ELEMENTAL ANALYSIS OF CONCRETE USING REFLECTED PROMPT GAMMA-RAYS

BY

ZAMEER KALAKADA

A Thesis Presented to the

DEANSHIP OF GRADUATE STUDIES

KING FAHD UNIVERSITY OF PETROLEUM & MINERALS

DHAHRAN, SAUDI ARABIA

In Partial Fulfillment of the
Requirements for the Degree of

MASTER OF SCIENCE

In

CIVIL ENGINEERING

MARCH 2012

KING FAHD UNIVERSITY OF PETROLEUM & MINERALS

DHAHRAN 31261, SAUDI ARABIA

DEANSHIP OF GRADUATE STUDIES

This thesis, written by **ZAMEER KALAKADA** under the direction of his thesis advisor and approved by his thesis committee, has been presented to and accepted by the Dean of Graduate Studies, in partial fulfillment of the requirements for the degree of **MASTER OF SCIENCE IN CIVIL ENGINEERING**.

Thesis Committee

Prof. Omar S. Baghabra Al-Amoudi(Advisor)

Prof. Akhtar A. Naqvi (Co-Advisor)

Prof. Mohammed Maslehuddin (Member)

Dr. Shamshad Ahmad (Member)

Dr. Salah U. Al-Dulaijan (Member)

15 APR 2012

Dr. Nedal T. Ratrout
Departmental Chairman

Dr. Salam A. Zummo
Dean of Graduate Studies

6/5/12
Date

عمادة الدراسات العليا
DEANSHIP OF GRADUATE STUDIES

DEDICATED TO

MY PARENTS & MY WIFE

ACKNOWLEDGEMENTS

All praise is due only to **ALLAH** subhana wa ta' aala, the sustainer of the worlds, the most compassionate, the most merciful for bestowing me patience, health and knowledge to complete this work successfully. May the peace and blessings of Allah Subhanahu wa ta'aala be upon Prophet Mohammed (Sal allahu alahi wa sallam).

I would like to thank King Fahd University of Petroleum and Minerals for providing tremendous research facilities and financial assistance during the course of my MS program.

I acknowledge my sincere appreciation and thanks to Prof. Omar S. Baghabra Al- Amoudi for his supervision and constructive guidance throughout this research. I would like to acknowledge sincere gratitude and appreciation to my co-advisor Prof. Akhtar A. Naqvi for his constant encouragement, untiring efforts and valuable time spent during all the stages of this work. I am grateful to my committee Dr. Mohammad Maslehuddin, Dr. Shamshad Ahmad and Dr. Salah U. Al-Dulaijan for their guidance and cooperation during this work. I am also indebted to the Department Chairman, Dr. Nedal T. Ratrout, and other faculty members for their support.

Lastly, but not the least, special thanks are due to my parents, wife and family members for their untiring efforts and encouragement during the all stages of my life.

TABLE OF CONTENTS

LIST OF TABLES

LIST OF FIGURES

THESIS ABSTRACT

NAME: **ZAMEER KALAKADA**

TITLE: **ELEMENTAL ANALYSIS OF CONCRETE USING REFLECTED PROMPT GAMMA-RAYS**

MAJOR: **CIVIL ENGINEERING**

DATE: **MARCH 2012**

Corrosion of reinforcing steel, mainly caused by chloride ions, is the number one durability problem faced by the construction industry. There is a desire to develop a non-destructive concrete corrosion monitor to determine the concentration of chloride ions in concrete. The Prompt Gamma Neutron Activation Analysis (PGNAA) technique offers a prompt, non-destructive, in-situ technique to detect the elemental composition of concrete. Therefore, a PGNAA setup will be designed and tested to detect prompt gamma-rays reflected from concrete specimens. Monte Carlo calculations will be carried out to determine the optimum size of the neutron moderator, sample and detector shielding.

The chloride concentration was measured in chloride-contaminated FA, BFS and SPZ cement concrete specimens at 6.11, 5.72 and 2.86+3.10 MeV chlorine prompt-gamma rays. In spite of interference between gamma-rays from chlorine and calcium, an excellent agreement was observed between the experimental and theoretical yield of 6.11, 5.72 and 2.86+3.10 MeV chlorine prompt gamma-rays. This shows the successful application of the portable neutron generator for evaluating the chloride contamination in the field.
A good correlation was noted between the gamma-ray yield at 5.72 and 6.11 MeV. Consequently, the chloride concentration can be determined from these relations:

Chloride (wt.%) = 5.72 MeV Gamma-Ray Counts / 3839

Chloride (wt.%) = 6.11 MeV Gamma-Ray Counts / 5293

However, the equation with 6.11 MeV is preferred as it has higher intensity and can detect low concentrations of chloride.

THESIS ABSTRACT (ARABIC)

الاسم: كالقاضي زمر

العنوان: أشعة غاما موجه باستخدام الخرسانة من العناصر تحليل وانعكست

الرئيسية: المدنية الهندسة

التاريخ: 2012 مارس

البناء صناعة تواجه التي المتانة 1 رقم المشكلة هي الكلوريد، أيونات عن أساسا ينجم وهو التسليح، حديد تآكل الخرسانة في الكلوريد أيونات تركيز لتحديد ملموسة تآكل رصد مدمرة غير وضع في رغبة هناك .والتشييد عن للكشف تقنية الموضع في مدمرة، وغير الفوري، يقدم تقنية (PGNAA) التنشيط تحليل موجه غاما والنيوترون غاما الفوري للكشف واختبار PGNAA الإعداد برنامج تصميم سيتم ولذلك، .الخرسانة من العنصري التركيب النيوترونية، وسيط من الأمثل الحجم لتحديد الحسابات كارلو مونتي وسيجري .ملموسة عينات من المنعكسة الأشعة التدريع عن للكشف وعينة.

و 6.11 ،5.72 على الخرسانة عينات BFS SPZو القدم، كرة اتحاد الملوثة كلوريد في الكلوريد تركيز قياس تم والكالسيوم، الكلور من جاما أشعة بين التداخل من الرغم على .موجه غاما أشعة 3.10+ الكلور فولت إلكترون 2.86 الكلور فولت إلكترون 3.10+ 2.86 و 6.11 ،5.72 من والنظرية التجريبية الغلة بين ممتاز اتفاق على لوحظ وقد المجال هذا في كلوريد تلوث لتقييم المحمولة النيوترون للمولد الناجح التطبيق على يدل وهذا .غاما أشعة موجه تحديد يمكن ذلك، على وبناء .فولت إلكترون 6.11 و 5.72 على غاما اشعة العائد بين جيدة علاقة وجود ولوحظ العلاقات هذه من كلوريد تركيز:

كلوريد (wt.٪) = 5.72 التهم غاما أشعة فولت إلكترون / 3839

كلوريد (wt.٪) = 6.11 التهم غاما أشعة فولت إلكترون / 5293

منخفضة تركيزات عن الكشف ويمكن كثافة أعلى فعلت كما فولت إلكترون 6.11 مع المعادلة في ويفضل ذلك، ومع كلوريد من.

CHAPTER 1

INTRODUCTION

1.1 Elemental Analysis of Concrete

Cement, the most important ingredient in concrete, is known since the construction of pyramids in old Egypt, where it was used as a binding agent. At present, concrete is one of the most widely produced materials on the earth, with usage above dozens of billions of tons. The concrete industry involves millions of dollars being the basis of the development of the society. Concrete is subjected to severe degradation problems. Apart from structural design failures, the most important cause of concrete deterioration is reinforcement corrosion. In the past three decades, this problem has reached alarming proportions leading to very high repair costs, sometimes above the initial construction cost, or in extreme situations, to the final collapse of the structure.

Reinforcement corrosion, mainly caused by chloride ions, is a serious problem facing the building construction industry. Several billion dollars are spent worldwide to repair the damage caused by reinforcement corrosion. Therefore, it is desired to develop a concrete corrosion monitor to determine the chloride concentration in concrete non-destructively. PGNAA technique offers a relatively non-destructive in-situ technique to determine the concentration of chloride ions in concrete. In order to analyze the chloride ions in

concrete, the intensity of backward-emitted gamma-rays (reflection mode) from the structure has to be detected.

A PGNAA setup was designed and tested in this thesis project to detect prompt gamma-rays from concrete specimens in the reflection mode. Monte Carlo calculations were carried out to determine the optimum size of neutron moderator, specimen size and detector shielding. Finally, theoretical calibration curves of elemental concentration of chloride contaminated Fly ash, super pozz and blast furnace slag cement concrete specimens versus prompt gamma-ray yield were generated for comparison with the experimental results.

In this study, Fly ash, super pozz and blast furnace slag cement concrete samples with varying chloride concentrations were prepared. Thereafter, prompt gamma-rays reflected back from these specimens were measured. The elemental concentrations versus gamma-ray yield curves were generated from the results. Finally, prompt gamma-ray yield was measured in reflection mode from the chloride contaminated- Fly ash, super pozz and blast furnace slag cement concrete specimens. The chloride concentration versus prompt gamma-ray yield calibration curves for Fly ash, super pozz and blast furnace slag cement concretes were also generated.

1.2 Significance of This Research

Billions of dollars can be saved in public and private sectors if corrosion of reinforcement is detected at an early stage. Since the presently utilized techniques involve difficult and time consuming process of sample retrieval and analysis, there is a critical need for a nondestructive test method that can detect chlorides in concrete to assess the existing condition of reinforced concrete structures.

The data developed in this study will be utilized to design a portable monitor for the detection of chloride concentration in concrete structures with different types of cements.

1.3 Objectives

The general objective of this study was to assess the suitability of PGNAA technique in determining the chloride concentration in cement concretes. The specific objectives were the following:

1. Design and testing of a PGNAA set-up to assess the chloride concentration in concrete,
2. Determine the chloride concentration in cement concretes, and
3. Verify the Monte Carlo simulations by experimental results.

CHAPTER 2

LITERATURE REVIEW

2.1 Corrosion of Reinforcing Steel in Concrete

Deterioration of concrete structures due to reinforcement corrosion is the major durability problem facing the construction industry in the Arabian Gulf and worldwide [1]. Reinforcement corrosion is mainly attributed to the diffusion of chloride ions to the surface of the reinforcing steel. The exact process by which the chloride ions initiate reinforcement corrosion is not very well understood [2]. Whatever be the process, billions of dollars are being utilized annually to repair and rehabilitate deteriorated concrete structures in North America, Europe and the Arabian Gulf [3-4]. Considering the damaging attributes of chloride ions on reinforcement corrosion, building codes often place limitations on the acceptable chloride concentration [2,4]. Preventive measures against corrosion require maintaining the chloride and sulfate concentration in concrete below the threshold limits specified by the Codes of Practice. This requires monitoring the chloride concentration in concrete, preferably using a non-destructive technique.

The most important causes of reinforcement corrosion are: (i) depassivation of the reinforcing steel due to the chloride ions ingress and (ii) total depassivation of the reinforcement due to acidification of the interstitial solution in consequence of reactions of the cement matrix with carbon dioxide present in the atmosphere [5].

The harmful chloride ions may be present in concrete as contamination from the ingredients, or they may diffuse from the external environment. This situation results from exposure of the structures to water and marine atmospheres or to the use of de-icing salts (NaCl, $CaCl_2$ and $MgCl_2$); an essential practice in cold climates [2]. After initiation of the corrosion process, the corrosion products (iron oxides and hydroxides), occupying a volume several times larger than that of the original iron, cause internal stresses that result in cracking and spalling of the concrete cover. At this stage, forced intervention of aggressive agents, oxygen and humidity is facilitated through these cracks leading to the total loss of structural integrity [6].

2.2 Corrosion Process

Corrosion is an electrochemical process in which anodic and cathodic half-cell reactions take place. In a good quality concrete, the pH is in the range of 12.5-13.5 and in the absence of chlorides, the following anodic reaction takes place leading to the formation of iron cations.

$$Fe \rightarrow Fe^{2+} + 2e^{-} \quad (2.1)$$

The cathodic reaction balances this reaction by producing hydroxyl anions as follows:

$$1/2O_2 + H_2O + 2e^{-} \rightarrow 2OH^{-} \quad (2.2)$$

The products of both these reactions combine together and in a later stage produce a stable film that passivates the reinforcing steel. The stability of this passive film depends

on the availability of oxygen that controls the cathodic reaction and on the pH of the pore solution at the interface of steel and concrete [7].

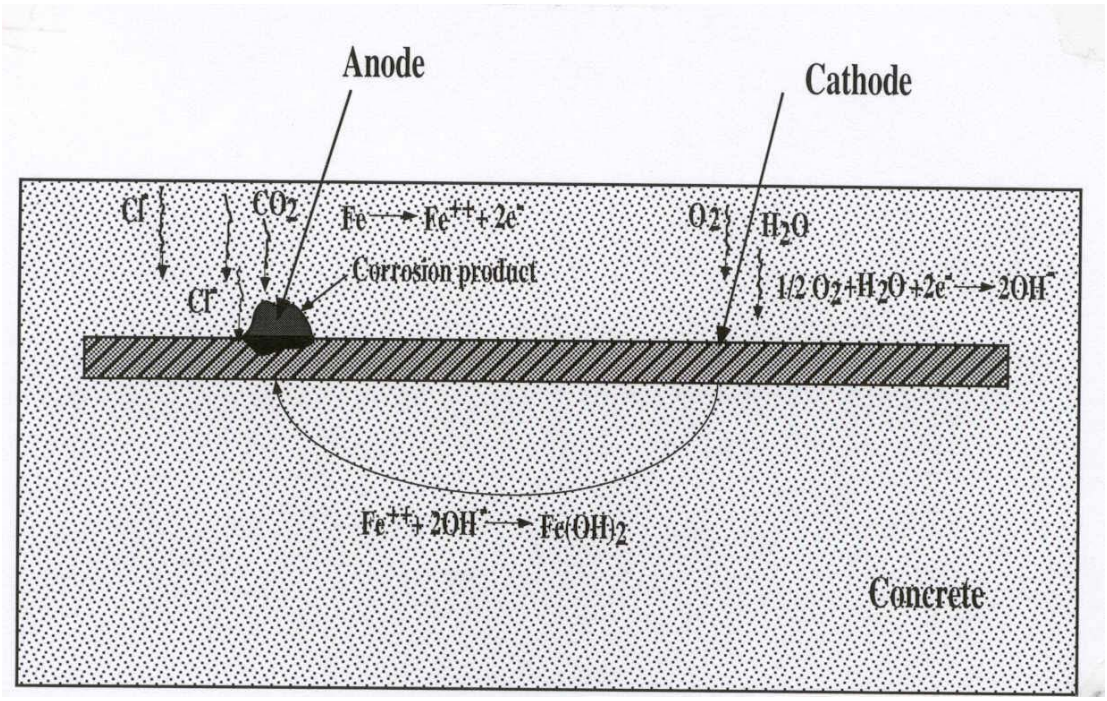

Figure 2.1: Schematic representation of the mechanisms of corrosion.

2.2.1 Chloride-Induced Corrosion

Chloride ion acts as an essential catalyst in the corrosion reaction. Chloride ions initiate the corrosion reaction by depassivating the oxide film on the steel surface, allowing the iron to dissolve into solution. However, depassivation of steel does not necessarily occur through a direct reduction of alkalinity in the electrolyte by the chloride-induced reaction. Some researchers now believe that the chloride ions also react directly by migrating through the film [8]. The actual mechanism of migration, however, is not very well understood or agreed upon. Ogura and Ohama [9] suggested that nucleation sites are related to microscopic inclusions and grain boundaries on the metal surface.

Chloride ions also cause a shift of potential of the steel. Non-uniform penetration of chloride ions to the level of the steel produces differences in potential and leads to the formation of "macro" corrosion cells. Non-uniform penetration is a general occurrence, and results from such factors as variations in concrete cover and local differences in concrete quality. On reaching the iron substrate, the chloride ions act as a catalyst for the oxidation of iron by taking an active part in the reaction. According to Uhlig [10], chloride ions oxidize the iron to form $FeCl_3$ and draws its unstable ferrous ion into solution, where it reacts with the available hydroxyl ions to form $Fe(OH)_2$. This releases the Cl^- ions back into solution, as seen in the following reaction [11]:

$$Fe + 3Cl^- \rightarrow FeCl_3 + 3e^- \quad (2.3)$$

$$FeCl_3 + 3OH^- \rightarrow Fe(OH)_3 + 3Cl^- \quad (2.4)$$

The electrons released in the oxidation reaction (Eq. 2.3) flow through the steel to the cathode. This process results in an increase in the concentration of chloride ions and a reduction of the pH at the points of corrosion initiation. The lowered pH at these sites contributes to the continual breakdown of the passive oxide film [11]. Equation 2.4 indicates that three chloride ions are released as a byproduct indicating that once the chloride ion reaches the metal surface, no more chlorides are required for further corrosion and depending on the electrical resistivity of concrete either general or local corrosion proceeds.

Further, concrete, acting as a conducting medium has a wide variation in its electrical resistivity. Resistivity values ranging from about 10 to 10,000 k.Ω.cm have been reported

by researchers studying concrete with different moisture induced ionic contents. An increase in temperature or addition of moisture and ions, such as chlorides, to hydrated concrete results in a large drop in the resistivity. High water-cement ratio, chloride-bearing saturated concrete provides the lowest resistivity to corrosion current, while low water-cement ratio, well cured, dry concrete provides the highest.

Another form of chemical protection provided by cement is its ability to bind chlorides. The chemical compound that is primarily known to have the chloride binding capacity is tricalcium aluminate (C_3A). It is reported that chloride ions react with C3A in cement paste to form tricalcium chloroaluminate ($C_3A.CaCl_2.10H_2O$), known as Friedl's salt [12-14]. Because of this reaction, a threshold concentration of chloride ions must be present for destroying the passive film. From this viewpoint, the American Concrete Institute [15] limits the water-soluble chlorides to 0.15% by weight of cement. ACI [16], adopting a more conservative approach, has suggested that the acid-soluble chloride concentration should not be more than 0.2% by weight of cement. The British Standard BS 8110 allows a total chloride content of 0.4%. Rasheeduzzafar et al. [17] indicated that the chloride threshold limits for cements with up to 8% C_3A agree very well with the ACI [15] limit of 0.15% water-soluble chlorides, as well as with the BS 8110 limit of 0.4% acid-soluble chlorides. Additionally, they reported that ACI, BS and Australian Code limits, however, appear to be conservative for concretes prepared with high C_3A cements. Lambert et al. [18] suggested that the critical level of chloride below which there was no significant probability of corrosion was around 1.5% by weight of cement. They attributed the

increased chloride tolerance in their specimens compared to BS 8110 limit of 0.4% to the protective nature of concrete produced under well-controlled conditions of the laboratory.

Research findings, however, have shown that cement alkalinity also significantly influences chloride binding and, hence, the free chlorides [19-21]. Taking into account the combined effect of chloride and alkalinity, Hausmann [22] suggested the critical Cl^-/OH^- to be around 0.6. Gouda [23], using pH values of the electrolyte representative of the concrete pore solution, indicated that the threshold Cl^-/OH^- was 0.3. Lambert et al. [18] investigated the relationship between Cl^-/OH^- and corrosion current density in various cements. Their investigation indicated that the passive conditions of steel in concrete, characterized by corrosion current density (I_{corr}) substantially lower than 100 nA/cm^2 were maintained until a threshold Cl^-/OH^- ratio of approximately 3 was exceeded. There was a considerable scatter in the values of I_{corr} recorded at Cl^-/OH^- ratios in excess of 3 and even at Cl^-/OH^- ratios as high as 15 to 20, there were instances of bars suffering no significant corrosion. Mangat and Molloy [24] indicated that a universal threshold Cl^-/OH^- level is not applicable to different concretes. In their investigation, reinforcing steel corrosion was observed in the control matrix when the pore fluid Cl^-/OH^- ratio was 13, while at values of 17 and 18, in silica fume cement concrete, reinforcement corrosion was insignificant. Similarly, minimal reinforcement corrosion in the silica fume cement and blast furnace slag cement mortar specimens placed in the aggressive sabkha environment even at Cl^-/OH^- of 3.3 and 6.5, respectively, was reported by Al-Amoudi et al.[25].

Corrosion of steel in concrete is initiated when the passive film is destroyed locally due to the presence of chloride ions. The breakdown procedure was studied by a large number

of authors. Jovancicevic et al. [26] explained and criticized a number of models proposed to explain the passive film breakdown by the chloride ions. The authors reported three general models: (i) adsorption-displacement, (ii) chemico-mechanical and (iii) migration-penetration.

The first model proposed by Leckie and Uhlig [27, 28] and Kolotorkyn [29] suggested that breakdown involves adsorption of Cl^- with simultaneous displacement of O^{2-} resulting in the film destruction. In the second model, Hoar [30] stated that when the repulsive forces between adsorbed ions are sufficiently large, chloride ions lower the interfacial surface tension resulting in the formation of cracks and flaws which in turn leads to the weakening of the passive film. Chao et al. [31] developed the third model and stated that Cl^- reaches the steel filling the O^{2-} vacancies, resulting in the formation of complexes with Fe^{2+}. Due to the faster iron dissolution, the decrease of oxygen vacancies at the interface caused by Cl^- leads to the formation of voids resulting in the pit growth. This results in the formation of soluble iron complexes and conversion of the amorphous layer into a crystalline layer. The solubility of these products releases chlorides, making them available for further reaction with iron resulting in localised acidification and finally in the breakdown of the passive film. The formation of iron oxides and hydroxides occupy larger volume than the original iron, leading to the creation of internal forces that decrease the adhesion at the steel/concrete interface.

2.2.2 Chloride Threshold Content

Tuutti [6] stated that from the point of view of reinforcement corrosion, the service life of a concrete structure can be subdivided into an incubation period (t_1) and a propagation period (t_2). The incubation period (t_1) corresponds to the chloride penetration within the porous material and its accumulation in the vicinity of the reinforcement. Its duration depends on the thickness and quality of the concrete cover as well as on the chloride concentration required to start the corrosion process. The propagation period (t_2) corresponds to the stage when the chloride ions depassivate the reinforcing steel surface, leading to the development of corrosion and very often to the local failure of the structure.

Chloride threshold level is defined as the chloride concentration at the steel/concrete interface resulting in a significant corrosion rate, leading to corrosion-induced deterioration [32]. The determination of the chloride threshold level has been one point of increasing interest. However, this parameter is affected by a large number of factors that are mainly dependent on the characteristic of the steel/concrete system, such as:

(i) the interstitial solution chemistry and pH,

(ii) water to cement ratio,

(iii) concrete composition, namely cement type, use of additives such as fly ash and other mineral admixtures,

(iv) pore and capillary structure, and

(v) Curing period and curing and exposure temperature.

Glass et al. [33, 34] reported several chloride threshold values obtained by different authors in different conditions: (i) outdoor concrete structures and (ii) laboratory experiments using mortar, concrete pastes and solutions. It was shown that the total chloride content, expressed in wt% cement, is in the range of 0.17 to 2.5, thus changing by about 15 times. These large differences clearly indicate that the quantification and prediction of the chloride content in concrete can be a difficult task. As there are a large number of variables affecting the process, the error involved can be significantly high. Thus, it is fundamentally important to constantly monitor the state of reinforcement steel in order to detect the onset of corrosion.

2.2.3 Chloride Monitoring Techniques

It is important to determine the chloride ion distribution in a structure under investigation to be able to determine its susceptibility to corrosion. Chloride profiles (chloride concentration versus depth from the surface) provide valuable information on the source of chloride ions and the apparent rate of diffusion of the chloride ions in concrete. The rate of diffusion can be used to calculate when the chloride ion concentration at the steel/concrete interface will exceed the threshold value required to initiate the corrosion, if it has not already exceeded.

The chloride content in concrete can be determined through analysis of powdered concrete samples. Samples can be collected on-site at different depths up to and beyond the depth of the reinforcing steel using a hammer drill. Extreme care should be exercised

to avoid inadvertent contamination of the samples. Alternatively, core can be retrieved and powdered samples can be obtained at different depths in the laboratory.

Chloride ion in concrete exists in two forms, chemically bound and soluble in the concrete pore water. The chloride ion content of concrete is usually measured in the laboratory using wet chemical analysis. The total chloride (or acid soluble) test method measures the sum (i.e., total) of all chemically bound and free chloride ions in the concrete. The water soluble test method measures only the free ions soluble in pore water. The water soluble chloride ions are linked to the initiation of corrosion. Because the water soluble test method is not very accurate or repeatable, the general practice is to use the acid soluble test method [35]. Most researchers have used the acid soluble and reported varying threshold values for corrosion initiation depending on design of the concrete mix [35].

While several analytical techniques are available to measure the chloride concentration in concrete, these methods are destructive and laborious as they involve the tedious work of obtaining core specimens or powder samples from a structure and are not very accurate. As such, there is a need to develop an accurate and non-destructive technique to monitor in-situ chloride concentration in a structure [36]. The available techniques to quantify chloride ions in concrete, in particular the wet analysis methods, tend to be inaccurate due to the small sample size and the associated uncertainties during sampling and testing stages. Other techniques, for example PGNAA and X-ray fluorescence (XRF) technique [37], can be utilized to determine the elemental composition of bulk specimens. Both these techniques have their own advantages and limitations.

X-ray fluorescence (XRF) spectroscopy is a technique that can be used for direct analysis of solid metal samples, thin metal films, petroleum products, cement, coal and various other materials. XRF is a fast technique and non-destructive to the sample. It is frequently used for analyses performed in the field and for industrial quality control. An X-ray tube is used to irradiate the sample with a primary beam of X-rays. Some of the impinging primary X-rays are absorbed by the sample elements in a process known as the photoelectric effect [37]. The photoelectric effect occurs when all the energy of a primary X-ray is absorbed by an electron in an atom's innermost electron shell. This causes excitation and ejection of the absorbing electron (photo-ejection). The electron vacancies caused by the photoelectric effect are filled by electrons from higher energy states, and X-rays are emitted (fluorescence) to balance the energy difference between the electron states. The X-ray energy is characteristic of the element from which it was emitted [37].

The XRF technique requires specialized sampling methodology and sample preparation, and is associated with difficulties in analyzing low atomic number elements, such as C and O. Moreover, this technique is excluded from the non-destructive category. On the other hand, the PGNAA technique is a fast and multi-elemental nuclear technique for analysis of bulk materials. This technique determines precisely the concentration of light elements, such as C, S, F, Al, Si, P, Cl, Ca, Va and Fe in the range of 0.1% to 50% [37]. Another main advantage of this technique is its capability of analyzing very large specimens.

2.3 Neutron Activation Analysis

Neutron activation analysis (NAA) technique is a very popular nuclear non-destructive method used for the elemental analysis of samples. The principle of this technique is that elements can be made radioactive by exposure to neutron irradiation. NAA is a sensitive analytical technique useful for performing both qualitative and quantitative multi element analysis of major, minor and trace elements in specimens from almost every conceivable field of scientific or technical interest. For many elements and applications, NAA offers sensitivities that are superior to those attainable by other methods, on the order of parts per billion or better [38].

The basic essentials required to carry out an analysis of specimens by NAA are a source of neutrons, instrumentation suitable for detecting gamma-rays, and a detailed knowledge of the reactions that occur when neutrons interact with target nuclei. The sequence of events occurring during the most common type of nuclear reaction used for NAA, namely the neutron capture or (n, gamma) reaction, is illustrated in Figure 2.2. When a neutron interacts with the target nucleus via a non-elastic collision, a compound nucleus is formed in an excited state [38].

The excitation energy of the compound nucleus is due to the binding energy of the neutron with the nucleus. The compound nucleus will almost instantaneously de-excite into a more stable configuration through emission of one or more characteristic prompt gamma-rays. In many cases, this new configuration yields a radioactive nucleus which also de-excites (or decays) by the emission of one or more characteristic delayed gamma-rays, but at a much

slower rate according to the unique half-life of the radioactive nucleus. Depending upon the particular radioactive species, half-lives can range from fractions of a second to several years.

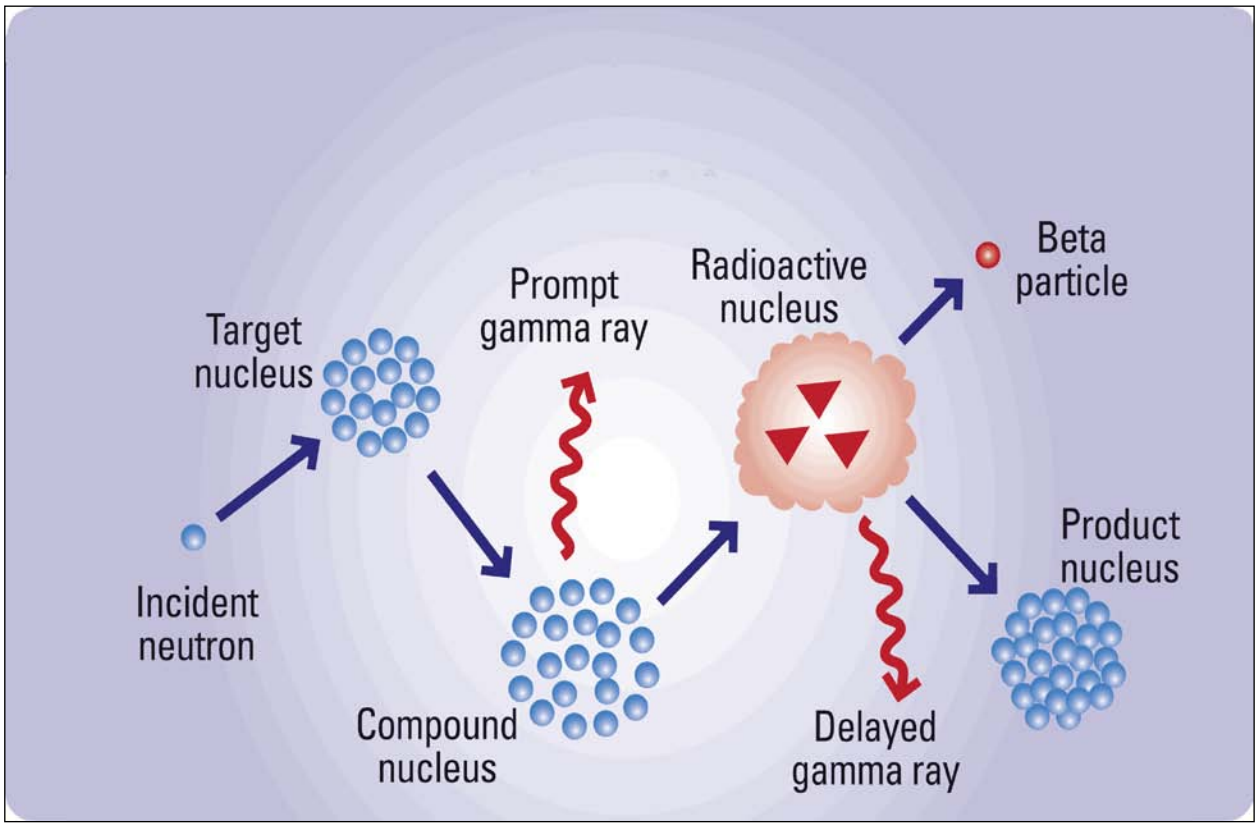

Figure 2.2: Diagram illustrating the process of neutron capture by a target nucleus followed by the emission of gamma rays.

With respect to the time of measurement, NAA falls into two categories: (1) prompt gamma-ray neutron activation analysis (PGNAA), where gamma-ray measurements take place during irradiation, or (2) delayed gamma-ray neutron activation analysis (DGNAA), where the gamma ray measurements are carried out after a specific delay after irradiation.

2.4 Theory of PGNAA

When a nucleus absorbs a neutron, a compound nucleus is formed with excitation energy equal to the binding energy ($BE_{Neutron}$) of the neutron plus the kinetic energy of the neutron ($K_{Neutron}$). For about 80% of the stable nuclei, the binding energy ranges from 6 to10 MeV.

Excitation Energy = $K_{Neutrons} + BE_{Neutrons}$

The excitation energy is rapidly shared among several nucleons followed by almost instantaneous decay (~10^{-13} to 10^{-14} s) with the following possible reaction products:

- Inelastic scattering, in which the neutron is emitted along with one or more gammas.
- Radiative capture (n, γ), in which one or more capture gammas are emitted.
- Similar to radiative capture except particles are emitted e.g., (n,α), (n,p), (n,d), (n,n') …, (n,2n).
- Fission or if enough energy spallation or evaporation [39]

Of the four processes, radiative capture is the most common form of decay for compound nuclei formed by the absorption of a thermal neutron, and it is the fundamental process for PGNAA.

Nucleus has different energy levels and when it is in its excited state, the excitation energy is shared by nucleons within the nucleus. These nucleons almost simultaneously go through a series of discreet energy transitions to get to the ground state. The transitions, starting at the capture state, are called primary transitions, two or more transitions are called secondary transitions, and the final transitions reaching the ground

state are called ground-state transitions. Each transition releases a gamma ray with energy equal to the energy of the transition (E_T) minus the recoil-energy (E_R) of the nucleus [39].

$E_\gamma = E_T - E_R$

Where $E_R = P^2/2M = E^2_\gamma/2Mc^2$

since, $E^2 = P^2c^2 + m^2c^4$ (Relativistic relation between energy and momentum)

P = Momentum, M = Mass of nucleus and

c = speed of light.

In case of radiative capture, the recoil energy can be as high as several keV for light elements but is typically less than 0.1% of the transition energy for most elements [40]. Thus, as the nucleons return to the ground state, the energy released is discrete and characteristic of the nuclear energy levels within the nucleus, and since the energy levels of the nuclei are characteristically different for different elements, the gammas released from radiative capture, which range from 50 keV to greater than 10 MeV, are distinct for differing elements [39].

In PGAA, it is important to consider radiative capture of both thermal and epithermal neutrons. For thermal neutrons, the energies of the capture states are very sharply defined due to low kinetic energy of the neutrons. Thus, the probability of decay through various transitions is essentially constant and, therefore, the distribution of the gammas produced is essentially constant. This is important for determining information such as the quantities of elements through PGNAA. For epithermal neutrons, the increased kinetic energy of the neutrons results in greater excitation energy of the compound nucleus. For

these higher exited states, the transition to the ground state tends to be less-well defined, often resulting in an increase or change in the number of different energy gammas released due to de-excitation through different discrete energy levels of the nucleus. Hence, for most applications, it is desirable to reduce the epithermal component of the beam as much as possible.

2.5 Prompt Gamma Neutron Activation Technique

The Prompt Gamma-Ray Neutron Activation Analysis (PGNAA) technique is one type of Neutron Activation Analysis (NAA) techniques. It is one of the popular techniques commonly used to analyze the concentration of elements in bulk specimens [41-46]. This technique is non-destructive and ideally suited for in-situ measurements. The sample is irradiated in a neutron beam and the gamma-rays from the radiative capture are detected. PGNAA studies can be carried out via Thermal Neutron Capture (TNC) reaction or fast Neutron Inelastic Scattering (NIS) reactions. Depending upon the elements to be studied, either of the reactions can be chosen for PGNAA studies. For TNC-based prompt gamma-ray analysis, the intensity of thermal-neutron source is of primary importance [47-49], while for NIS-based prompt gamma-ray analysis, fast neutron intensity and energy are critical for the analysis [50,51]. In addition, because of its accuracy and reliability, PGNAA is generally recognized as the "referee method" of choice when new procedures are being developed or when other methods yield results that do not agree.

2.5.1 Development of PGNAA

Neutron radioactive capture, the mechanism for PGNAA, was first observed by Lea [52] when high energy gamma-rays were measured during the irradiation of paraffin wax and liquid hydrogen using a Polonium-Beryllium neutron source. Amaldi [53] identified this to be due to neutron capture followed by the emission of energy in the form of gamma-rays equal to the binding energy of the nucleus. Since then, capture gamma rays have been studied extensively, resulting in the measurement of capture gamma-rays for a large number of isotopes using gamma spectroscopy.

Before 1962, scintillation spectrometers were used. Groshev [54] reported that these scintillators were efficient in counting but had poor resolution of ~8% for 0.7 MeV and 20 % for 0.1 MeV. A compilation of the gamma rays measured for specific isotopes up until this time using these methods was studied by Groshev [54], Bartholomew [55] and Greenwood [56]. These studies contributed significantly to the knowledge of the nuclear energy levels, properties of isotopes, and provided much of the data necessary for PGNAA but were not practical because of their poor counting efficiencies.

The first studies using PGNAA for elemental analysis were conducted using sodium iodide scintillation spectroscopy. Even though sodium iodide detectors provide good sensitivity, their poor resolution made it difficult to differentiate between the different gamma energies, and the background. Bernard [57] solved the background problem by taking a series of measurements. Lussie [58] showed that this method could be used successfully to measure moisture content in calcium nitrate from hydrogen capture

gamma-rays, hydrogen content in paraffin and polystyrene, and could possibly be used for isotopic analysis of at least three of the four stable-iron isotopes.

The major limiting factor of the early PGNAA facilities was the resolution of the available detectors. This, however, changed when the first lithium drifted germanium Ge(Li) detectors were produced in 1962. These detectors had efficiencies of approximately 0.3-0.8%, as opposed to the sodium iodide detectors which were approximately 8-20%. One of the first applications of a Ge(Li) detector with a PGNAA facility was at the University of Washington Research Reactor by Lambard and Isenhour [59] who compared the results of two Ge(Li) detectors to that of a NaI(Tl) detector; increase in resolution which was obtained by using the Ge(Li), as opposed to the NaI(Tl) detector, made it possible to use PGNAA practically and efficiently for a much wider range of elements. After the implementation of Ge(Li) detector, PGNAA has been implemented successfully at over 40 research reactors throughout the world [60].

Among some of the best PGNAA facilities are the state-of-the-art facilities at the National Institute of Standards and Technology (NIST), and the University of Texas. The facilities at NIST include a thermal PGNAA facility and a cold PGNAA facility. The thermal PGNAA facility at NIST has a neutron beam which is extracted vertically from the NIST research reactor from a region within the D_2O approximately 0.5m from the nearest fuel element [61]. The resulting neutron beam in this facility had a measured thermal flux of 2 x 10^{-8} cm^{-2} s^{-1} and an epithermal flux of 1.1 x $10^{-8}cm^{-2}$ s^{-1}. Since the initial installation of this facility, several changes have been made which greatly enhanced the detection

capabilities. The reported thermal neutron flux for the new system was 3.0 x10^{8} cm^{-2} s^{-1} with epithermal flux of 1.1 x 10^{5} cm^{-2} s^{-1} with a relatively uniform beam diameter of approximately 2.0 cm. Overall, the sensitivities of the new instruments were 5-50% better than that of the old instrument.

The cold PGNAA facility at NIST utilizes a cold-neutron-source, the flux measured is 1.5 x 10^{8} cm^{-2} s^{-1}. The advantage of this facility over the thermal one is that it has higher sensitivities in part due to the higher absorption cross-section and the background is lowered due to the absences of fast neutron and gamma-rays in the beam. The PGNAA facility at the University of Texas and the facility in Budapest have reported thermal neutron fluxes of 5.3 x 10^{6} cm^{-2} s^{-1} and 5.0 x 10^{7} cm^{-2} s^{-1} respectively [62,63]. The reactor at the University Texas is a 1.1 MW Mark II TRIGA® reactor, and the reactor at the Budapest facility is a 10 MW tank type light water-cooled reactor [64]. Thermal PGNAA neutron facility at NIST was used as a guide for the design and construction of the PGNAA facility at Oregon State University. However, as far as neutron fluxes, the University of Texas facility was a better representation of expected fluxes since the reactor power and type are very similar to that of the 1.1 MW reactor at OSU.

2.5.2 PGNAA of Concrete

The elemental analysis of concrete using PGNAA can be done either with radio-isotope neutron sources [65-69] or accelerator-based neutron sources [70-73]. The radio-isotope neutron sources used successfully are ^{252}Cf [65] and ^{241}Am-Be [66]. Collico Savio et al. [74] did the elemental analysis of concrete samples by the neutron-induced prompt

gamma-ray technique ((PGNAA), using a radio-isotopic neutron source. Gamma-rays from capture of neutrons in concrete have been studied in the energy region from 0.3 to 10.5 MeV using an HPGe detector and Am-Be neutron source. This work presented the results of primary studies of the (n, γ) radiation produced in concrete specimens by an Am-Be source, which provided information on the relative amounts of the constituents in the sample. The analysis of the neutron capture gamma-ray spectra was accomplished using simplifying assumptions about neutron and gamma transport in the media, focusing on the concentrations of Ca, Si and Cl. Relative concentrations of Ca , Si and Cl have been obtained with reasonable accuracy and a 4% relative error for the Si to Ca ratio was reported [74]. The elemental identification is done by correlating the gamma-energies with the specific nuclei and the concentrations can be obtained from the intensities of the corresponding gamma-rays.

High gamma-ray dose and permanent radiation hazards are the problems encountered during the PGNAA of concrete using radio-isotope neutron sources. Another drawback of this analysis is the frequent replacement of neutron source due to its half-life. An accelerator-based PGNAA setup can be used as an alternative for radio-isotope neutron source based PGNAA setup. In case of an accelerator-based PGNAA setup, fast neutrons are produced by a compact accelerator.

The accelerator-based PGNAA set-up has certain benefits over the radio-isotope neutron source-based PGNAA setup due to the controlled mechanism of neutron production. It is user-friendly as it has got less radiation hazard. Furthermore, the on-off control of the

accelerator power ensures that the accelerator-based PGNAA setup has radiation hazards only when in use. An accelerated-based PGNAA setup which is a thermal neutron capture based was designed at KFUPM to analyze large samples of bulk materials [71-73]. Previously, the chloride concentration in blended cement concretes, such as FA, SF and BFS, were measured utilizing the accelerator-based PGNAA setup at KFUPM [47, 48, 75]. The previous PGNAA studies for the measurement of chlorine concentration in the cement concrete specimens were based upon the measurement of chlorine prompt gamma-ray intensities transmitted through the concrete specimen [47, 48, 75]. Although this setup was suitable for laboratory tests, it was not suitable for use in the field. For the detection of chloride in a concrete structure, a neutron source and gamma-ray detector are required to be placed side by side in order to carry out chlorine prompt gamma-ray scan of the concrete structure from one side only. Further, the set-up has to be portable and has to be built either around a portable radio-isotope neutron source or a portable neutron generator [76]. The set-up designed in the present study satisfies all these requirements. It is built around a portable neutron generator MP320 obtained from Thermo fisheries, USA. In this set-up, the detector and the moderated neutron source are placed side by side; the details of the set-up are given in the next section.

CHAPTER 3

METHODOLOGY OF RESEARCH

The experimental work was carried out in several stages. In the first stage, PGNA set-up was designed to analyze the elemental composition of concrete. In the second stage, the set-up was optimized using Monte Carlo simulations to determine the size of the major components of the set-up. The parameters optimized were size of the concrete specimen and moderator thickness. In the third stage, tests were conducted on BGO, $LaBr_3$:Ce and $LaCl_3$:Ce detectors to select the most appropriate one for the set-up. Based on the test results, a BGO detector was chosen to perform the PGNAA of concrete specimens. Lastly, the experimental results were compared with the simulation results.

3.1 Monte Carlo Simulations using MCNP Code

Monte Carlo methods have been extensively used in the design and response calculation of PGNAA experimental set-up, analysis of PGNAA data and assessing the detection limits of the PGNAA set-up and the prediction of detector response [77, 78]. In particular, Monte Carlo code is valuable in minimizing the time spent on system calibration and optimization, and assessing the detection limits [77-79]. Modeling of PGNAA process requires a Monte Carlo code capable of modeling neutron and photon interactions and transport. The Monte Carlo code MCNP4B has been specially designed for the transport of neutral particles, such as neutrons and gamma-rays [80].

Monte Carlo simulations were carried out to design a 2.5 MeV neutron source-based prompt gamma-ray neutron activation analysis (PGNAA) set-up for the elemental analysis of plain and chloride-contaminated FA, BFS and SPZ cement concrete specimens. The prompt gamma-rays produced by the capture of thermal neutrons in the specimen nuclei were used for the analysis. In these simulations, the moderator and sample size of the PGNAA setup were optimized. Monte Carlo simulations were experimentally validated through thermal neutron intensity measurements as a function of moderator thickness using a cylindrical (52 mm diameter and 2 mm thick) enriched-Lithium glass thermal neutron detector.

3.1.1 Use of MCNP Code to Design a Set-up

MCNP is a general-purpose Monte Carlo N-particle code that can be used in several transport modes: neutron only, photon only, electron only, combined neutron/photon transport where the photons are produced by neutron interactions, neutron/photon/electron, photon/electron, or electron/photon [80]. The neutron energy regime is from 10^{-11} MeV to 20 MeV, and the photon and electron energy regimes are from 1 KeV to 1000 MeV. The code requires the following information related to the set-up to be designed, such as: (i) Geometry, (ii) Materials and their cross-sections, (iii) Type and energy of the radiation, such as neutron, photon, or electron to be transported and (iv) Data to be recorded and the variance reduction techniques to improve the data uncertainity [80].

EXPERIMENTAL GEOMETRY

The geometry of the MCNP treats an arbitrary three-dimensional configuration of user-defined materials in geometric cells bounded by first and second degree surfaces and fourth degree elliptical tori. Cells are bound by surfaces. MCNP treats geometric cells in a Cartesian coordinate system.

MATERIALS SPECIFICATION

MCNP uses continuous-energy nuclear and atomic data libraries. Each data table available to MCNP is listed on a directory file, XSDIR. Users may select specific data tables through unique identifiers for each table, called ZAIDs. This identifier generally contains the atomic number Z, mass number A, and library specifier ID. Over 500 neutron interaction tables are available for approximately 100 different isotopes and elements. Photon interaction tables exist for all elements from Z=1 to Z=94. Cross sections for nearly 2000 dosimetry or activation reactions involving over 400 target nuclei in ground states are part of the MCNP data package.

NEUTRON AND GAMMA SOURCE SPECIFICATIONS

MCNP allows the user to specify a wide variety of source conditions without modifying the code. Independent probability distributions can be specified for the source variables of energy, time, position, and for other parameters, such as starting cell(s) or surface(s).

OUTPUT TALLIES SPECIFICATIONS

Various tallies related to particle current, particle flux, and energy deposition can be used in MCNP. All tallies are function of time and energy as specified by the user and are normalized to be per starting particle except for a few special cases with critical sources. MCNP provides seven standard neutron tallies, six standard photon tallies, and four standard electron tallies.

ESTIMATION OF MONTE CARLO ERRORS

The tallies are printed in the output accompanied by a second number R, the estimated relative error defined as the estimated standard deviation of the mean S_x divided by the estimated mean x. For a well-behaved tally, R will be proportional to $1/\sqrt{N}$ where N is the number of histories/runs. An interval is said to be reliable if the R obtained is less than 0.10.

VARIANCE REDUCTION TECHNIQUE

Variance is the square of the standard deviation. For a given MCNP run, the computer time consumed, T is proportional to N. Thus $R=\sqrt{C/T}$, where C is a positi ve constant which depends on the tally choice and/or the sampling choices. There are two ways to reduce R: (i) increase T and/or (ii) decrease C. First approach is often limited due to computer budgets, however; MCNP has special variance reduction techniques for decreasing C.

3.2 Geometry of the KFUPM PGNAA Setup

The geometry of the set-up used for simulations is shown in Figure 3.1. The PGNAA set-up mainly consists of a portable neutron generator, a cylindrical 25 cm x 8 cm (diameter x height) High density polyethylene (HDPE) moderator, and a cylindrical 5 cm x 5 cm (diameter x height) BGO gamma-ray detector. The concrete specimen was placed on one side of the neutron generator target-plane location, with the symmetry axis aligned at right angle to the neutron generator axis. The HDPE moderator is placed between the specimen and the neutron generator with its symmetry axis aligned with the axis of the concrete specimen. The BGO detector views the concrete specimen at an angle of 45° with respect to its symmetry axis, as shown in Figure 3.1. In order to prevent undesired gamma-rays and neutrons from reaching the detector, lead, tungsten and paraffin neutron shielding are inserted between the neutron generator, moderator and the BGO detector, as shown in Figure 3.1. The paraffin neutron shielding is made of a mixture of paraffin and lithium carbonate mixed in equal weight proportions.

The yield of prompt gamma-rays due to thermal neutron capture is needed to be optimized in the design of the PGNAA set-up. Since the yield depends upon the concentration of the elements of interest in the specimen as well as the thermal neutron flux available at the position of the specimen, it requires optimization of the size of the specimen and the moderator [47].

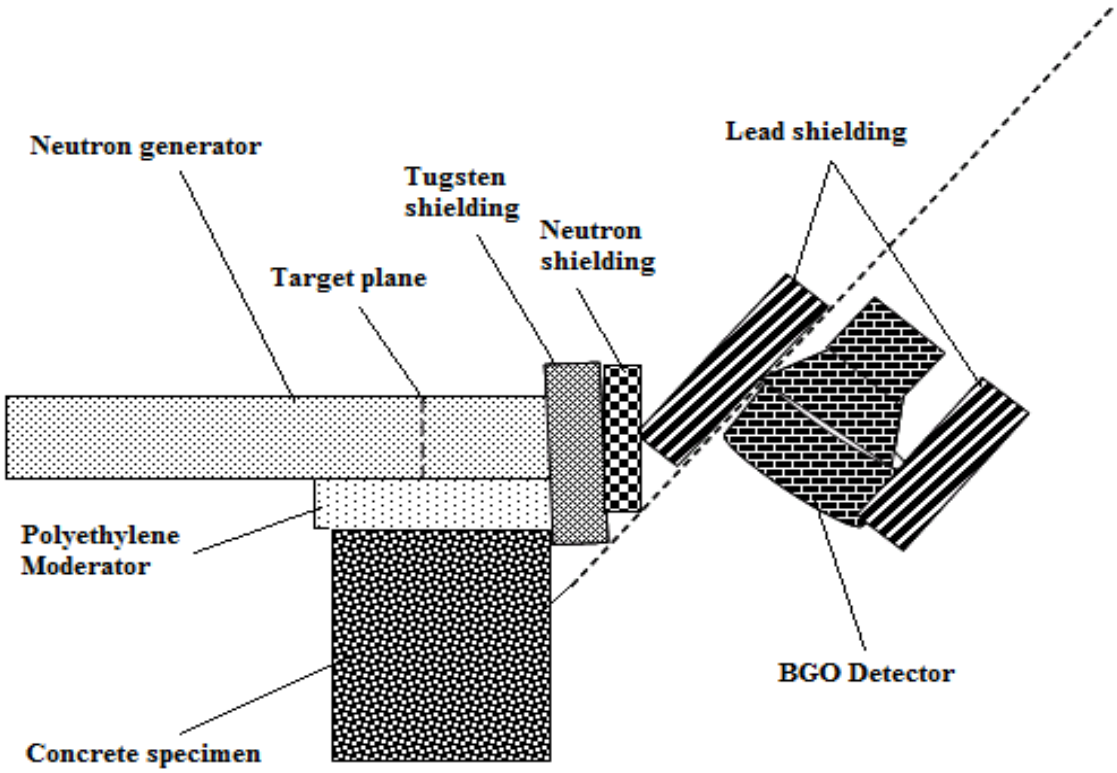

Figure 3.1: Schematic of the PGNAA set-up for Elemental and Chloride Gamma-Ray Measurements.

3.2.1 Specimen Size Optimization

Cylindrical cement concrete specimen 12.5 cm in radius and 14 cm high were used. This size was similar to the size used previously in the transmission type PGNAA set-up [47, 48, 75]. The calculated yield of prompt gamma-rays from concrete specimen plotted as a function of specimen radius and length are shown in Figure 3.2 and Figure 3.3 respectively. For the reflected gamma-ray measurements, it was assumed that the

specimen is large enough to emit prompt gamma-ray intensity in backward direction to be detected by the BGO detector.

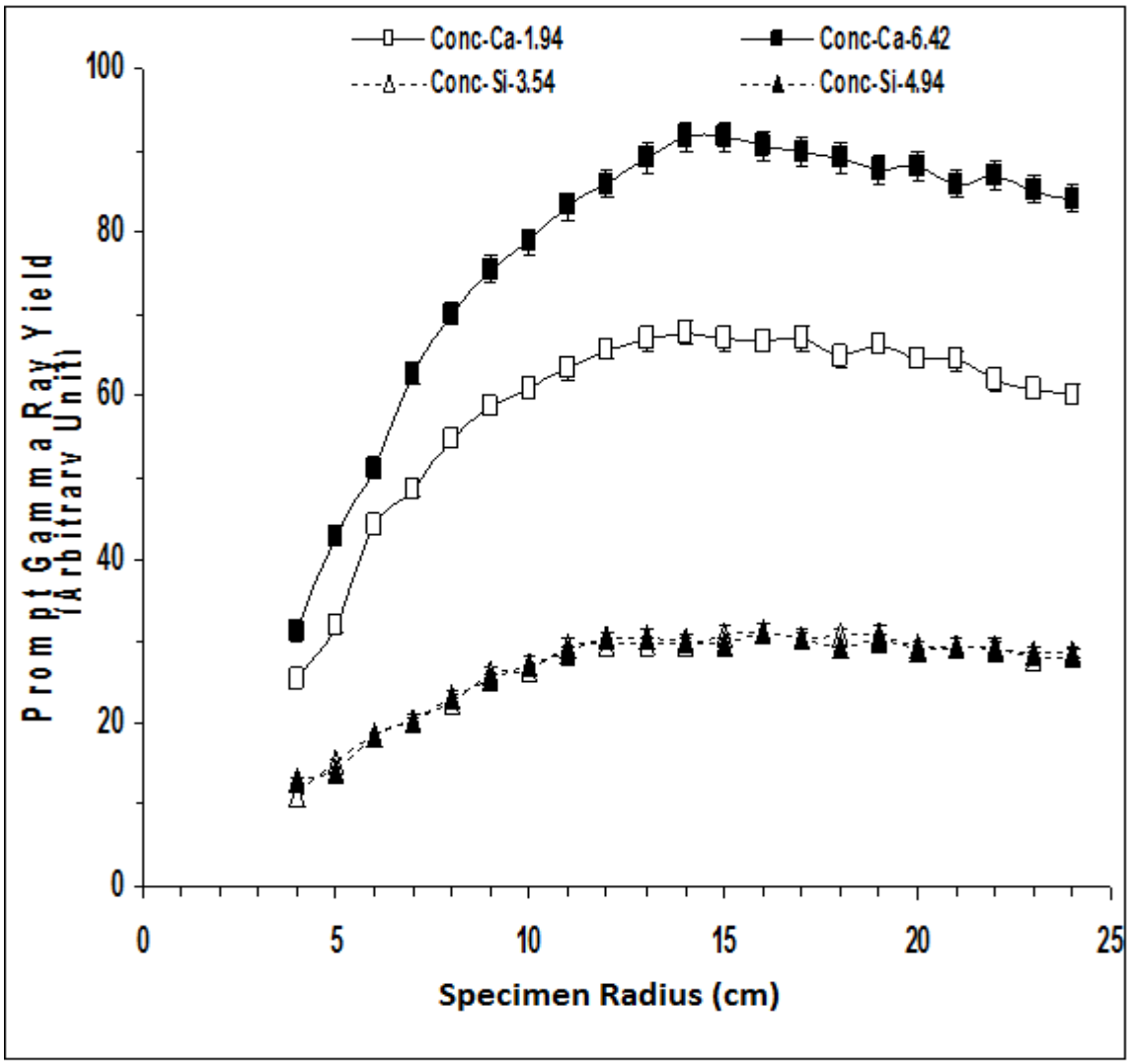

Figure 3.2: Calculated yield of prompt gamma rays from calcium and silicon in concrete specimen plotted as a function of specimen radius.

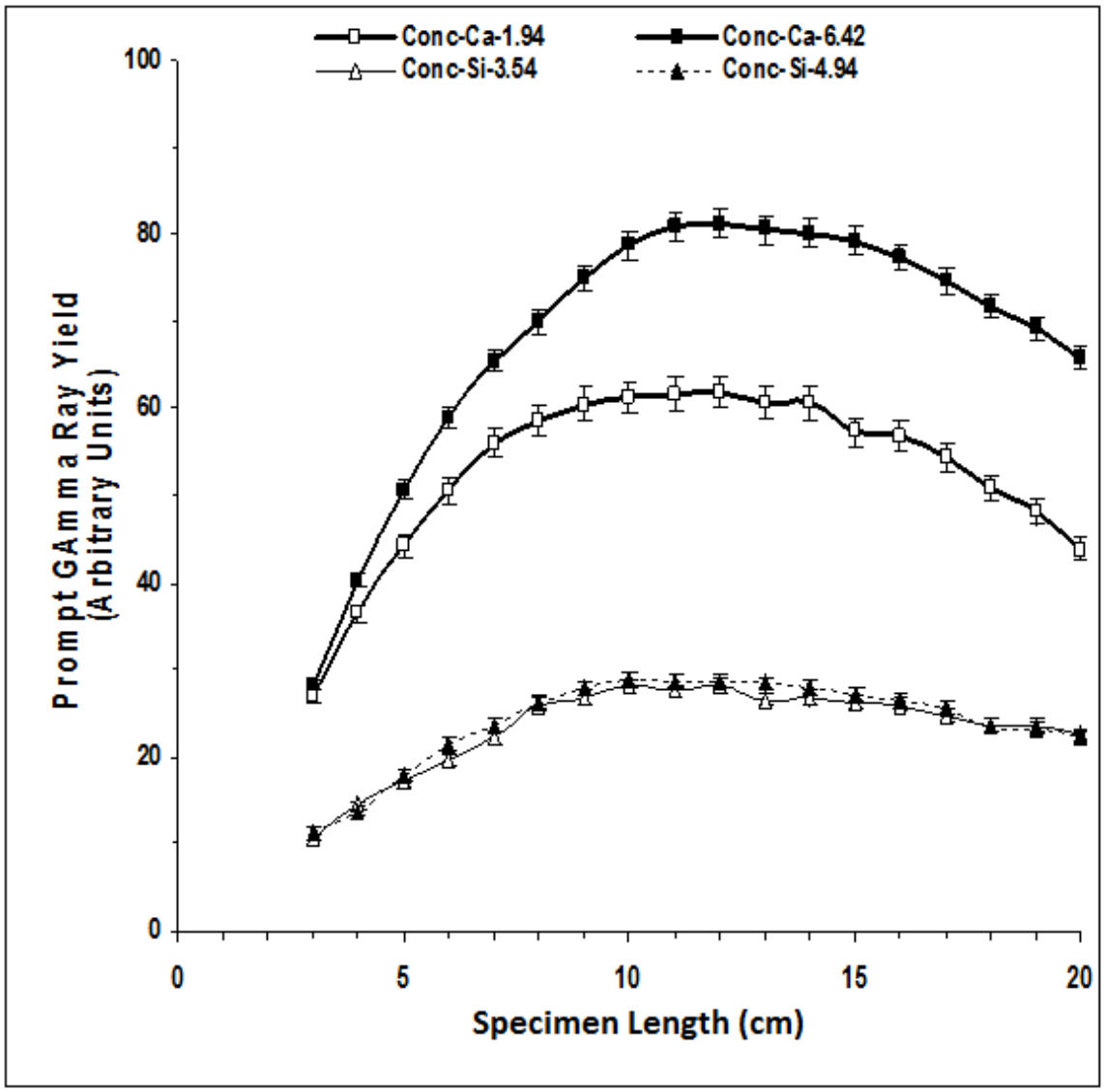

Figure 3.3: Calculated yield of prompt gamma rays from calcium and silicon in concrete specimen plotted as a function of specimen length.

3.2.2 Moderator Length Optimization

In this study, the optimum moderator size was determined through thermal neutrons yield calculations in the specimen volume as a function of the moderator thickness. The thermal neutron yield calculations for different neutron moderator thicknesses were carried out using code MCNP4B2 [80] and following the procedure described in Reference 48. The thermal neutron intensity increases with increasing the moderator thickness for 10 cm thickness and then remains constant over 10 to 14 cm thickness and starts decreasing with a further increase in the moderator thickness, as shown in Figure 3.4. The decrease in the thermal neutron intensity is due to decreasing neutron flux in the moderator.

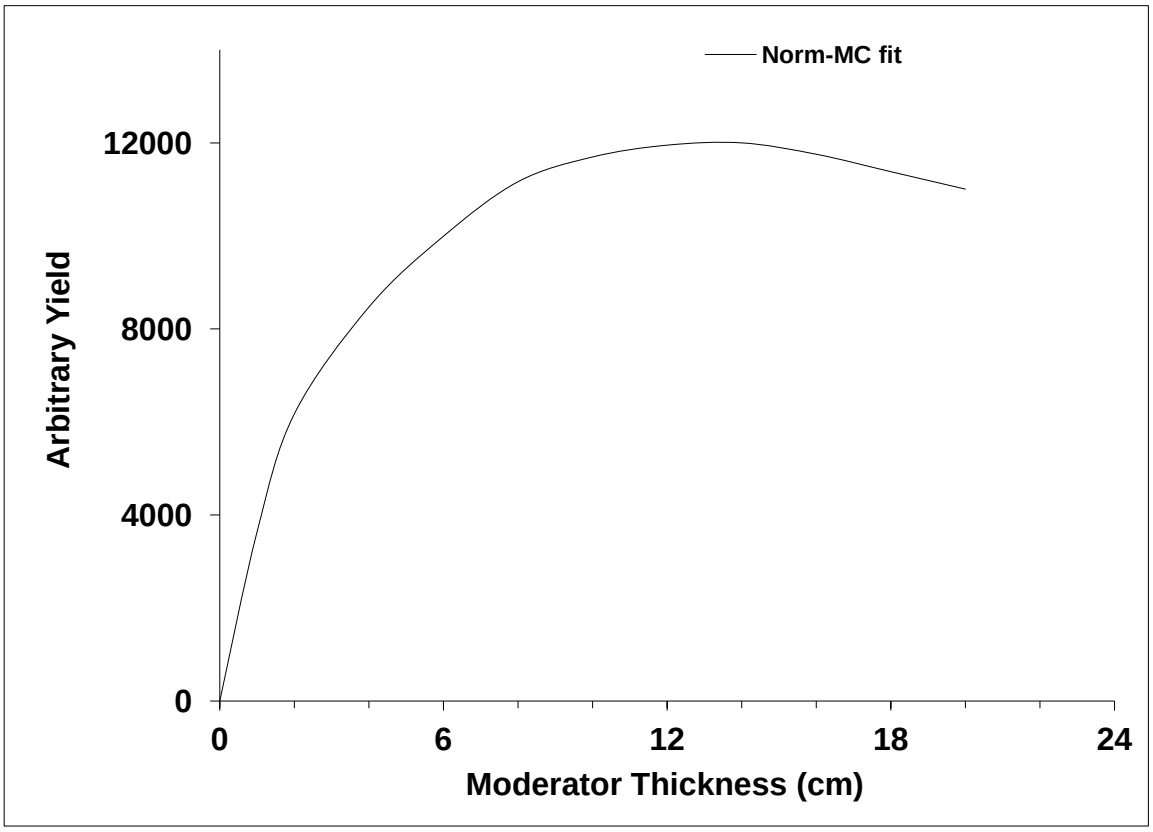

Figure 3.4: Calculated yield of prompt gamma rays from concrete specimen plotted as a function of moderator thickness.

3.3 Chlorine Gamma-Ray Calculations from Blended Cement Concrete Specimens

Monte Carlo simulations for 1.96, 2.86, 4.98, 5.72 and 6.11 MeV gamma-rays from BFS cement concrete specimens containing 0.5-4.0 wt.% chloride by weight of the cementitious material were carried out. The Monte Carlo yield obtained from the simulations are shown in Figures 3.5 and 3.6.

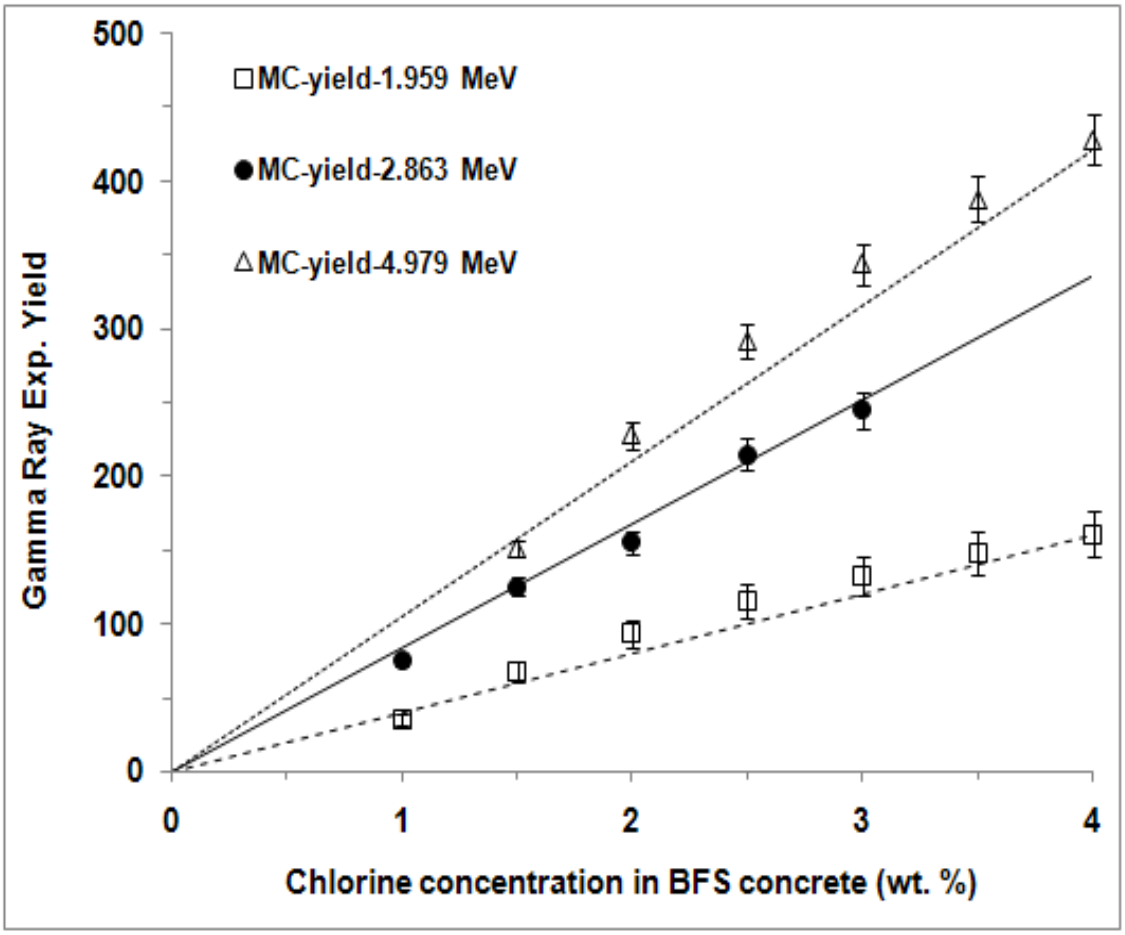

Figure 3.5: Monte Carlo yield for 1.96, 2.86 and 4.98 MeV gamma-rays from BFS concrete specimens containing 0.5-4.0 wt % chloride by weight of cementitious material.

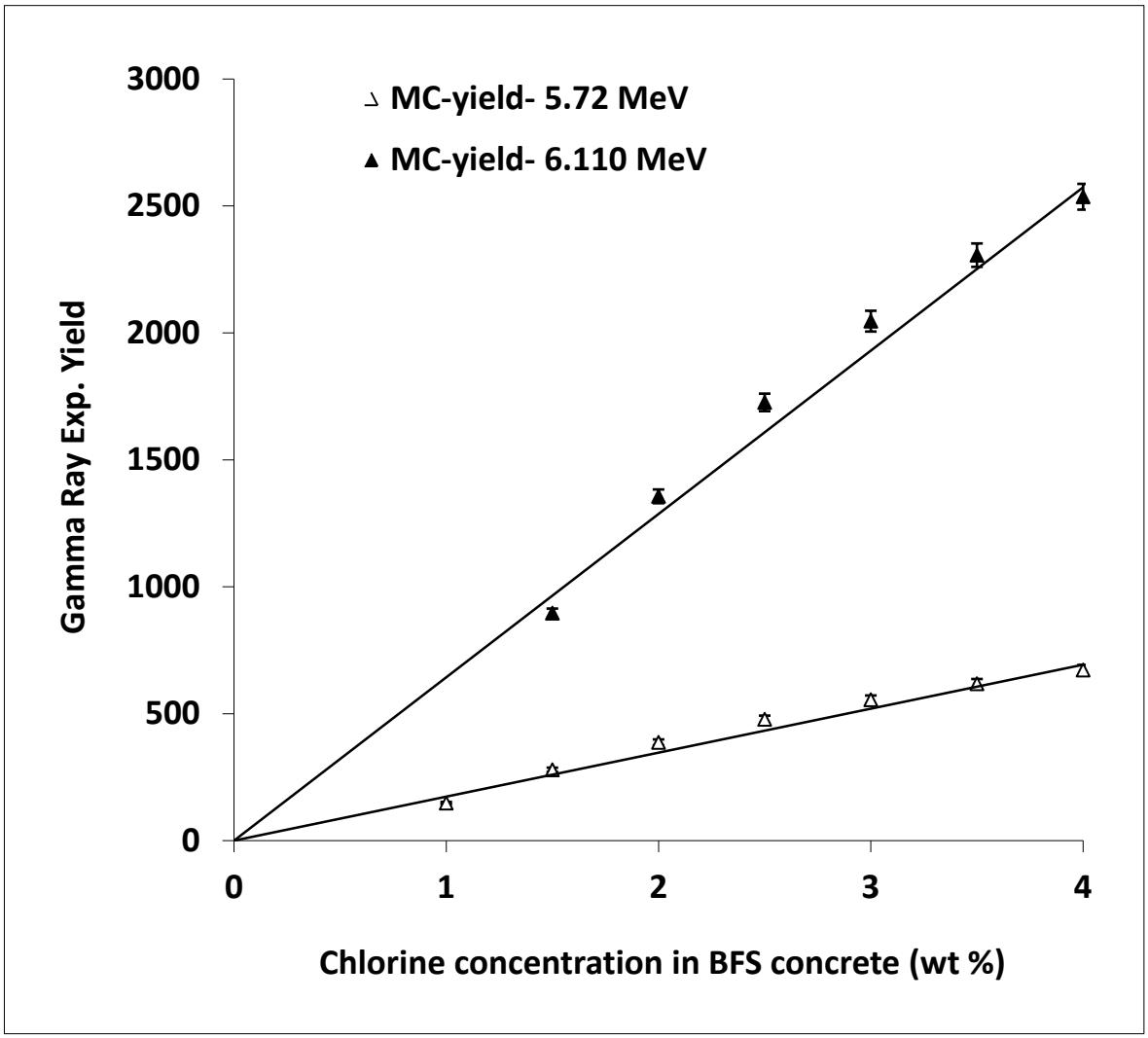

Figure 3.6: Monte carlo yield for 5.72 and 6.11 MeV gamma ray from BFS concrete specimens containing 0.5-4.0 wt % chloride by weight of cementitious material.

3.4 Thermal Neutron Flux Measurements from the PGNAA Setup

Monte Carlo simulations were experimentally validated by Lithium glass thermal neutron detector. The Li-glass was placed at right angle to the neutron generator axis at a distance of 120 cm from the target plane location. The thermal neutron yield was measured for fixed time for 1-14 cm thick moderators. A pulsed beam of 2.5 MeV neutrons was produced via D(d,n) reaction using MP320 portable neutron generator. The neutron generator was operated with 70 keV deuteron beam with a pulse width of 5 milli-seconds and a frequency of 250 Hz. The pulsed neutron beam improves the signal to background ratio in the PGNAA studies. The typical beam current of the generator was 70 μA. The thermal neutron spectra were acquired in PC-based data acquisition system utilizing multi-channel buffer modules.

Figure 3.7 shows the thermal neutron spectra of Lithium glass detector for 1 cm to 14 cm thick moderators. Data for each moderator thickness was acquired for 1,800 seconds. Due to overlapping of thermal neutron pulse height spectra of moderators with thickness in excess of 8 cm, only few representative pulse height spectra are shown in the Figure 3.7 over this thickness range. The thermal neutron peaks in the spectra were integrated and normalized to the same counting time, in case if they were different. Figure 3.8 shows integrated yield of thermal neutrons as a function of moderator thickness. The yield of thermal trend of neutrons as a function of moderator follows the same trend as the normalized calculated yield shown by solid line.

There is an excellent agreement between the experimental yield and the calculated yield shown as solid line in Figure 3.8. Further, the results show an optimum thickness of the moderator to be 9 to 10 cm. A moderator thickness of 9 cm was chosen as optimum thickness of the moderator.

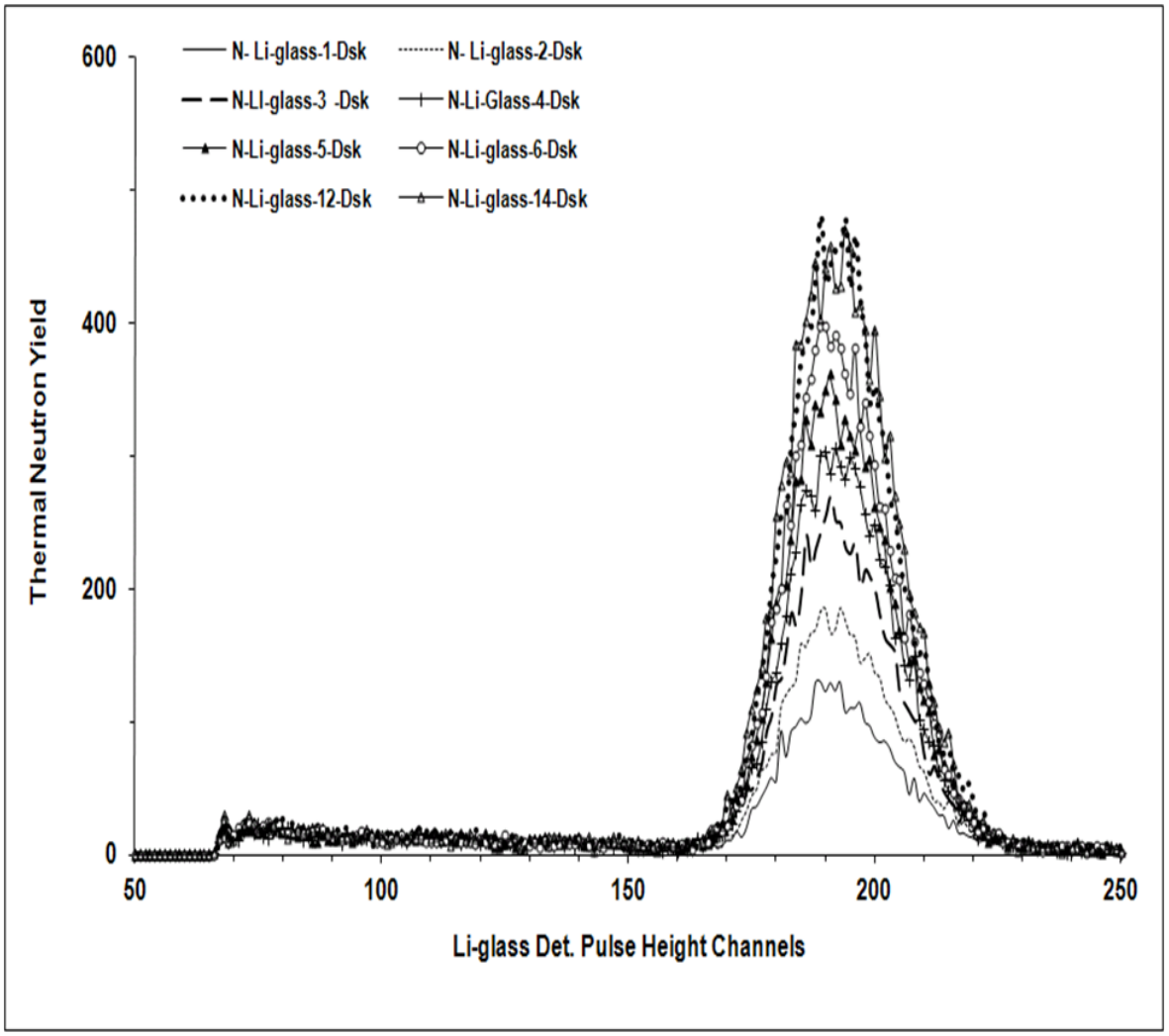

Figure 3.7: Pulse height spectrum of thermal neutrons recorded by an enriched Lithium glass scintillator for different moderator thicknesses.

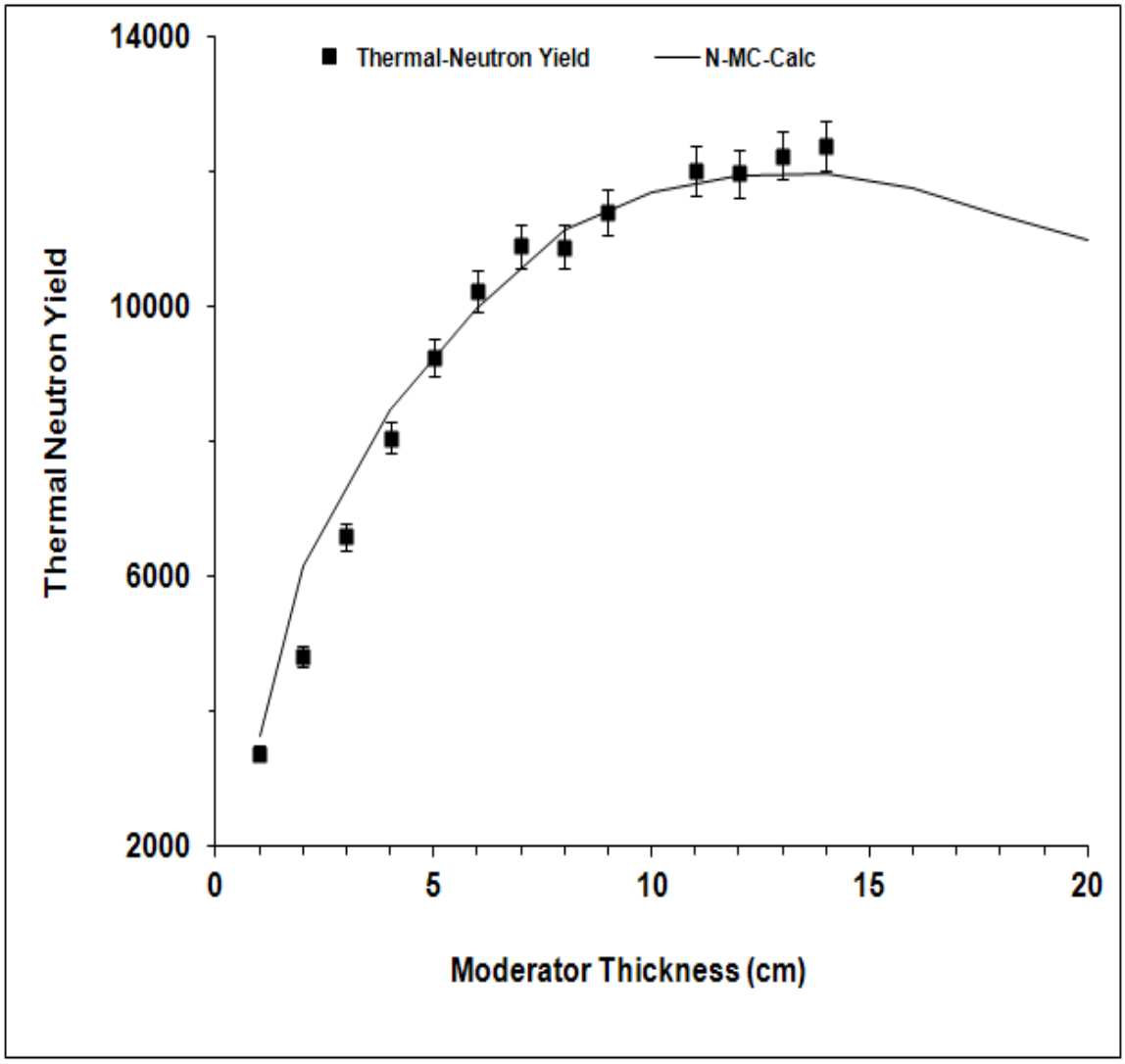

Figure 3.8: Integrated thermal neutron yield plotted as a function of 2-14 cm thick HDPE moderator. Also plotted is normalized calculated thermal neutron yield obtained by Monte Carlo simulations.

3.5 Performance Test of Gamma-Ray Detectors

The performance of the gamma-ray detector was evaluated by performing analysis of water sample with BGO, $LaBr_3$:Ce and $LaCl_3$:Ce detectors. This was done to select the optimum detector for the concrete testing. The experimental set-up and the sample preparation are common in all detector tests, as addressed below.

3.5.1 Experimental Set-up

The experimental set-up consisted of a cylindrical specimen placed inside a cylindrical moderator made of high density polyethylene, as shown in Figure 3.9. The moderator had a cylindrical cavity that can accommodate a specimen with a maximum diameter equal to the external diameter of the moderator. A gamma-ray detector was placed with its longitudinal axis aligned along the major axis of the moderator. The Longitudinal axis of the specimen was at right angle to the neutron beam axis. Lead shielding of 3 mm and a 50 mm paraffin shielding were provided at the detector in order to ward off unwanted gamma-rays and neutrons from reaching the detector. Neutron shielding was made up of a mixture of paraffin and lithium carbonate mixed in equal weight proportions. The results of the Monte Carlo simulations showed that the optimum dimensions for radius and length are 9.00 and 14.0 cm, respectively, for a moderator of 25 cm outer diameter.

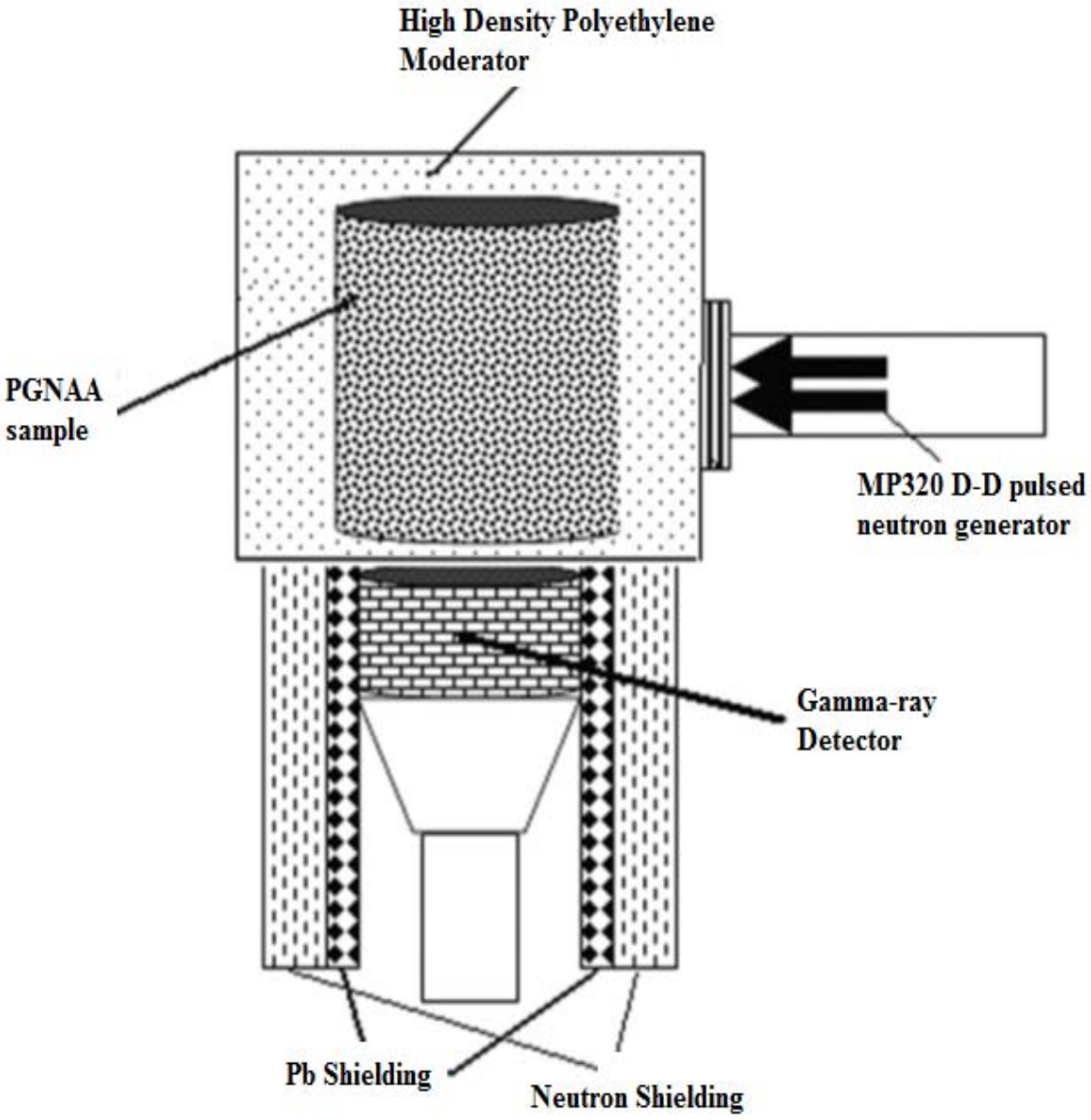

Figure 3.9: Schematic representation of the MP320 portable neutron generator used to measure the prompt gamma-ray yield.

3.5.2 Sample Preparation

Cd contaminated water samples were prepared by mixing Cd compounds with water. The sample was poured in cylindrical plastic bottles of 145 mm length and 90 mm internal diameter. They were then irradiated in the MP320 generator-based PGNAA setup. A pulsed beam of 2.5 MeV neutrons was produced with 70 keV voltage and a current of 70 μA through D (d,n) reaction using the portable neutron generator. The prompt gamma-ray data from Cd contaminated water samples was acquired for 25 min.

3.6 Cd Concentration Measurement in Water Samples Using BGO Detector

The Cd concentration was measured using the KFUPM BGO detector. It has an energy resolution of 11% for 662 keV gamma-rays from ^{137}Cs source. This BGO detector was chosen to detect prompt gamma-rays because of its higher resistance to neutron radiation damage [84]. The performance of the BGO detector was tested for low energy prompt gamma-rays from Cd contaminated water samples using the KFUPM neutron generator model MP320 PGNAA set-up [48].

3.6.1 Activation Spectrum of BGO Detector

During the irradiation of the samples, the BGO detector, although well shielded, was also exposed to thermal neutrons and it registered the prompt gamma-rays due to the capture of thermal neutrons in Bi and Ge element present in the BGO detector, as shown in Figure 3.10. The energies and intensities of prominent prompt gamma-rays due to capture of

thermal neutrons in the detector material and cadmium elements are listed in Table 3.1 [43].

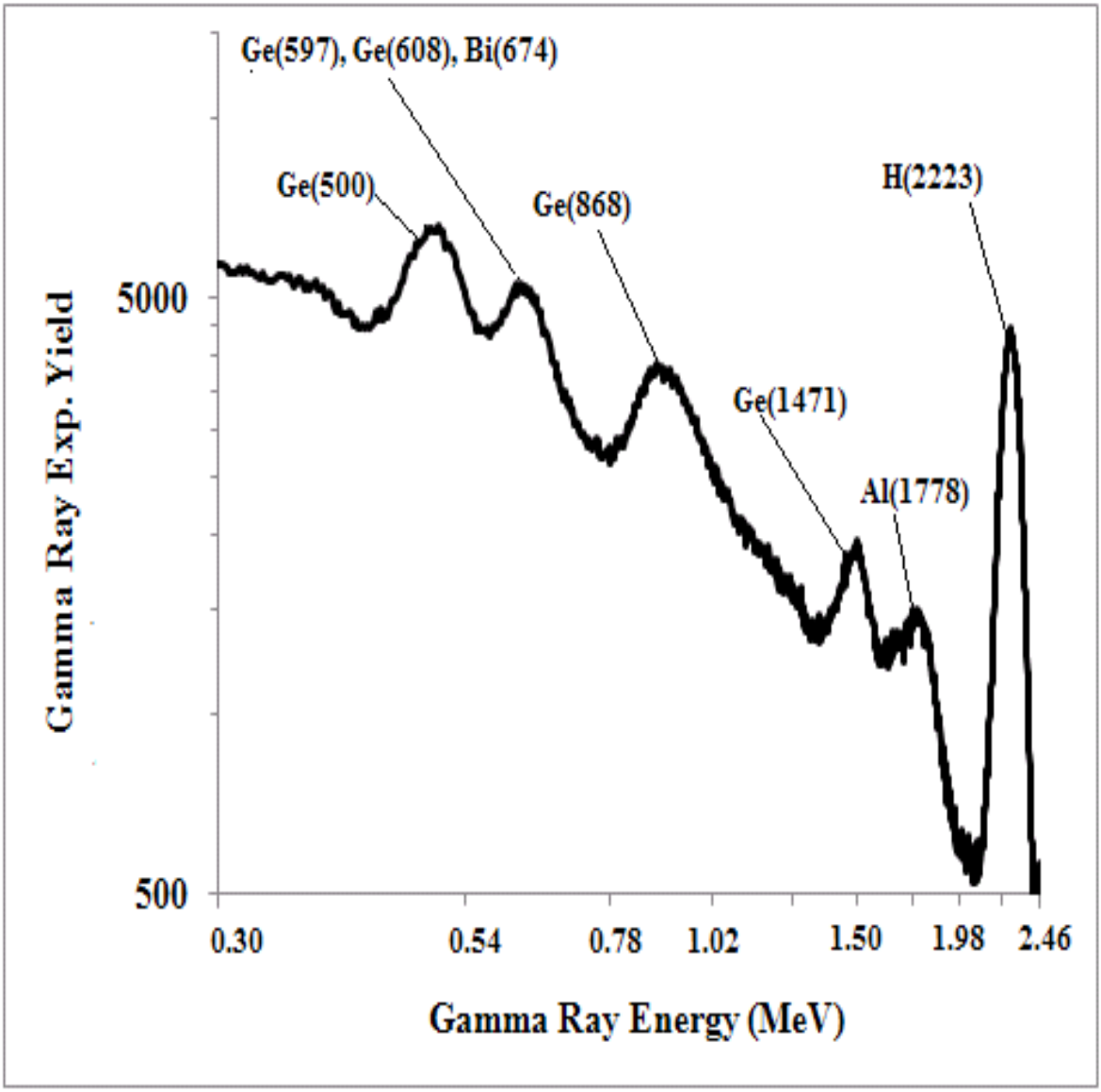

Figure 3.10: Prompt gamma-ray spectrum due to activation of the BGO detector caused by the capture of thermal neutrons in Bi and Ge elements present in the BGO detector.

Table 3.1: Energies and partial elemental cross section $\sigma_\gamma^z(E_\gamma)$-barns of prominent capture gamma-rays of Bismuth, cadmium and germanium [43].

Element	Gamma-ray energy (keV)	$\sigma_\gamma^z(E_\gamma)$-barns
Bi	162	0.008
Cd	320	0.0115
	674	0.0026
	2505	0.0021
	2828	0.00179
	4054	0.0137
	4171	0.0171
	245	274
Ge	558	1860
	651	359
	175	0.164
	493	0.133
	500	0.162
	596	1.100
	608	0.250
	868	0.553
	961	0.129
	1101	0.134
	1204	0.141
	1472	0.083

3.6.2 Prompt Gamma-Ray Analysis of Water Samples

Figures 3.11 through 3.13 show the pulse height spectra of a BGO detector from Cd contaminated water samples. Figure 3.11 shows the pulse height spectra of prompt gamma-rays of water samples containing 0.625, 1.250, 2.500 and 5.000 wt% Cd superimposed by the background spectrum taken without the sample. The interference of 558 keV prompt gamma-ray from cadmium peak with 500 keV peak of germanium in the BGO detector can be seen in Figure 3.11. As the cadmium peak included the contribution of germanium peaks, such as Ge(500), Ge(597), Ge(608) and bismuth peak Bi(674), the difference spectra of cadmium peaks for 0.625, 1.250, 2.500 and 5.000 wt% concentration are obtained by subtracting the background spectra from each of them. The difference spectra of cadmium peaks for 0.625, 1.250, 2.500 and 5.000 wt% cadmium concentration was shown in Figure 3.12. Lastly, the difference spectra peaks are integrated to obtain the integrated yield as a function of cadmium concentrations, as shown in Figure 3.13. There is an excellent agreement between the theoretical yield and the experimental yield of prompt gamma-ray from cadmium measured by BGO detector as a function of Cd concentration in the water samples. This indicates an exceptional performance of BGO detector in detecting low energy prompt gamma-rays.

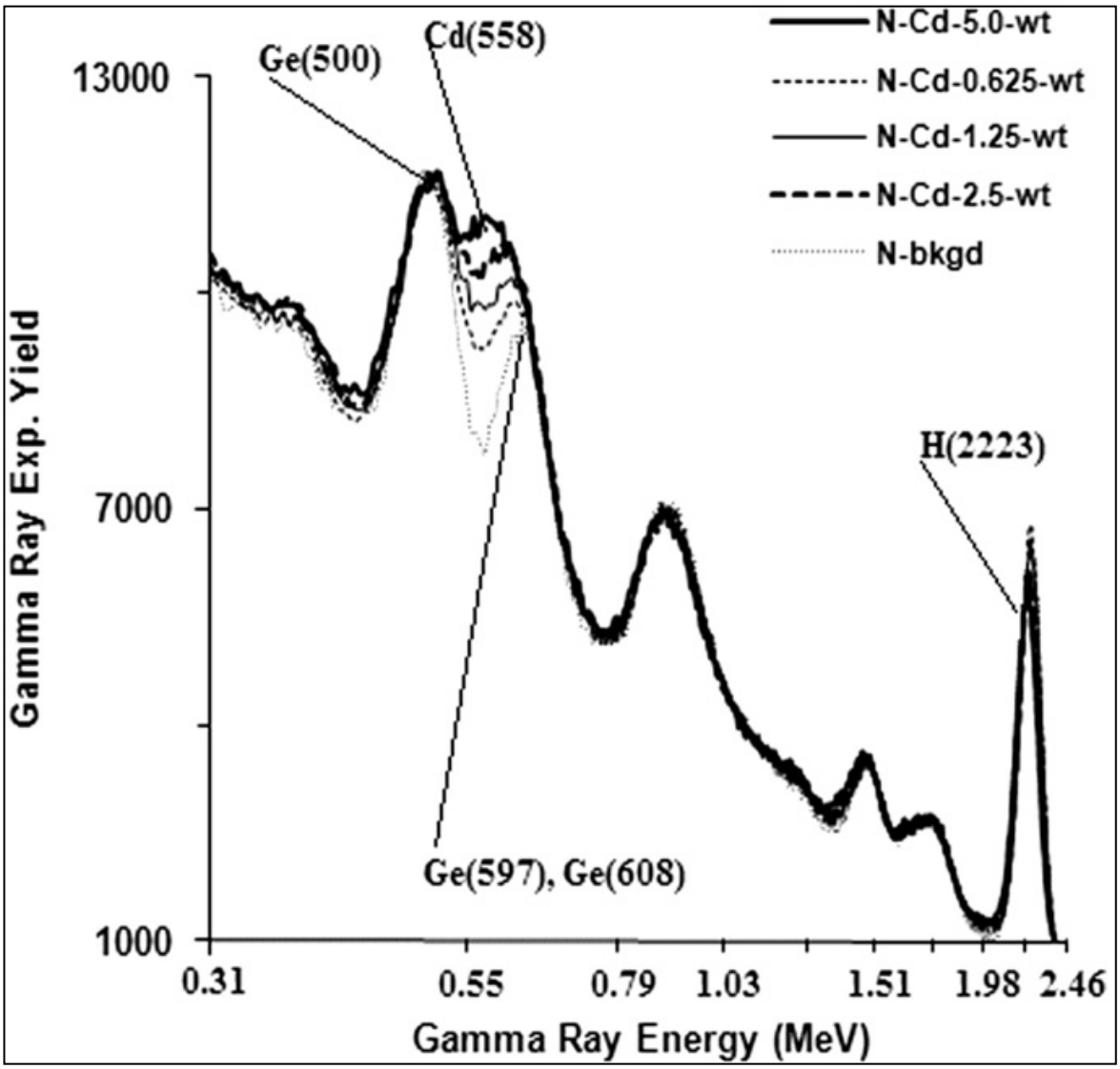

Figure 3.11: Experimental pulse height spectra of cadmium peak from water samples containing 0.625, 1.250, 2.500 and 5.000 wt% cadmium showing interference of 558 keV cadmium peak with 500 keV Ge peak. (The background spectrum taken with pure water sample is also superimposed for comparison).

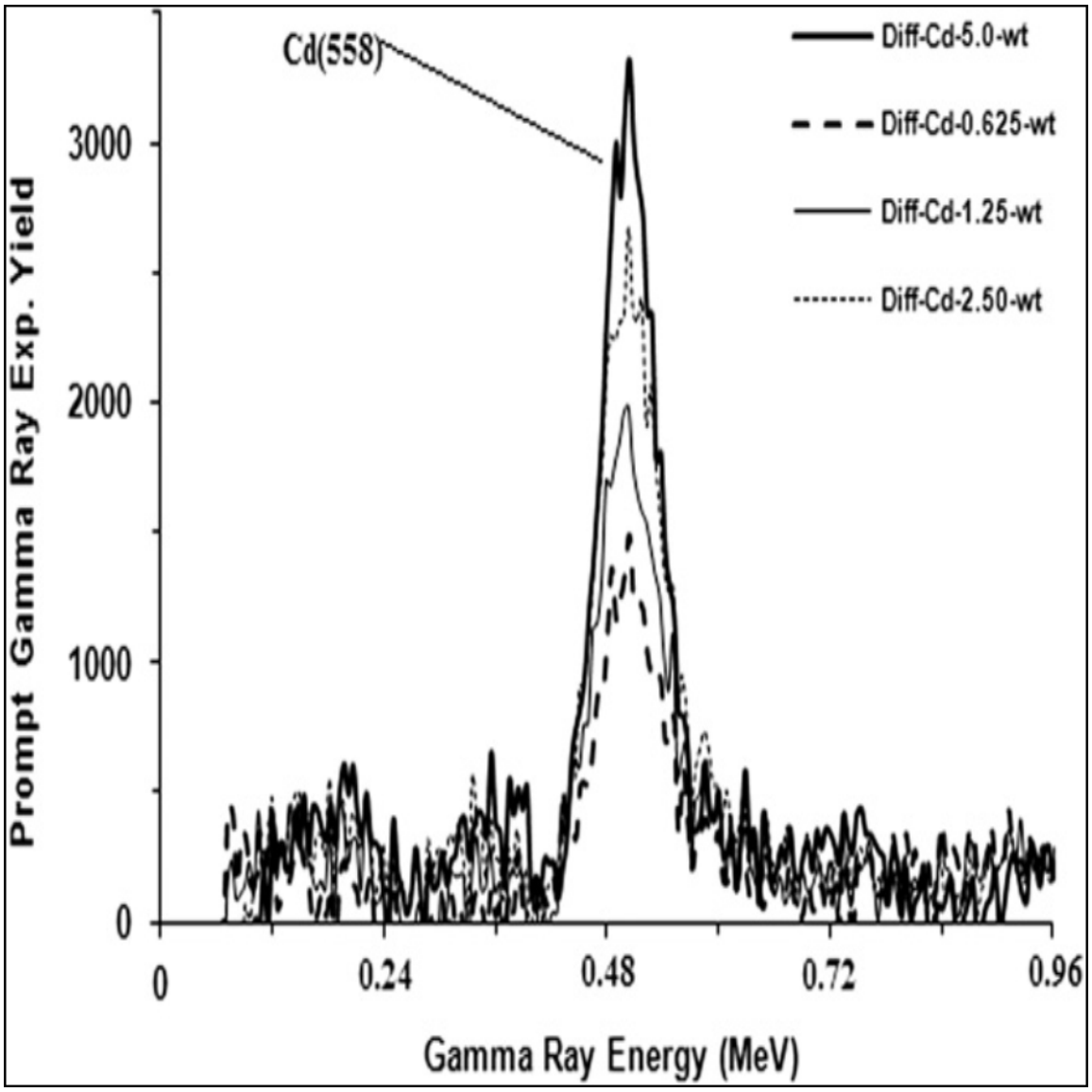

Figure 3.12: Enlarged prompt gamma-ray experimental pulse height spectra for the cadmium-contaminated water samples after background subtraction.

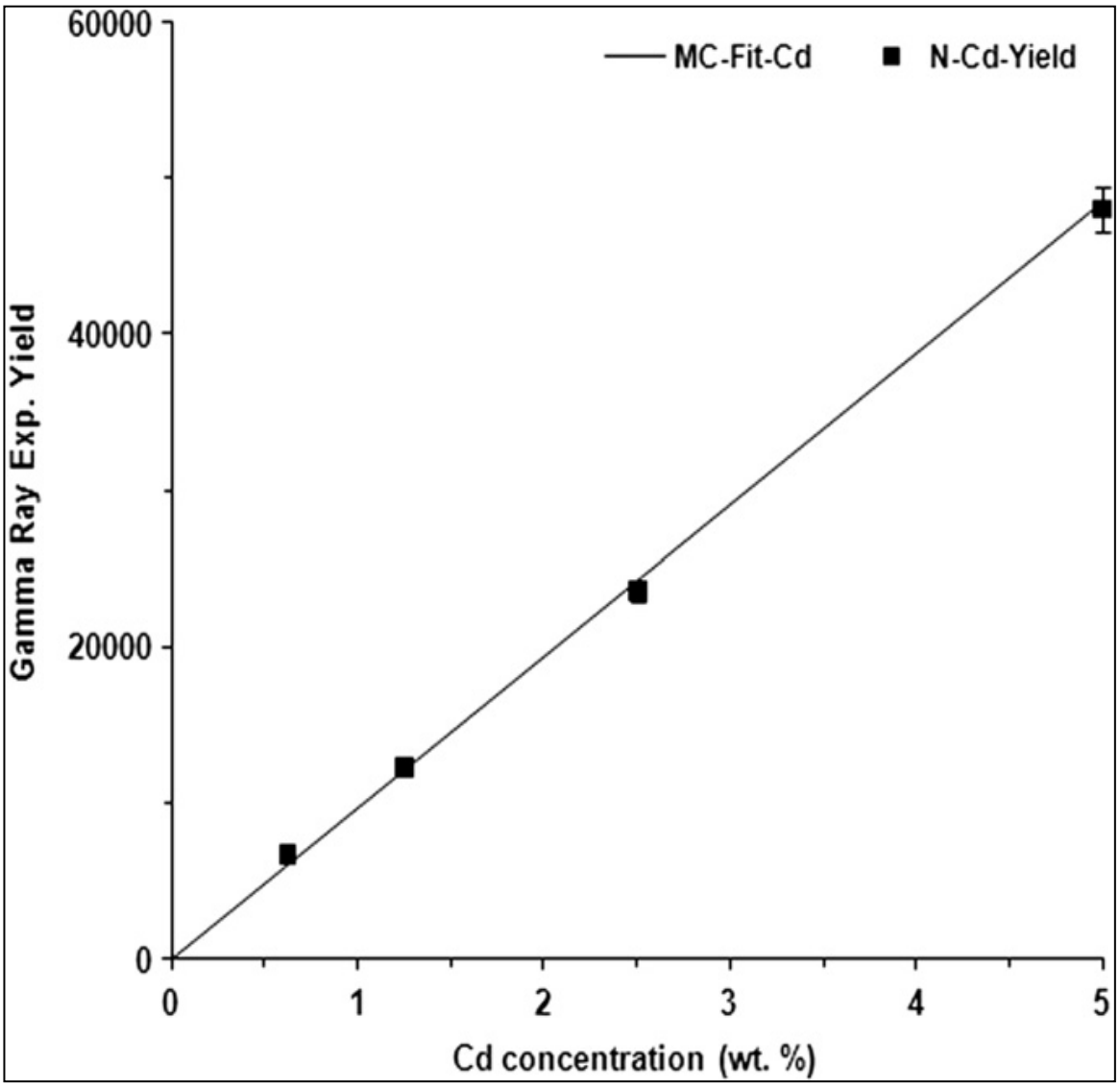

Figure 3.13: Integrated yield of 558keVpromptgamma-ray of cadmium from four water samples plotted as a function of cadmium concentration. The solid line shows normalized-calculated yield of the gamma-rays obtained through Monte Carlo calculations.

3.7 Cd Concentration Measurement in Water Samples Using $LaBr_3$:Ce Detector

Recently, lanthanide-halide $LaBr_3$:Ce and $LaCl_3$:Ce gamma-ray detectors are available in large crystal sizes and they exhibit improved energy resolution and faster light decay time compared to conventional NaI and BGO gamma-ray detectors [85-88]. The response of a cylindrical (76 x 76 mm) (length x diameter) $LaBr_3$:Ce detector was measured for low energy prompt gamma-rays from cadmium contaminated water samples using a newly designed portable neutron generator-based Prompt Gamma Neutron Activation Analysis (PGNAA) set-up. For the same volume, $LaBr_3$ has approximately a factor of two higher energy resolution (FWHM less than 3% at 662keV), and 30% higher detection efficiency compared to NaI(Tl) detectors [85]. $LaBr_3$ detector has faster decay time of 60 ns and can operate over wide dynamic ranges of count rate with little variation in the energy resolution [85, 86].

3.7.1 Intrinsic Activity and Dead Time Measurement of $LaBr_3$:CeDetector

In the present study, intrinsic activity and beam associated background spectra of $LaBr_3$:Ce detector were studied in detail. The detector signal was acquired using standard NIM electronics modules. The detector signal, which was routed through a pre-amplifier, was processed through a spectroscopy amplifier with shaping time of 1 μs. Logical gate signal was generated for each signal processed by the amplifier using single channel analyzer and gate and delay generators modules. For dead time correction, one of the

outputs of the gates and delay generator was used to gate Multi-channel Buffer, while another output was used to calculate dead time correction.

Dead time DTC was calculated at the end of each experimental run from the integrated count in the stored spectrum N_{tot} and total gate signals N_{gates}, counted independently through the following relation:

$$DTC = [(N_{gates} - N_{tot})/N_{gates}] \quad (3.1)$$

Then, the dead time corrected experimental yield of counts under a peak $Y_{DTC\text{-}Corr}$ was obtained from experimental counts under the peak Y_{exp} using the following relation:

$$Y_{DTC\text{-}Corr} = Y_{exp}[1+DTC] \quad (3.2)$$

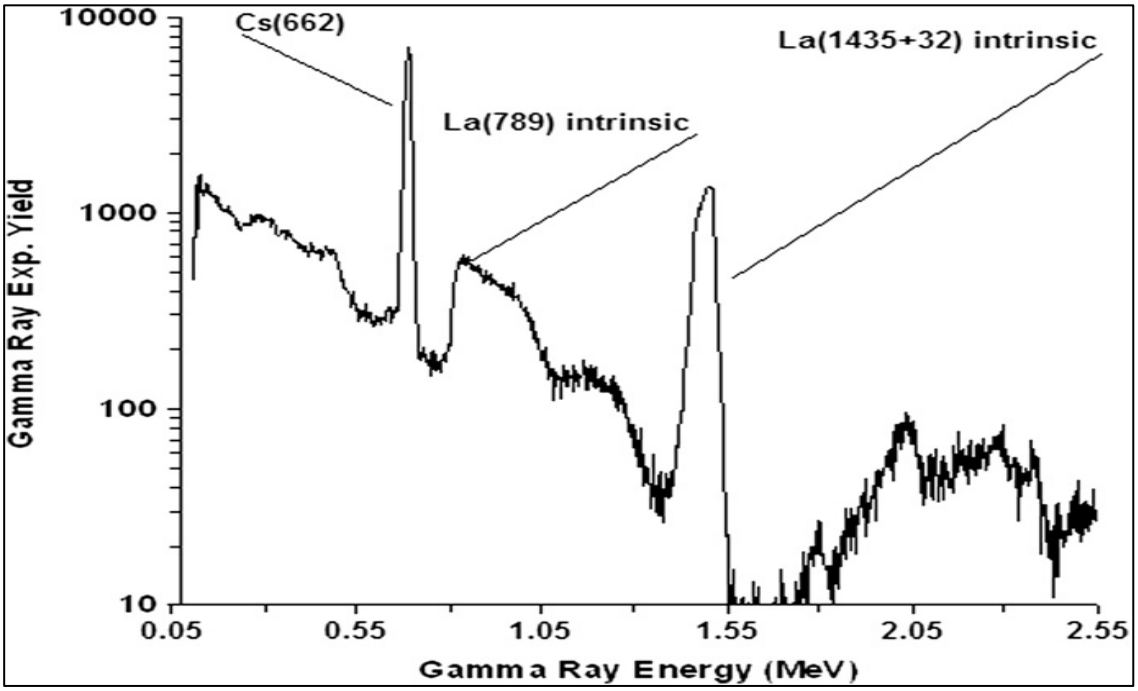

Figure 3.14: $LaBr_3$:Ce pulse height spectrum taken with ^{137}Cs source exhibiting ^{137}Cs peak along with detector intrinsic activity peaks due to La.

3.7.2 Activation Spectrum of $LaBr_3$:Ce Detector

During the irradiation of the samples, the $LaBr_3$:Ce detector, although shielded, is also exposed to thermal neutrons and it registered the prompt gamma-rays due to capture of thermal neutrons in La, Br, and Ce elements present in $LaBr_3$:Ce detector. This activation spectrum of the detector also contains additional peaks due to the intrinsic activity of the detector, as shown in Figure 3.15. Energies and intensities of the prominent prompt gamma-rays due to capture of thermal neutrons in lanthanum, cerium and barium are listed in Table 3.2 [87]. Also included are energies of gamma-rays due to intrinsic activity of the detector. All these peaks are present in the sample spectra taken with the detector and needed to be subtracted as the beam associated background.

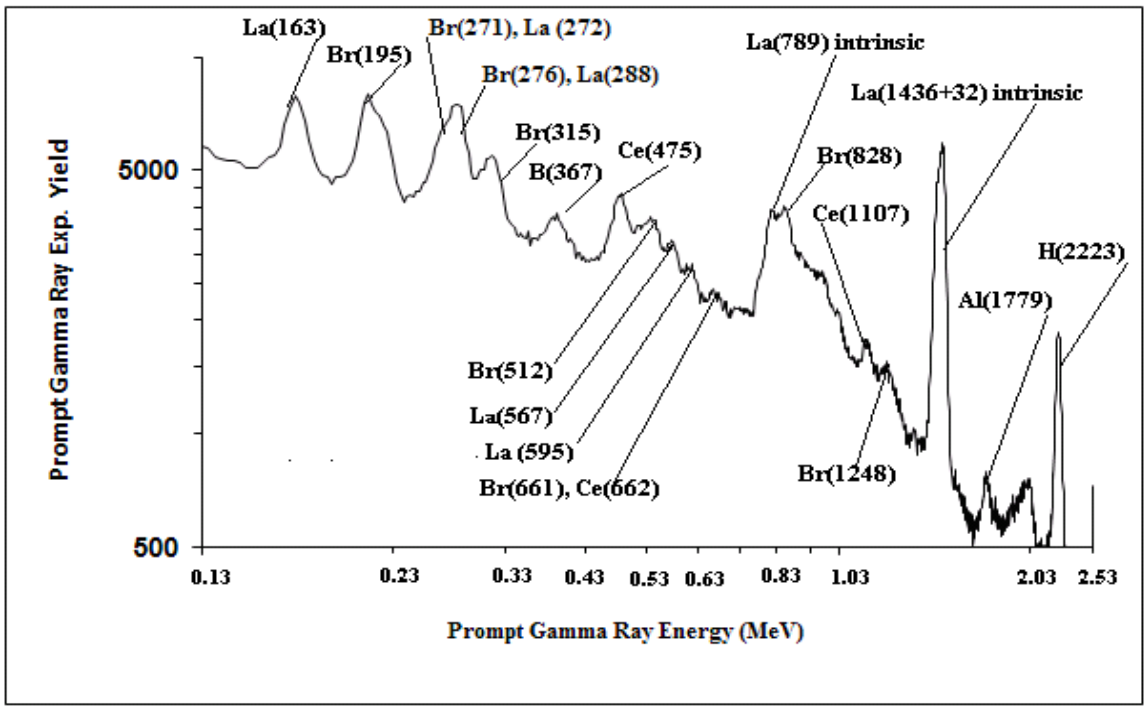

Figure 3.15: Prompt gamma-ray spectrum due to activation of the $LaBr_3$:Ce detector caused by capture of thermal neutrons in La, Br and Ce elements present in $LaBr_3$:Ce detector.

Table 3.2: Energies and partial elemental cross section $\sigma_\gamma^z(E_\gamma)$-barns of prominent capture gamma-rays of boron and cadmium [87].

Element	Gamma-ray energy(keV)	$\sigma_\gamma^z(E_\gamma)$-barns
Br	196	0.434
	271	0.462
	275	0.158
	315	0.460
	367	0.233
	513	0.21
	661	0.082
	828	0.285
	1248	0.0527
Cd	245	274
	558	1860
	651	359
Ce	475	0.082
	662	0.241
	1107	0.040
La	163	0.489
	272	0.502
	288	0.73
	567	0.335
	595	0.103
	789	intrinsic
	1436	intrinsic

3.7.3 Prompt Gamma-Ray Analysis of Water Samples

Figures 3.16 through 3.18 show the pulse height spectra of LaBr:Ce detector from cadmium contaminated water samples. Figure 3.16 shows the pulse height spectra of prompt gamma-rays from water samples containing 0.625, 1.250, 2.500 and 5.000 wt. % cadmium superimposed with background spectrum taken without sample. The 558 keV boron gamma-ray peak along with 1436 keV intrinsic activity peak and 2223 keV hydrogen capture peak from moderator is quite prominent. Figure 3.17 shows 558 keV cadmium peak on enlarged scale to show its interference with 567 keV peak from activation of lanthanum in LaBr:Ce detector. Since the cadmium peak contains the contribution of La(567) peak, the difference spectra of cadmium peaks for 0.625, 1.250, 2.500 and 5.000 wt.% concentrations were generated by subtracting the background spectrum from each of them. Figure 3.18 shows the difference spectra of cadmium peaks for 0.625, 1.250, 2.500 and 5.000 wt % cadmium concentrations. Finally, the peaks of the difference spectra were integrated to generate integrated yield as a function of cadmium concentration, as shown in Figure 3.19. There is an excellent agreement between the theoretical yield and the experimental yield of prompt gamma-ray from cadmium measured by $LaBr_3$:Ce detector as a function of the cadmium concentration in water samples.

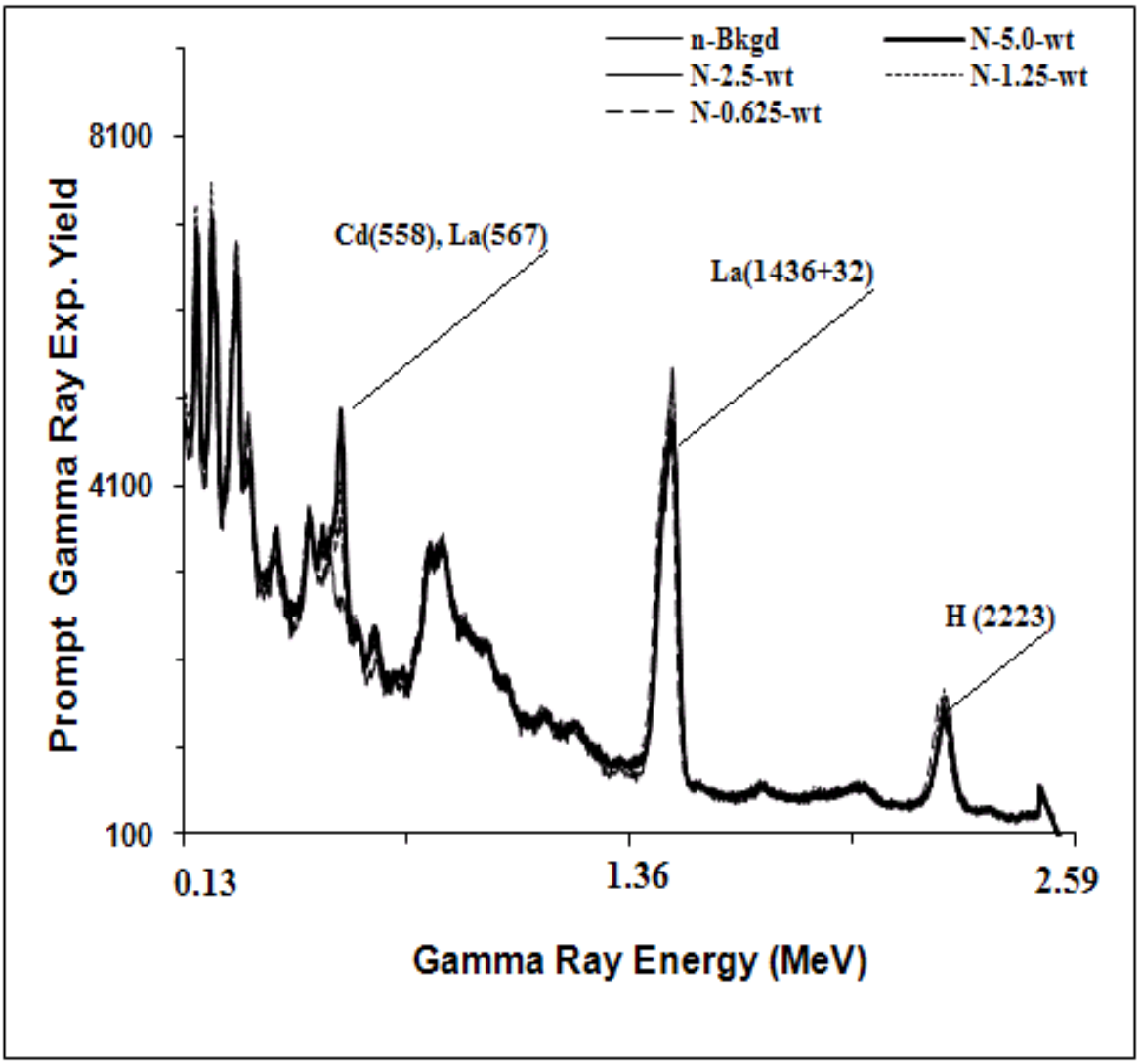

Figure 3.16: Prompt gamma-ray experimental pulse height spectrum from water samples containing0.625, 1.250, 2.500 and 5.000 wt % cadmium showing different peaks of prompt gamma-rays produced due to capture of thermal neutrons in the cadmium.

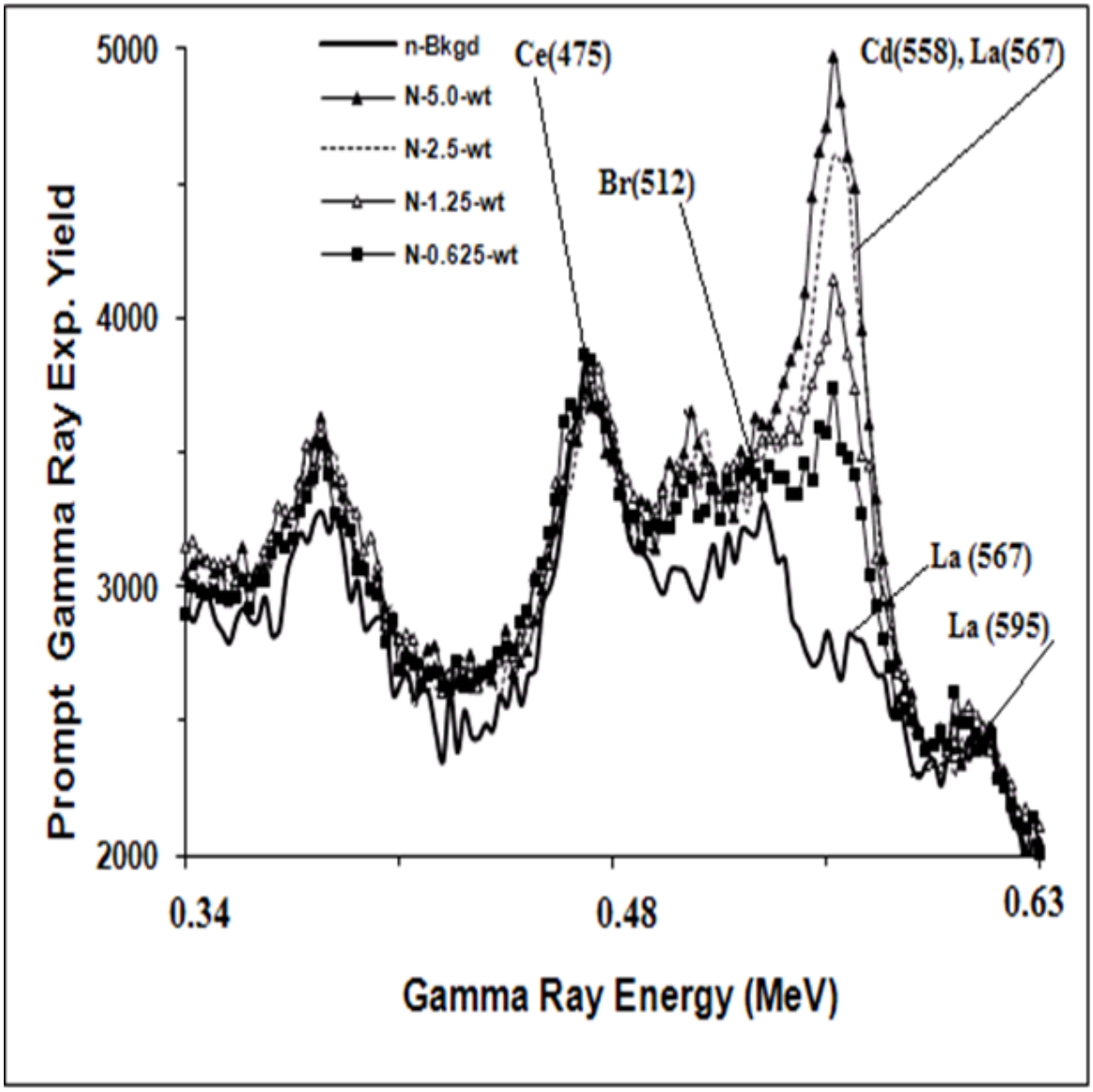

Figure 3.17: Enlarged prompt gamma-ray experimental pulse height spectra of cadmium peak from water samples containing 0.625, 1.250, 2.500 and 5.000 wt % cadmium showing interference of 558 keV cadmium peak with 567 keV La peak. (For comparison sake background spectrum taken with pure water sample is also superimposed)

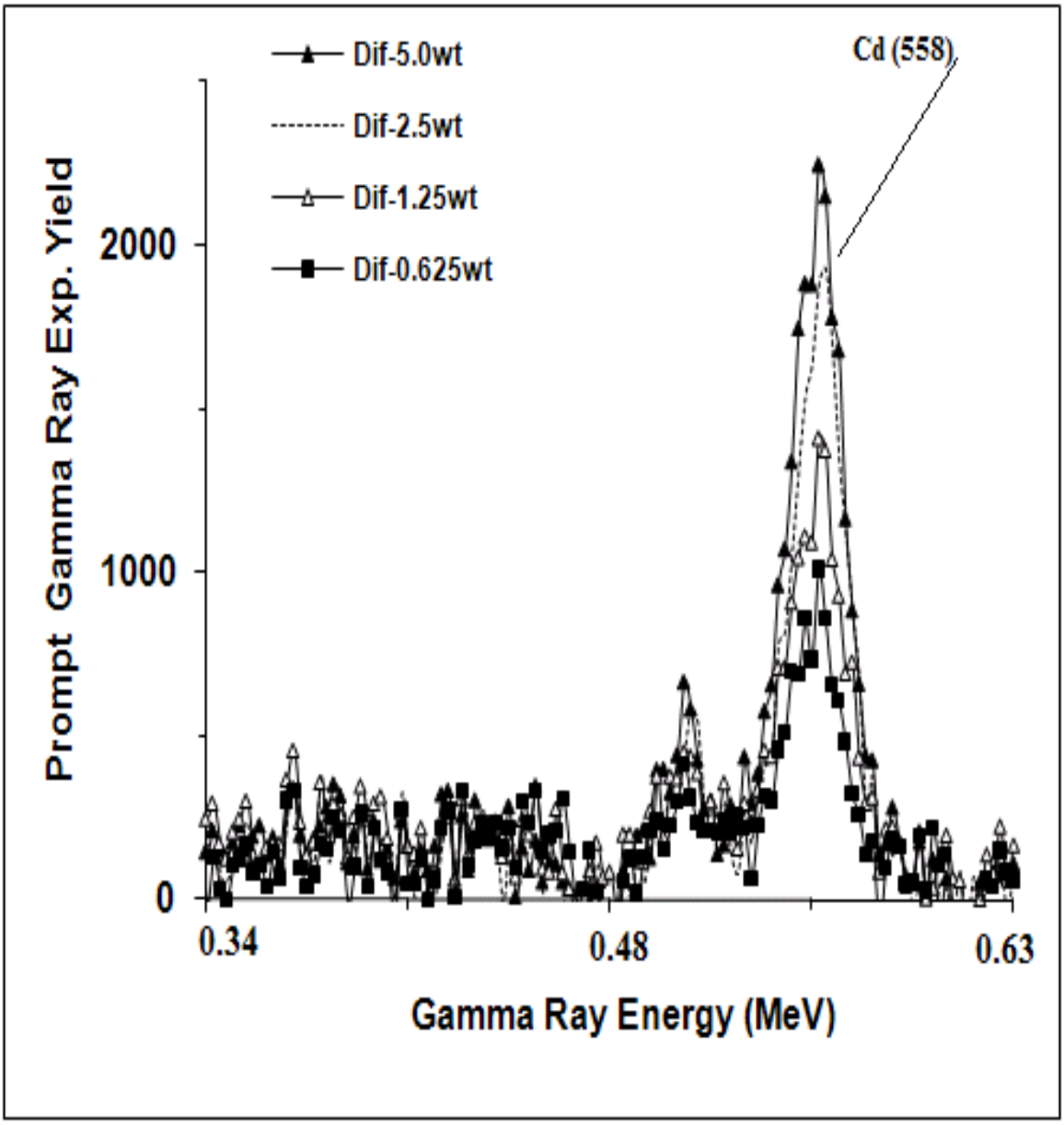

Figure 3.18: Enlarged prompt gamma-ray experimental pulse height spectra after background subtraction from the four cadmium-contaminated water samples.

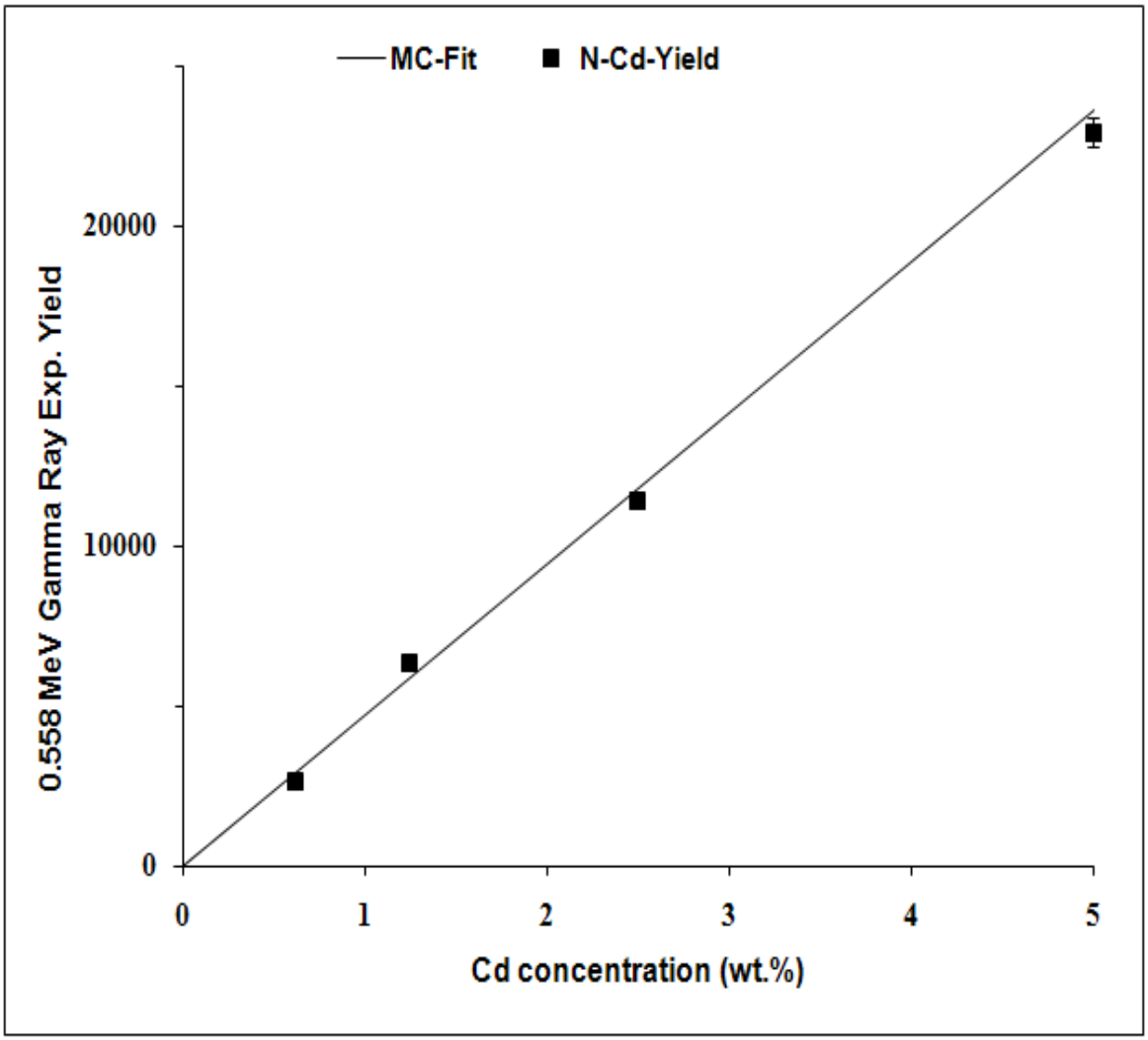

Figure 3.19: Integrated yield of 558 keV prompt gamma-ray of cadmium from four water samples plotted as a function of cadmium concentration. The solid line shows normalized-calculated yield of the gamma-rays obtained through Monte Carlo calculations.

3.8 Cd Concentration Measurement in Water Samples Using $LaCl_3$:Ce Detector

KFUPM has recently acquired a cylindrical (76 x 76 mm) (height x diameter) $LaCl_3$:Ce detector for prompt gamma-ray analysis of bulk samples. The $LaCl_3$:Ce gamma-ray detector model BrilLanCe 350 was acquired from Saint-Gobain Crystals, Europe. The performance of the $LaCl_3$:Ce detector was measured for low energy prompt gamma-rays from cadmium contaminated water samples using a newly-designed portable neutron generator-based Prompt Gamma Neutron Activation Analysis (PGNAA) set-up.

3.8.1 Activation Spectrum of $LaCl_3$:Ce Detector

In the PGNAA studies, gamma-ray detector was also irradiated with thermal and fast neutrons flux and detector register gamma-rays produced due to the interaction of neutrons with detector material. In the activation spectrum of the LaCl:Ce detector, it contains prompt gamma-rays due to capture of thermal neutrons in La, Cl, and Ce elements present in $LaCl_3$:Ce detector. It also contains additional peaks due to intrinsic activity of the detector, as shown in Figure 3.20. Energies and intensities of prominent prompt gamma-rays due to capture of thermal neutrons in lanthanum, cerium and chlorine are listed in Table 3.3 [43]. Also included are energies of gamma-rays due to intrinsic activity of the detector. All these peaks are present in the sample spectra taken with the detector and needed to be subtracted from the sample spectrum as the detector beam associated background.

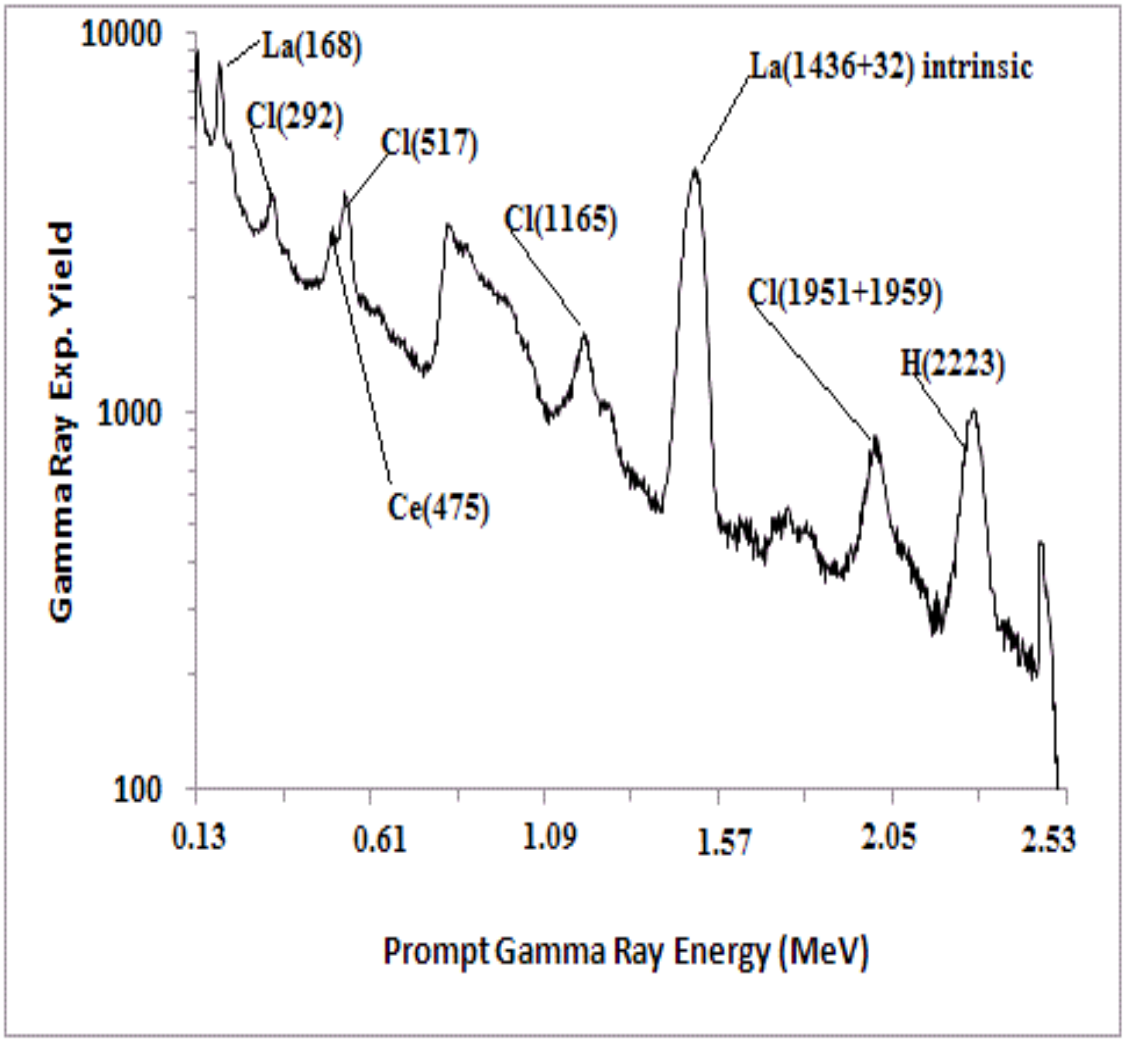

Figure 3.20: Prompt gamma-ray spectrum due to activation of the $LaCl_3$:Ce detector caused by capture of thermal neutrons in La, Cl and Ce elements present in $LaCl_3$:Ce detector.

Table 3.3: Energies and partial elemental cross section $\sigma_\gamma^z(E_\gamma)$-barns of prominent capture gamma rays of cadmium [43].

Element	Gamma-ray energy (keV)	$\sigma_\gamma^z(E_\gamma)$-barns
Cl*	517	7.58
	786	3.42
	788	5.42
	1164	8.90
	1601	1.21
	1951	6.33
	1959	4.10
	2863	1.82
	3061	1.13
Cd	245	274
	558	1860
	651	359
Ce	475	0.082
	662	0.241
	1107	0.040
La	163	0.489
	272	0.502
	288	0.73
	567	0.335
	595	0.103
	789	intrinsic
	1436	intrinsic

3.8.2 Prompt Gamma-Ray Analysis of Water Samples

Figure 3.21 shows the pulse height spectra of prompt gamma-rays from the water samples containing 0.0625, 0.125, 0.250 and 0.500 wt. % cadmium superimposed upon each other along with the background spectrum taken with pure water sample. Figure 3.22 shows 558 keV cadmium peak on enlarged scale to show its interference with 517 keV peak from activation of chlorine in $LaCl_3$:Ce detector. The cadmium peak is well resolved from the 517 keV chlorine peak. The difference spectra of cadmium peaks for 0.0625, 0.125, 0.250 and 0.500 wt % concentration were generated by subtracting the background spectrum from each of them. Figure 3.23 shows the difference spectra of cadmium peaks for 0.0625, 0.125, 0.250 and 0.500 wt % cadmium concentrations. Finally, the peaks of the difference cadmium spectra were integrated to generate integrated cadmium gamma-ray yield as a function of cadmium concentration.

3.8.3 Dead Time Correction

The integrated cadmium gamma ray yield data was corrected for dead time correction and neutron flux fluctuation using neutron monitor count for each cadmium concentration. The background of the difference spectra from the dead time corrected counts was subtracted from the corrected counts. Figure 3.24 shows dead time corrected and background subtracted counts of four cadmium samples as a function of cadmium concentration for cadmium contaminated water samples. The solid lines in Figure 3.24 represent the results of calculated yield of cadmium prompt gamma-ray obtained from Monte Carlo calculations. There is an excellent agreement between the theoretical yield

and the experimental yield of prompt gamma-ray from cadmium water samples measured as a function of cadmium concentration respectively as measured by $LaCl_3$:Ce detector.

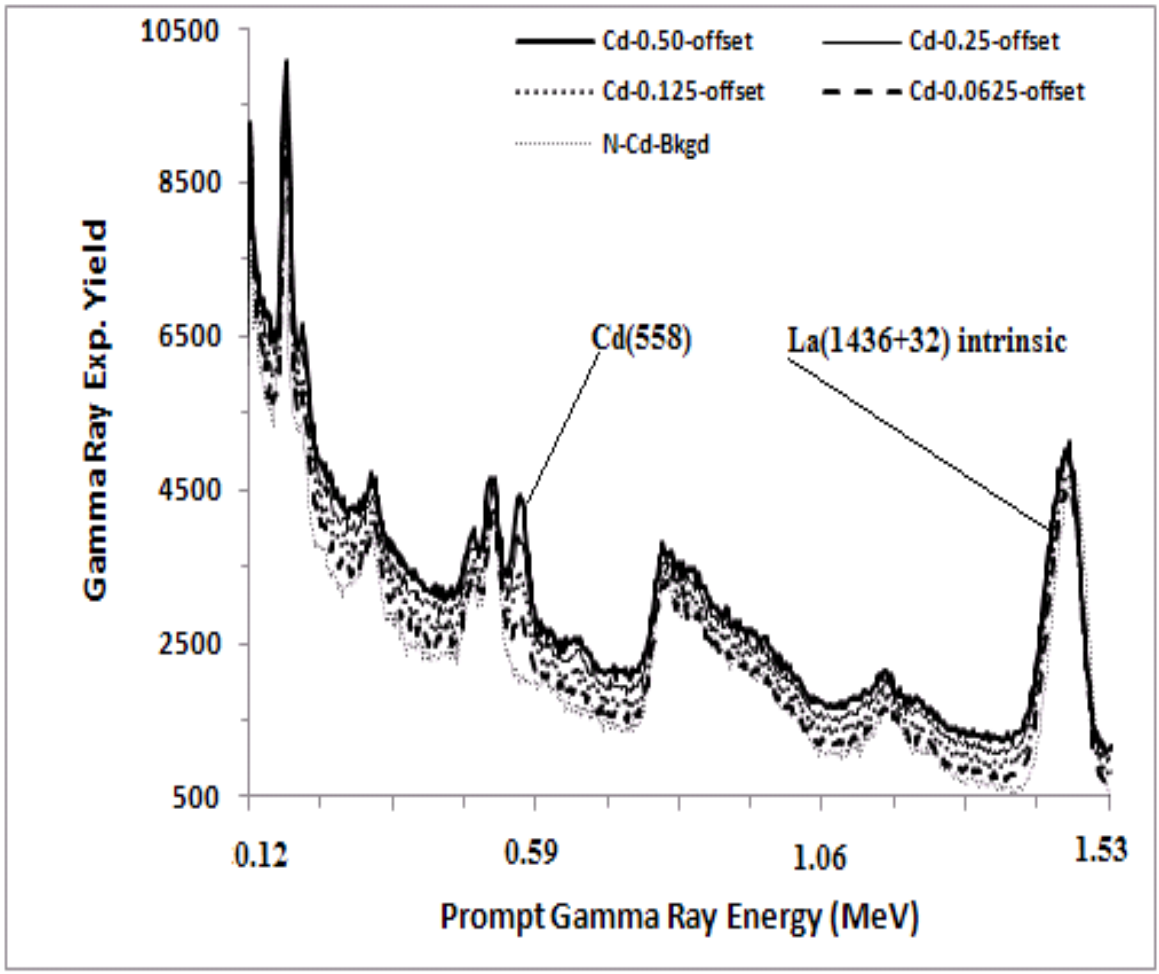

Figure 3.21: Prompt gamma-ray pulse height spectra of four cadmium contaminated water samples 0.0625, 0.125, 0.250 and 0.500 wt % cadmium, along with background spectrum taken with pure water sample, plotted with a constant vertical offset.

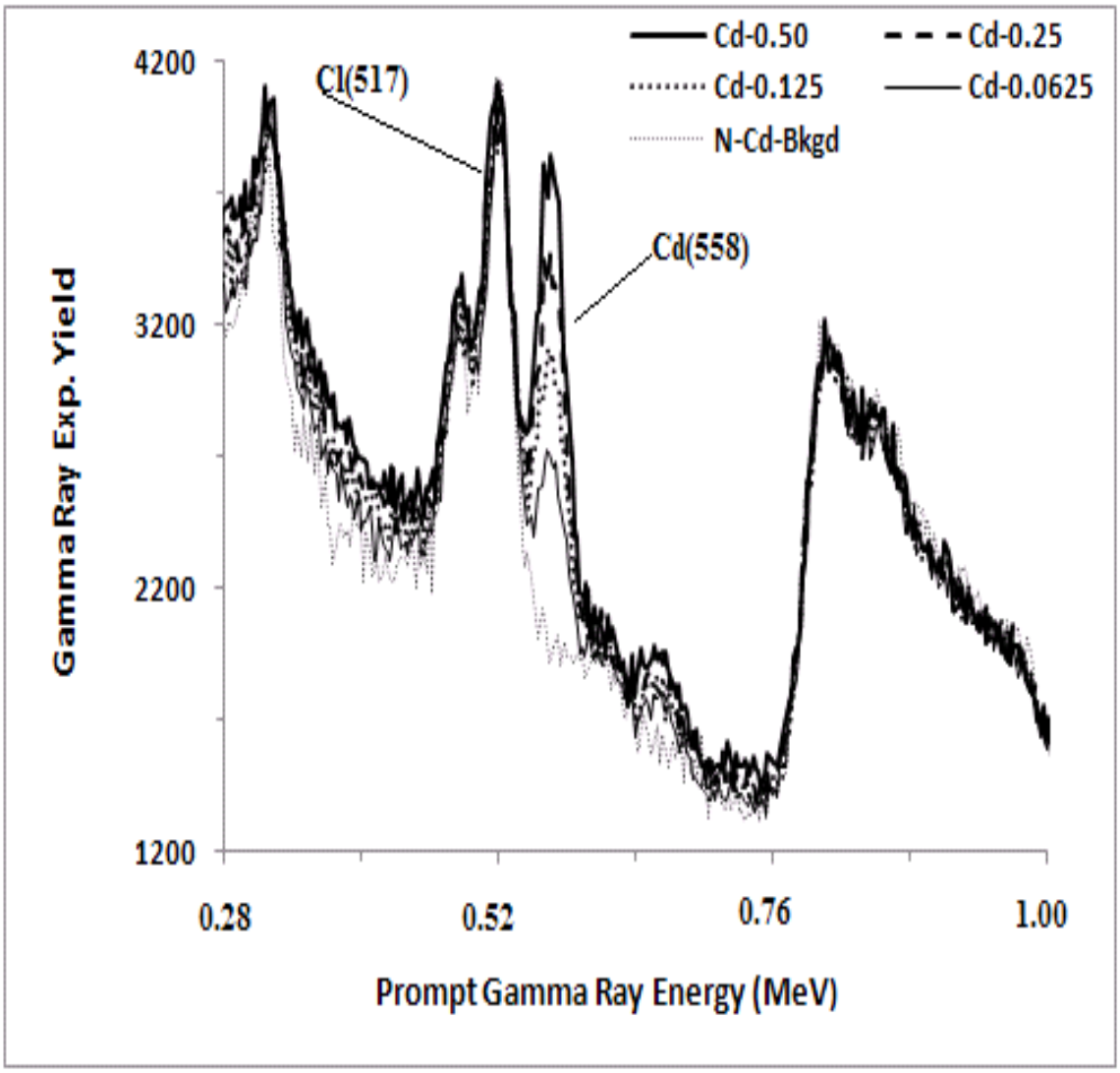

Figure 3.22:Enlarged prompt gamma-ray experimental pulse height spectra of water samples containing 0.0625, 0.125, 0.250 and 0.500 wt % cadmium, along with background pure water sample, showing interference of 558 keV cadmium peak with 567 keV La peak.

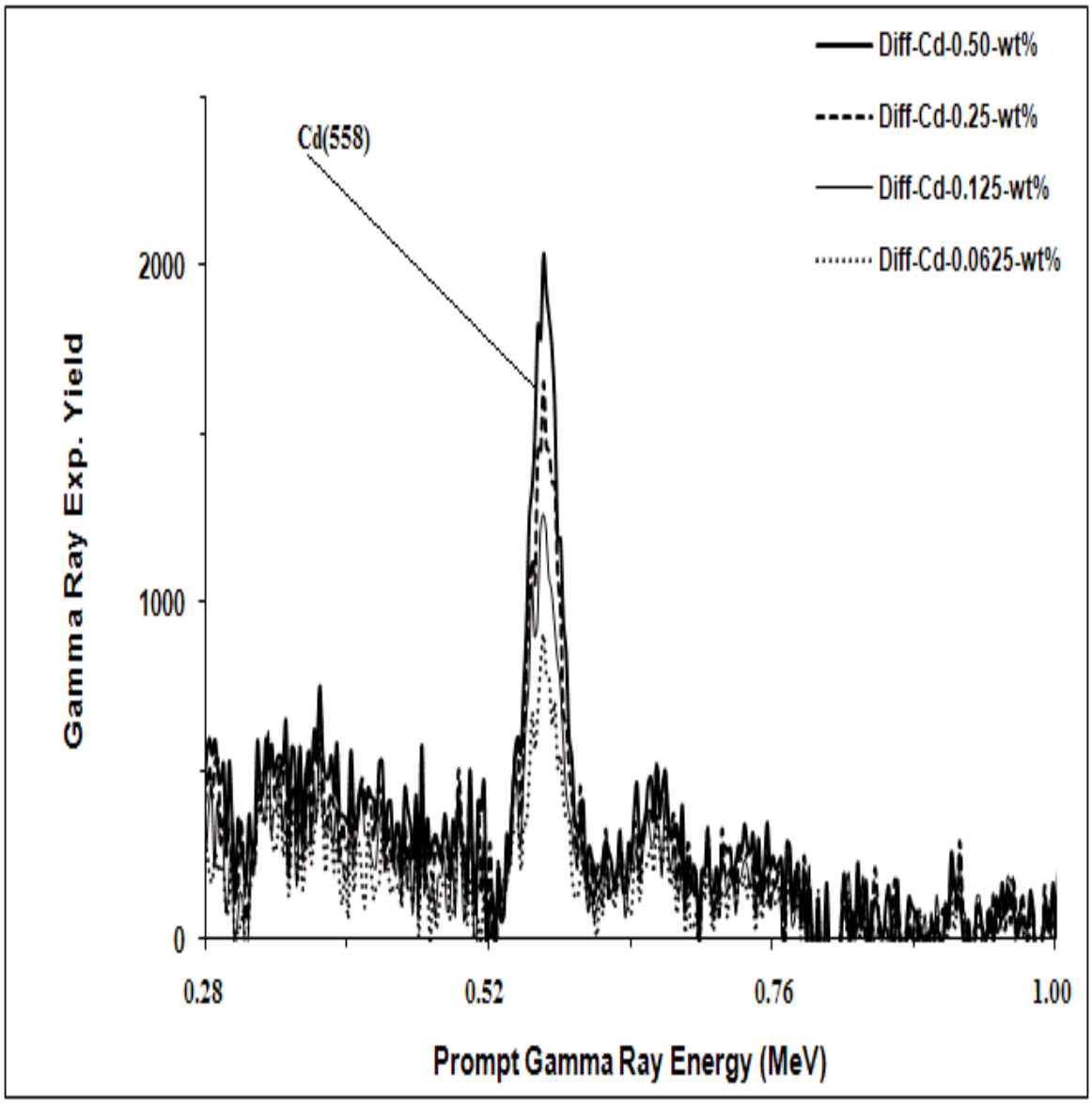

Figure 3.23: Enlarged prompt gamma-ray experimental pulse height spectra after background subtraction from the four cadmium-contaminated water samples.

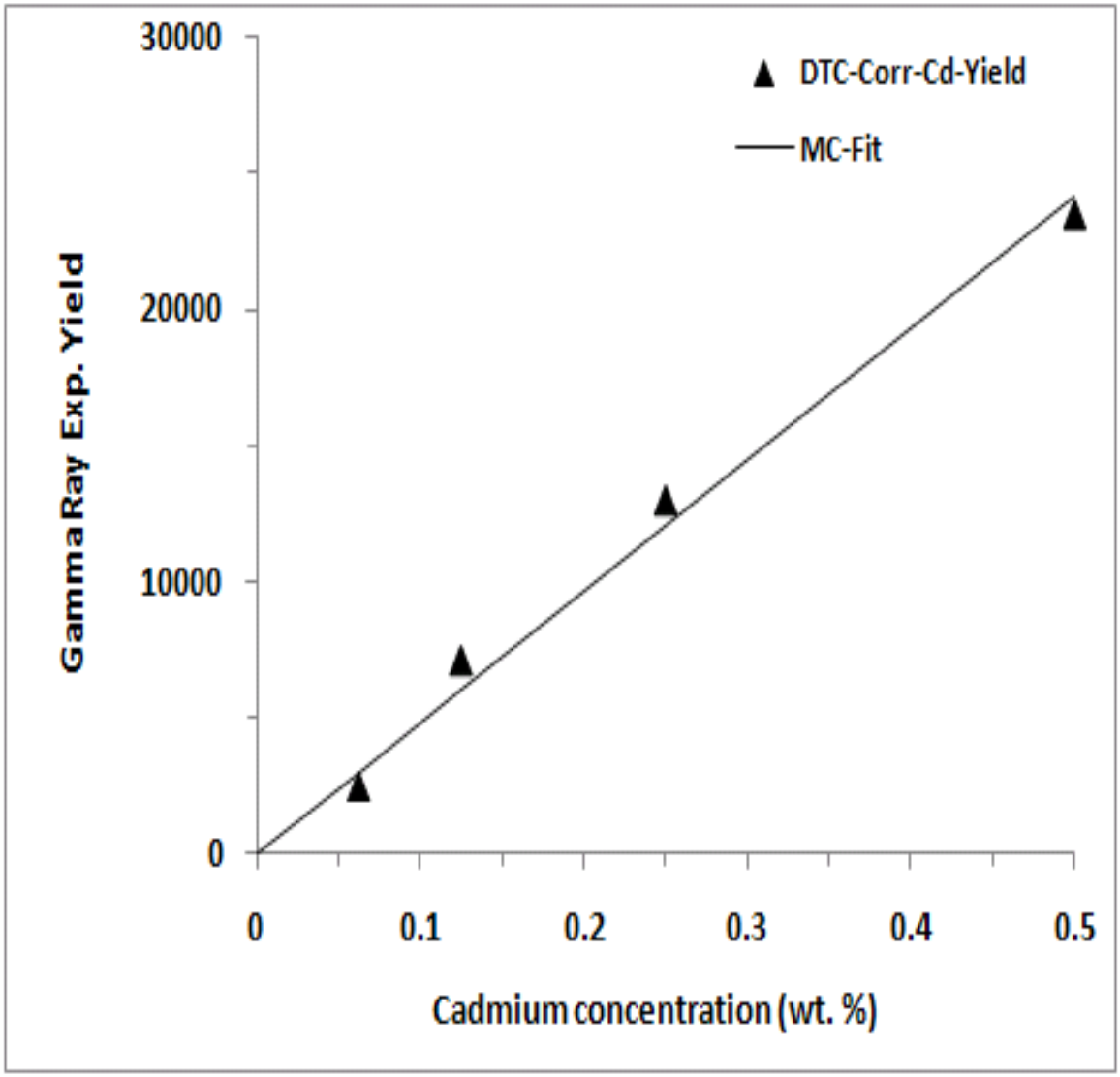

Figure 3.24: Dead time corrected integrated yield of 558 keV prompt gamma-ray of cadmium from four water samples plotted as a function of cadmium concentration. The solid line shows normalized-calculated yield of the gamma-rays obtained through Monte Carlo calculations.

3.9 Selection of Detector for Concrete Analysis

The results of the study show the excellent performance of the BGO, $LaBr_3$:Ce and $LaCl_3$:Ce detectors in detecting the low energy prompt gamma-rays. Lanthanum halide detectors ($LaBr_3$:Ce and $LaCl_3$:Ce) have good energy resolution of 2.9 - 4% for 662 keV gamma-rays from ^{137}Cs source, but are expensive and are not available in large crystal sizes [86]. BGO despite having poor energy resolution of 11% for 662 keV gamma-rays from ^{137}Cs source is preferred for neutron activation analysis of concrete due to its higher radiation hardness and large photo-peak efficiency [48]. So BGO detector was chosen to perform prompt gamma neutron activation analysis of concrete specimens.

CHAPTER 4

RESULTS AND DISCUSSION

4.1 Prompt Gamm-Ray Analysis of Blended Cement Concrete Specimens

Prompt gamma neutron activation analysis (PGNAA) of Fly ash, blast furnace slag and super pozz concrete specimens was performed to determine the chloride concentration. The chlorine concentration was measured in FA, BFS and SPZ cement concrete specimens contaminated with 0.8 to 3.5 wt. % chloride (by weight of the cementitious materials).

4.1.1 Experimental Procedure

Experimental set-up was the same as the one used in simulations. The details of the set-up are presented in Section 3.2. KFUPM has acquired a portable DD (using the deuterium + deuterium (DD)) reaction-based pulsed neutron generator model MP320, from Thermo-Fisher, USA to produce 2.5 MeV neutrons for the elemental analysis of bulk specimens [47, 48]. The chloride-contaminated FA, BFS and SPZ cement concrete specimens were irradiated in the newly designed portable neutron generator-based PGNAA set-up. The MP320 generator allows producing 2.5 MeV neutrons using 45-75 keV deuteron beam with 30 to 80 μA beam current for in-situ PGNAA studies in the field. The thermal neutron spectra were acquired in PC-based data acquisition system utilizing multichannel

buffer modules. The prompt gamma-ray data from the chloride-contaminated FA, BFS and SPZ cement concrete specimens were acquired for 120 minutes. For background subtraction, prompt gamma-ray data were also acquired from FA, BFS and SPZ cement concrete specimens without any chlorides.

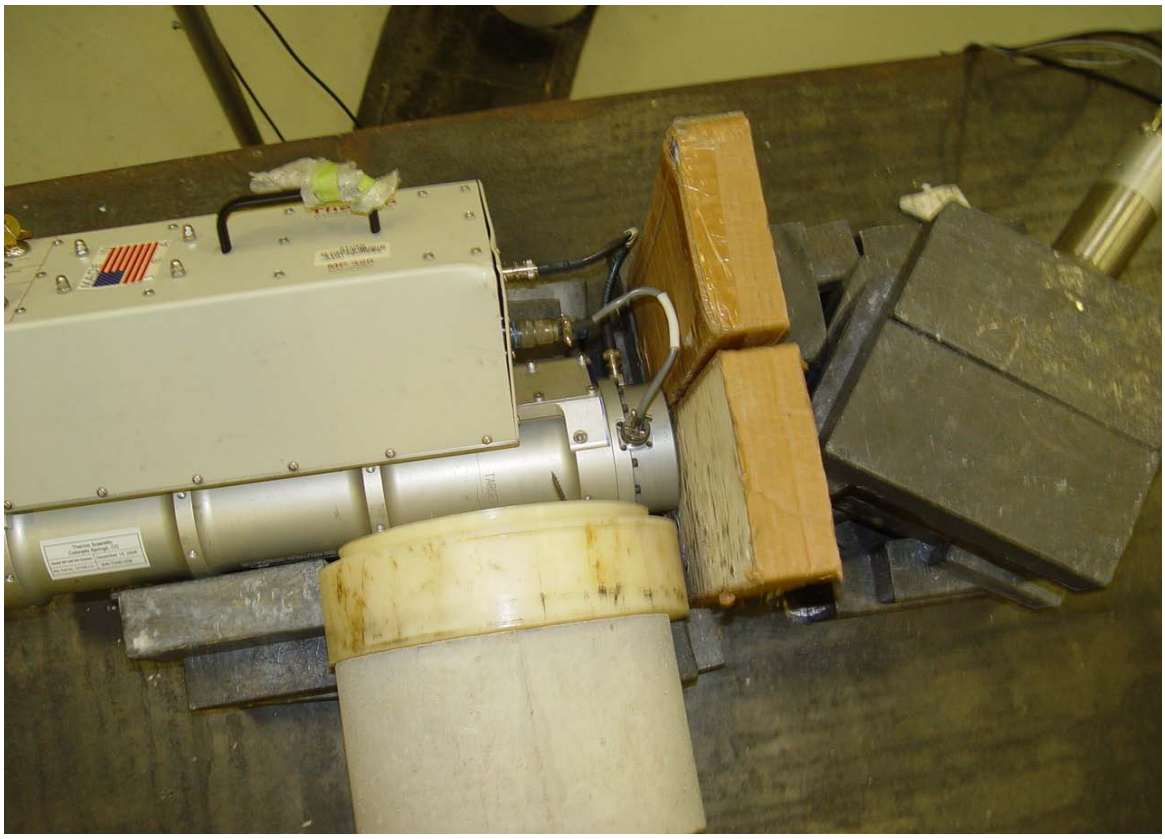

Figure 4.1: Photograph of the PGNAA setup for the Elemental and Chloride gamma-ray measurements.

4.1.2 Preparation of Concrete Specimens

Blended cement concrete specimens were prepared. The blended cement concrete specimens were prepared by mixing (5-80 wt %) of blast furnace slag (BFS), fly ash (FA) and superpozz (SPZ) as a replacement of cement. In addition, the chloride contaminated

blended concrete specimens were prepared by mixing 80 wt% BFS, 20 wt% FA and 10 wt% SPZ, as a weight replacement of cement. The chloride-contaminated concrete specimens were prepared with 0.4, 0.8, 1.5, 2.0, 2.5, 3.0 and 3.5% chloride (by weight of the cementitious materials).

The chemical composition of Fly ash, blast furnace slag, superpozz, and coarse and fine aggregates is shown in Table 4.1.

Table 4.1: Chemical Composition (wt. %) of Portland cement, Pozzolanic materials and coarse and fine aggregates.

Compound	Type V cement	Type I cement	Fly ash	Blast furnace slag	Silica fume	Super-pozz	Fine aggregate	Coarse aggregate
SiO_2	22.00	20.52	52.30	27.70	92.50	53.50	90.70	4.29
Al_2O_3	4.08	5.64	25.20	12.80	0.40	34.3	1.40	0.20
Fe_2O_3	4.24	3.80	4.6	1.20	0.40	3.6	0.48	0.23
CaO	64.07	64.35	10.0	44.0	0.50	4.4	-	-
$CaCO_3$	-	-	-	-	-	-	5.62	93.20
MgO	2.21	2.11	2.20	8.80	0.90	1.0	0.26	0.44
SO_3	1.96	2.1	0.60	3.10	0.50	-	0.2	0.4
K_2O	0.31	0.36	0.10	0.10	0.40	-	0.43	0.09
Na_2O	0.21	0.19	0.10	0.40	0.10	-	0.17	0.03

4.1.3 Concrete Mix Design

Concrete specimens were prepared with the following mix design parameters: a water-to-cementitious materials ratio of 0.45, cementitious material content of 370 kg/m^3 and a coarse-to-total aggregate ratio of 0.62. The chemical composition of concrete specimens

is given in Table 4.2. The bulk density and moisture content of the concrete specimens were assumed to be 2.2 g/cm^3 and 5 wt. %, respectively.

Table 4.2: Composition of Pozzolan cement concrete specimens.

Element (wt. %)	**Specimen 1 (20% FA)**	**Specimen 2 (80% BFS)**	**Specimen 3 (10% SPZ)**
H	0.774	0.727	0.788
C	5.349	5.677	5.545
O	49.607	49.840	50.142
Na	0.060	0.085	0.058
Mg	0.368	0.820	0.33
Al	1.043	1.132	0.895
Si	15.264	15.468	15.216
S	0.246	0.273	0.231
K	0.137	0.133	0.137
Ca	25.24	23.927	25.127
Ti	0.027	0.025	0.027
Fe	0.585	0.337	0.505
Lime/Silica	0.653	0.641	0.652

4.1.4 Preparation and Curing of Concrete Specimens

All the concrete ingredients were thoroughly mixed in a revolving drum mixer and thereafter poured in a specially designed 14 cm high and 12.5 cm radius molds. The concrete specimens were demolded after one day of casting and, thereafter, cured in water for a period of 13 days and finally dried in an electric oven at 70°C for two days.

4.2 Prompt Gamma-Ray Spectra of Chloride-Contaminated Concrete

The prompt gamma-ray spectra of blended cement concrete specimens, such as FA, BFS and SPZ with chloride contamination of 0.8 to 3.5 wt. % was generated in this study. Several prompt gamma-rays are emitted by chlorine due to capture of thermal neutrons. In this study, only chlorine prompt gamma-rays with energies in excess of 2.66 MeV were considered. Due to the poor energy resolution of the BGO detector, chlorine prompt gamma-ray with energies of 2.86, 3.10, 5.72, 6.11 and 6.62 MeV could only be resolved. The partial elemental cross section in barns $\sigma_\gamma^Z(E_\gamma)$for the production of gamma-rays E_γ from various elements Z in concrete assuming natural abundance is given in Table 4.3 [43], while the prompt gamma-ray partial elemental cross sections in barns $\sigma_\gamma^Z(E_\gamma)$for chlorine are listed in Table 4.4 [43].

Table 4.3: Energies and partial elemental cross section $\sigma_\gamma^z(E_\gamma)$-barns of capture gamma-rays of concrete [43].

Element	Gamma-rays energy (MeV)	$\sigma_\gamma^z(E_\gamma)$-barns
Calcium	1.942	0.352
	4.418	0.0708
	6.420	0.176
Silicon	3.539	0.1190
	4.934	0.1120
Aluminum	1.779	0.232
	7.724	0.0493
Iron	7.631	0.653
	7.646	0.549
Hydrogen	2.223	0.3326

Table 4.4: Energies and partial elemental cross section $\sigma_\gamma^z(E_\gamma)$-barns of prominent capture gamma-rays of BGO detector material and chlorine [43].

Element	Gamma-ray energy (keV)	$\sigma_\gamma^z(E_\gamma)$-barns
Bi	162	0.008
	320	0.0115
	674	0.0026
	2505	0.0021
	2828	0.00179
	4054	0.0137
	4171	0.0171
Cl	2863	1.820
	3062	1.130
	5715	1.82
	6111	6.59
	6620	2.530
	6628	1.470
Ge	175	0.164
	493	0.133
	500	0.162
	596	1.100
	608	0.250
	868	0.553
	961	0.129
	1101	0.134
	1204	0.141
	1472	0.083
	5450	0.028
	5518	0.029
	5817	0.028
	6037	0.045
	6117	0.043
	6251	0.019
	6276	0.021
	6390	0.030
	6418	0.018
	6707	0.039
	6717	0.020
	6916	0.031
	7091	0.017
	7260	0.027
	7415	0.016
	8030	0.012
	8498	0.012
	8731	0.013

4.2.1 Prompt Gamma-Ray Spectra of Chloride-Contaminated FA Cement Concrete Specimens

Figure 4.2 shows the prompt gamma-ray spectra from FA cement concrete specimens contaminated with 0.8, 1.5, 2.5, and 3.5 wt. % chloride in excess of 2.6 MeV gamma-ray energy. The figure shows chlorine prompt gamma-rays interfering with prompt gamma-rays from the materials in the FA cement concrete and the BGO detector. The full energy (F) and single escape (S) peaks of the prompt gamma-rays are marked in Figure 4.2. The partial elemental cross section in barns $\sigma_\gamma^z(E_\gamma)$ for the production of gamma-rays E_γ from various elements Z in concrete assuming natural abundance is given in Table 4.3 [43] while the prompt gamma-ray partial elemental cross sections in barns $\sigma_\gamma^z(E_\gamma)$ for chlorine are listed in Table 4.4 [43]. The calcium and silicon prompt gamma-ray peaks are located on the left hand side of the BGO detector sum peak. The full energy peak of calcium Ca(F) at 6.42 MeV is interfering with the full energy peaks of Ge(F) at 6.71 and 6.72 MeV of BGO detector material. Figure 4.2 also shows full energy prompt gamma-ray peaks from silicon Si(F) at 4.94 MeV and 3.54 MeV and a peak at 4.44 MeV which includes the single escape events from 4.94 MeV peak.

The main feature of the data in Figure 4.2 is the increased intensities of some peaks due to the interference of chlorine gamma-rays with those of concrete and BGO. The full energy peaks of 6.61 MeV gamma-rays from chlorine, 6.42 MeV gamma-rays from calcium and 6.71+ 6.72 MeV gamma-rays from Ge in BGO detector have strong interference. Although the full energy peak of 6.11 MeV prompt gamma-ray from chlorine interferes with the unlabeled single escape peak of 6.42 MeV gamma-ray from calcium, but due to

its highest intensity (6.59), 6.11 MeV prompt gamma-ray from chlorine is quiet prominent (see Figure 4.2). Similarly, single escape peak of 6.11 MeV from chlorine interferes with full energy peak of chlorine at 5.72 MeV. An unresolved broad prompt gamma-ray peak has been observed due to the interference of chlorine full energy peaks at 2.86 and 3.10 MeV. Finally, the chlorine gamma-ray yield from each of the chloride-contaminated FA cement concrete specimens was obtained after subtraction of normalized prompt gamma-ray spectra of pure FA cement concrete specimen. Figure 4.3 shows the subtracted spectra of chlorine prompt gamma-ray from FA cement concrete specimens containing 0.8, 1.5, 2.5, and 3.5 wt. % chloride. Prominent three chlorine full energy gamma-rays peaks corresponding to 2.86+3.10, 5.72 and 6.11 MeV energies are clearly shown in Figure 4.3.

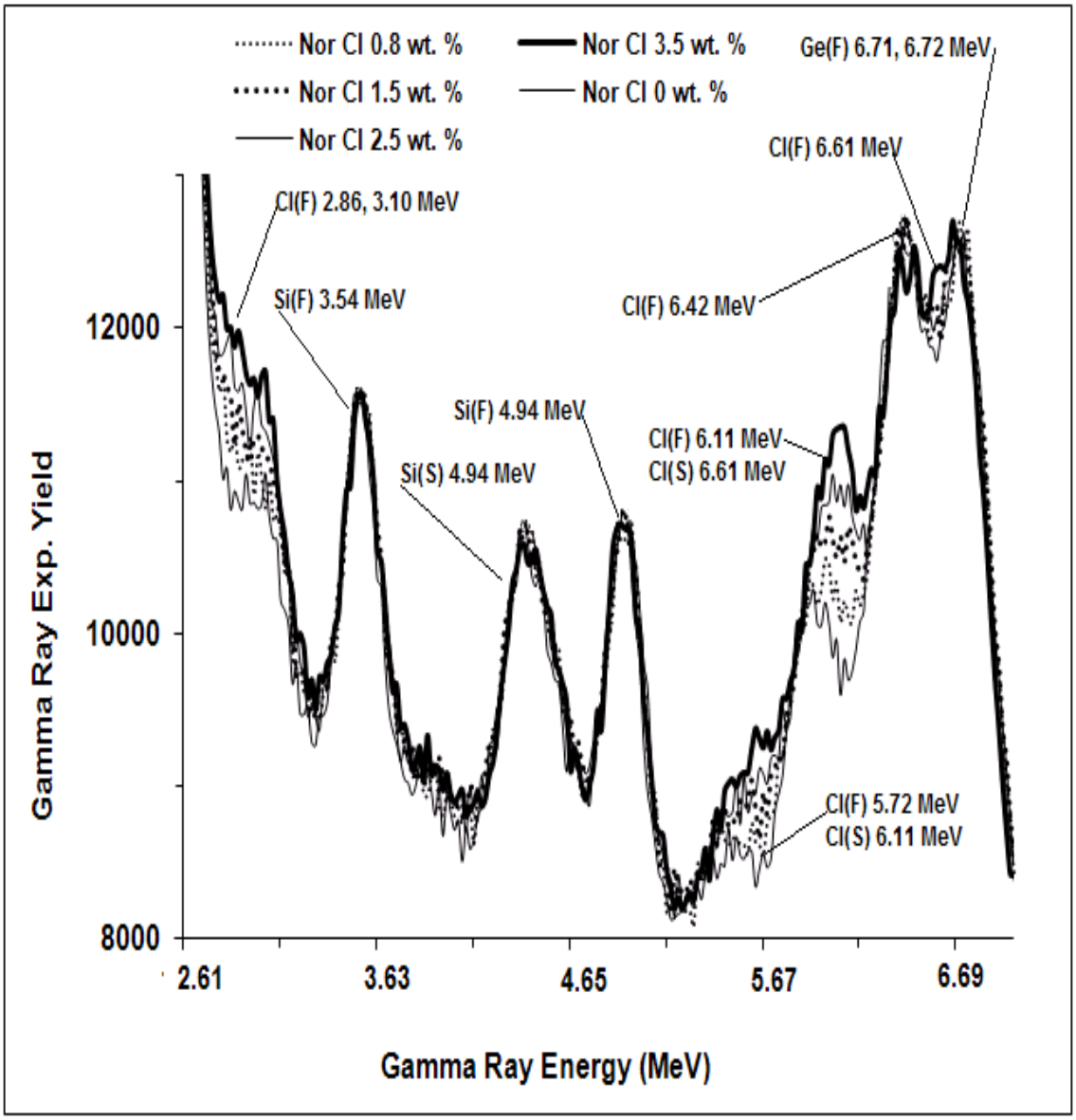

Figure 4.2: Enlarged experimental pulse height spectra of prompt gamma-rays of chloride-contaminated FA cement concrete containing 0.8, 1.5, 2.5 and 3.5 wt. % chlorine taken with the BGO detector (The background spectrum taken with uncontaminated FA cement concrete is also superimposed for comparison purposes).

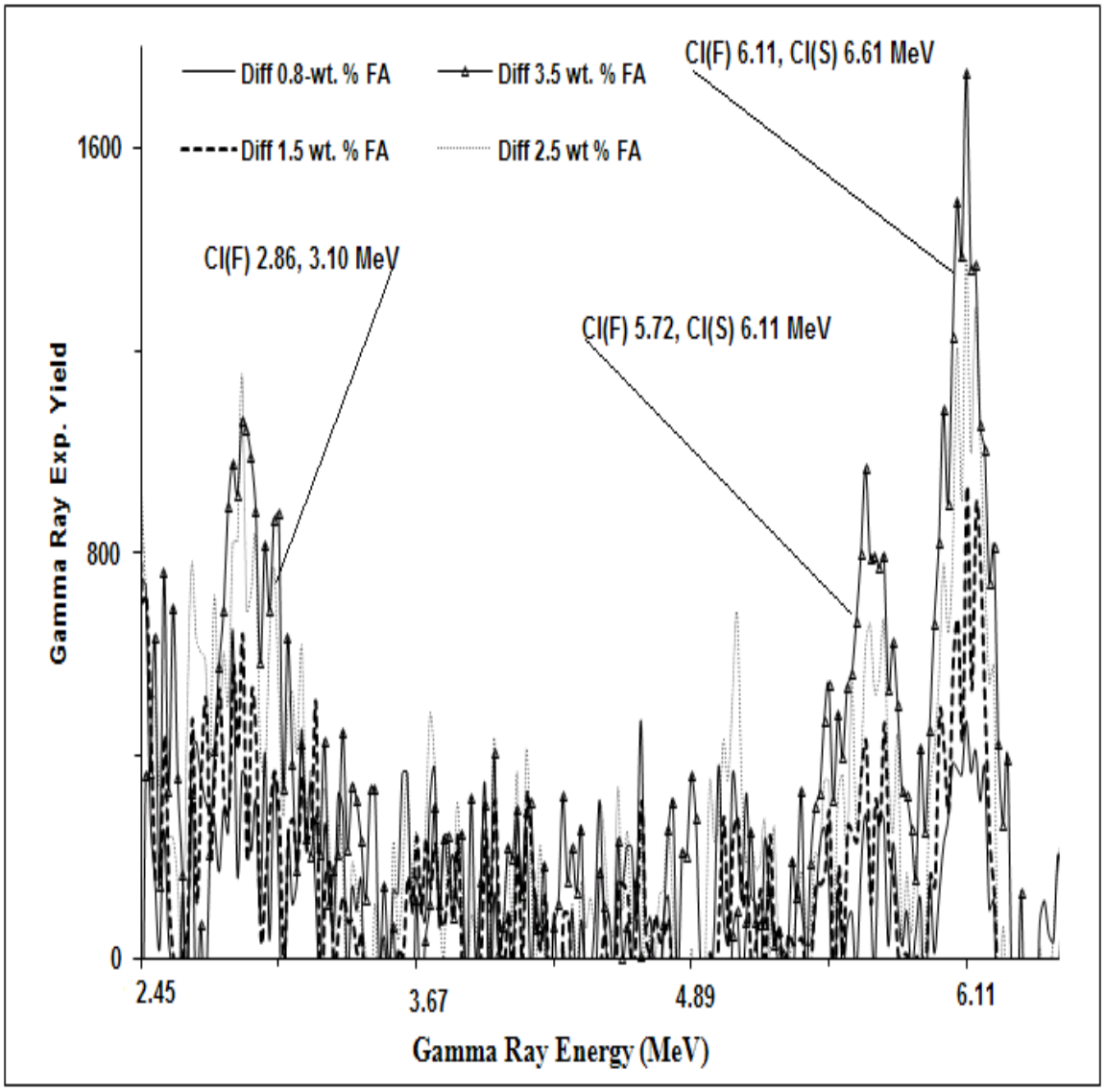

Figure 4.3: Enlarged prompt gamma-ray experimental pulse height spectra after background subtraction from the four FA cement concrete specimens, showing full energy and associated single escape prompt gamma-ray peaks for 2.86+3.1, 5.72 and 6.11 MeV.

4.2.2 Prompt Gamma Spectra of Chloride-Contaminated BFS Cement Concrete Specimens

Prompt gamma-ray spectra from BFS cement concrete specimens contaminated with 0.8, 2.0, and 3.5 wt. % chloride in excess of 2.66 MeV gamma-ray energy is shown in Figure 4.4. The interference of prompt gamma-rays of chlorine with BFS cement concrete constituents and BGO detector material can be seen in this figure whereby the full energy (F) and single escape (S) peaks of the prompt gamma-rays are marked. The sum peak in BGO detector is observed at 7.33 Mev with collective contributions of Ge prompt gamma-rays in excess of 7.0 MeV energy, as shown in Table 4.4. The calcium and silicon prompt gamma-ray peaks are located on the left hand side of the BGO detector sum peak. The full energy peak of calcium Ca(F) at 6.42 MeV is interfering with the full energy peaks of Ge(F) at 6.71 and 6.72 MeV of BGO detector material. Figure 4.4 also shows full energy prompt gamma-ray peaks from silicon Si(F) at 4.94 MeV and 3.54 MeV and a peak at 4.44 MeV which includes the single escape events from 4.94 MeV peak.

The key feature of the data in Figure 4.4 is the increased intensities of some peaks due to the interference of chlorine gamma-rays with those of concrete and BGO. The full energy peaks of 6.61 MeV gamma-rays from chlorine, 6.42 MeV gamma-rays from calcium and 6.71+6.72 MeV gamma-rays from Ge in BGO detector have strong interference. Although the full energy peak of 6.11 MeV prompt gamma-ray from chlorine interferes with the unlabeled single escape peak of 6.42 MeV gamma-ray from calcium, but due to its highest intensity (6.59), 6.11 MeV prompt gamma-ray from chlorine is quiet prominent in Figure 4.4 . Similarly, the single escape peak of 6.11 MeV from chlorine interferes with full

energy peak of chlorine at 5.72 MeV. An unresolved broad prompt gamma-ray peak has been observed due to the interference of chlorine full energy peaks at 2.86 and 3.10 MeV. Finally, the chlorine gamma-ray yield from each of the chloride-contaminated BFS cement concrete specimens was obtained after subtraction of normalized prompt gamma-ray spectra of pure BFS cement concrete specimen. Figure 4.5 shows the subtracted spectra of chlorine prompt gamma-ray from BFS cement concrete specimens containing 0.8, 2.0, and 3.5 wt. % chloride. Prominent three chlorine full energy gamma-rays peaks corresponding to 2.86+3.10, 5.72 and 6.11 MeV energies are clearly shown in Figure 4.5.

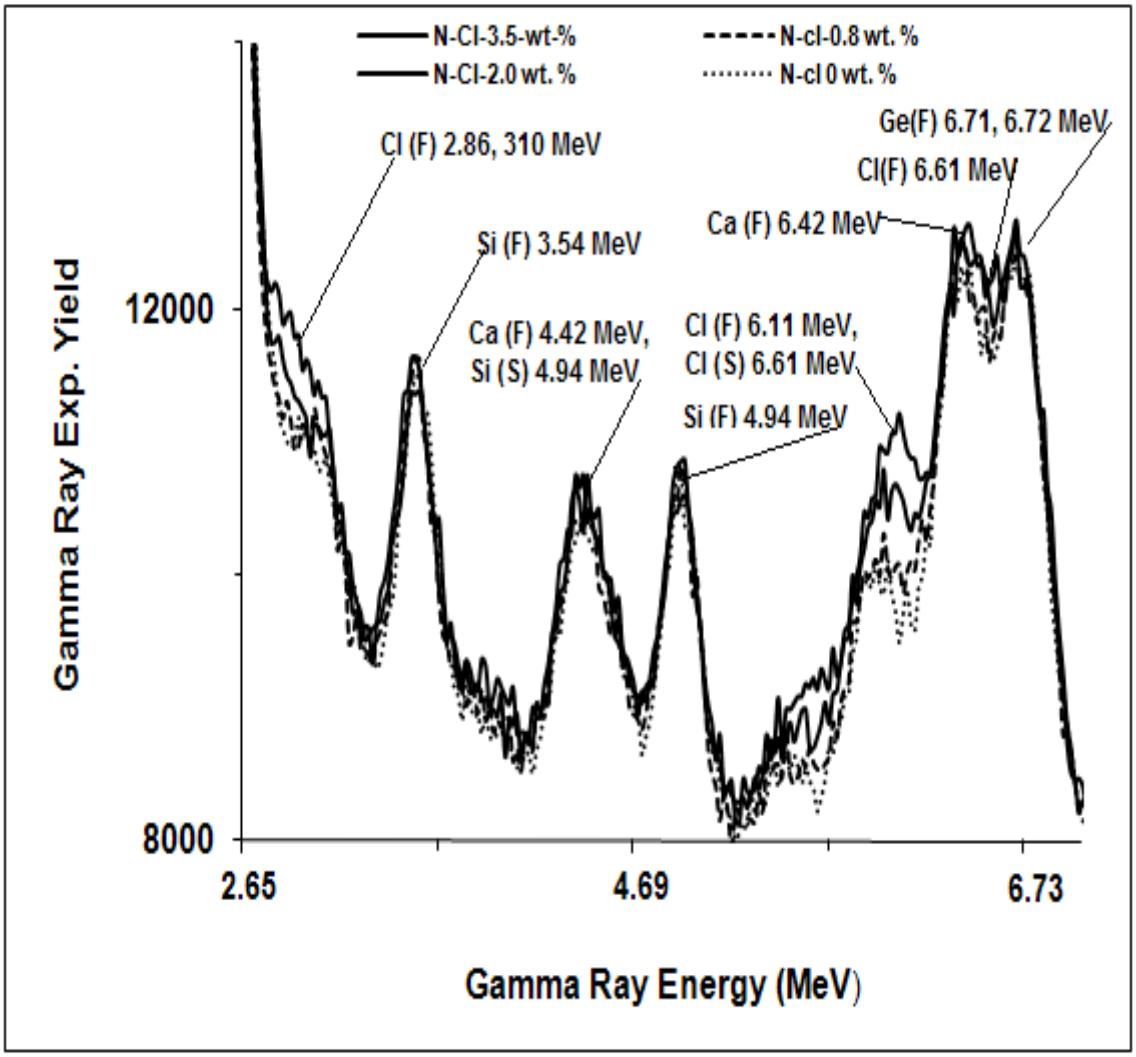

Figure 4.4: Enlarged experimental pulse height spectra of prompt gamma-rays of chloride contaminated BFS cement concrete containing 0.8, 2.0 and 3.5 wt. % chlorine taken with the BGO detector (The background spectrum taken with uncontaminated BFS cement concrete is also superimposed for comparison purposes)

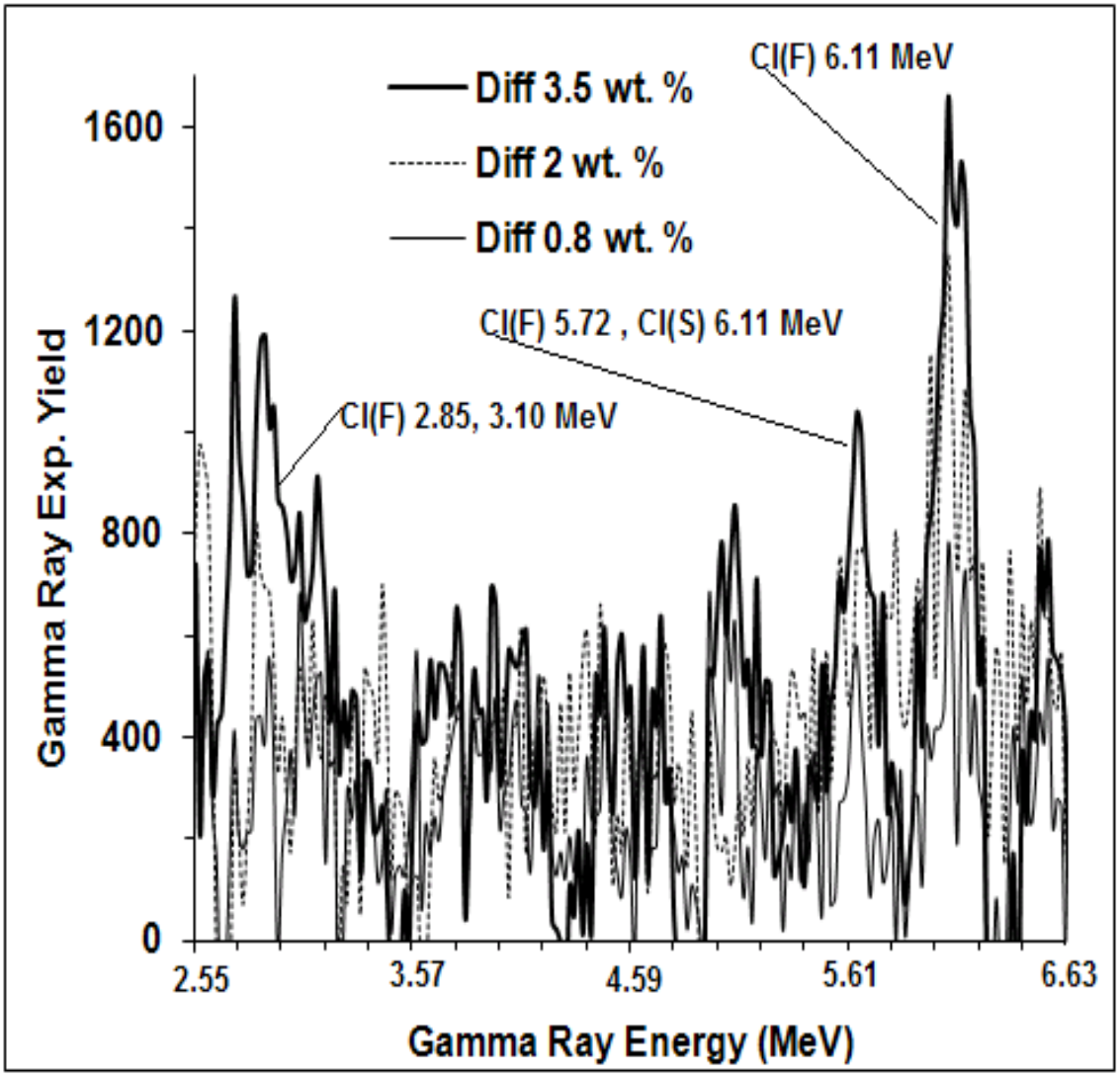

Figure 4.5: Enlarged prompt gamma-ray experimental pulse height spectra after background subtraction from the three BFS cement concrete specimens, showing full energy and associated single escape prompt gamma-rays peaks for 2.86+3.1, 5.72 and 6.11 MeV.

4.2.3 Prompt Gamma Spectra of Chloride-Contaminated SPZ Cement Concrete Specimens

Figure 4.6 shows the prompt gamma-ray spectra from SPZ cement concrete specimens contaminated with 0.8, 1.5, 2.5, and 3.5 wt. % chloride in excess of 2.66 MeV gamma-ray whereby the full energy (F) and single escape (S) peaks of the prompt gamma-rays are marked. The sum peak is observed at 7.33 MeV with collective contribution of Ge prompt gamma-rays in excess of 7.0 MeV energy, as reported in Table 4.4. Additionally, Figure 4.6 shows the prompt gamma-rays from chlorine interfering with prompt gamma-rays from SP cement concrete constituents and BGO detector material. The calcium and silicon prompt gamma-ray peaks are located on the left hand side of the BGO detector sum peak. The full energy peak of calcium Ca(F) at 6.42 MeV is interfering with the full energy peaks of Ge(F) at 6.71 and 6.72 MeV of BGO detector material. Figure 4.6 also shows full energy prompt gamma-ray peaks from silicon Si(F) at 4.94 MeV and 3.54 MeV and a peak at 4.44 MeV which includes the single escape events from 4.94 MeV peak.

The main feature of the data in Figure 4.6 is the increased intensities of some peaks due to the interference of chlorine gamma-rays with those of concrete and BGO. The full energy peaks of 6.61 MeV gamma-rays from chlorine, 6.42 MeV gamma-rays from calcium and 6.71+6.72 MeV gamma-rays from Ge in BGO detector have strong interference. Even though the full energy peak of 6.11 MeV prompt gamma-ray from chlorine interferes with the unlabeled single escape peak of 6.42 MeV gamma-ray from calcium, its highest intensity (6.59), 6.11 MeV prompt gamma-ray from chlorine is quiet prominent in Figure

4.6. Similarly, the single escape peak of 6.11 MeV from chlorine interferes with full energy peak of chlorine at 5.72 MeV. An unresolved broad prompt gamma-ray peak has been observed due to the interference of chlorine full energy peaks at 2.86 and 3.10 MeV. Finally, the chlorine gamma-ray yield from each of the chloride-contaminated SPZ cement concrete specimens was obtained after subtraction of normalized prompt gamma-ray spectra of pure SPZ cement concrete specimen. Figure 4.7 shows the subtracted spectra of chlorine prompt gamma-ray from SPZ cement concrete specimens containing 0.8, 1.5, 2.5, and 3.5 wt. % chloride. Three prominent chlorine full energy gamma-rays peaks corresponding to 2.86+3.10, 5.72 and 6.11 MeV energies are clearly shown in Figure 4.7.

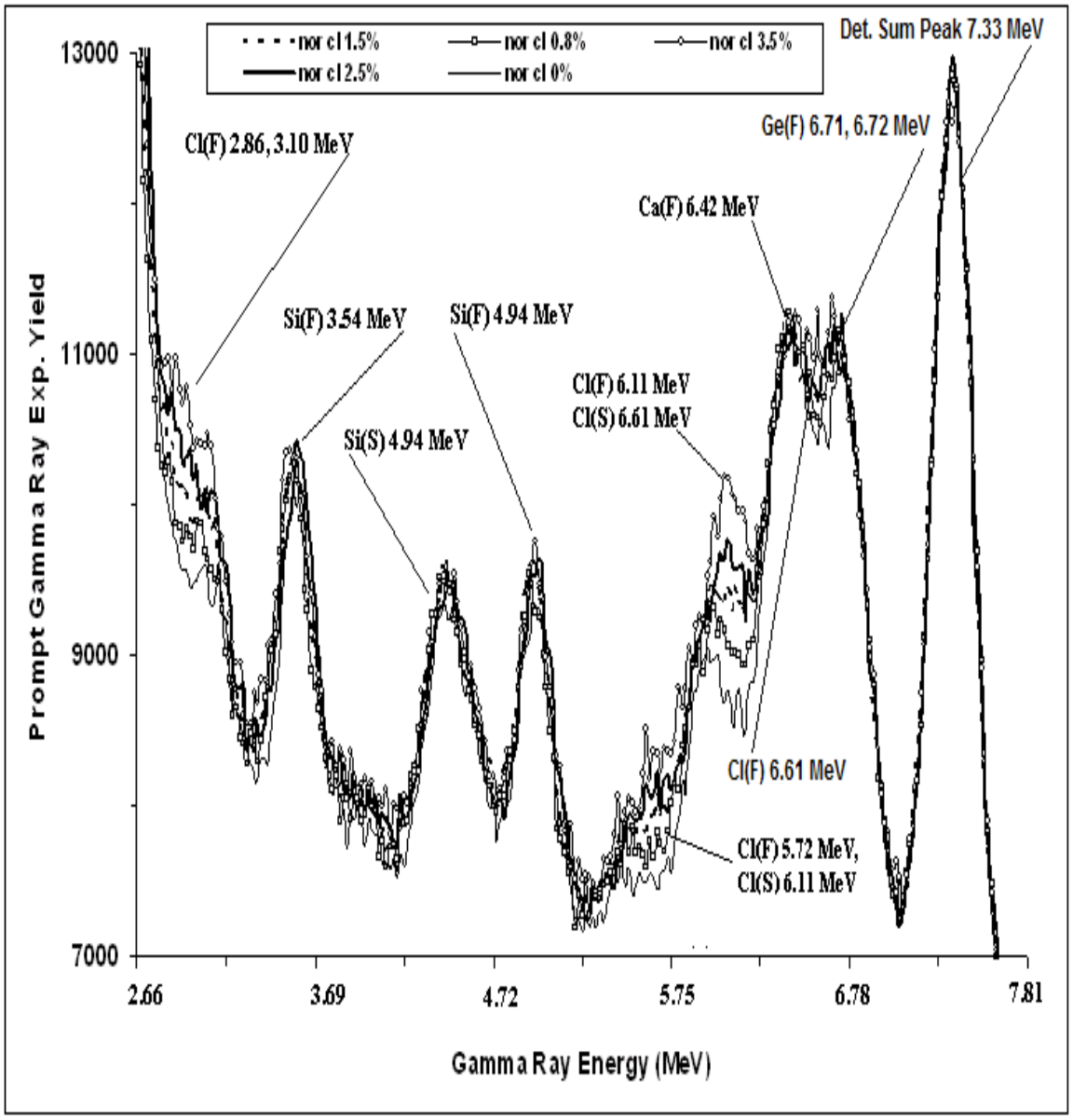

Figure 4.6: Enlarged experimental pulse height spectra of prompt gamma-rays of chloride contaminated SPZ cement concrete containing 0.8, 1.5, 2.5 and 3.5 wt. % chlorine taken with the BGO detector (The background spectrum taken with uncontaminated SPZ cement concrete is also superimposed for comparison purposes).

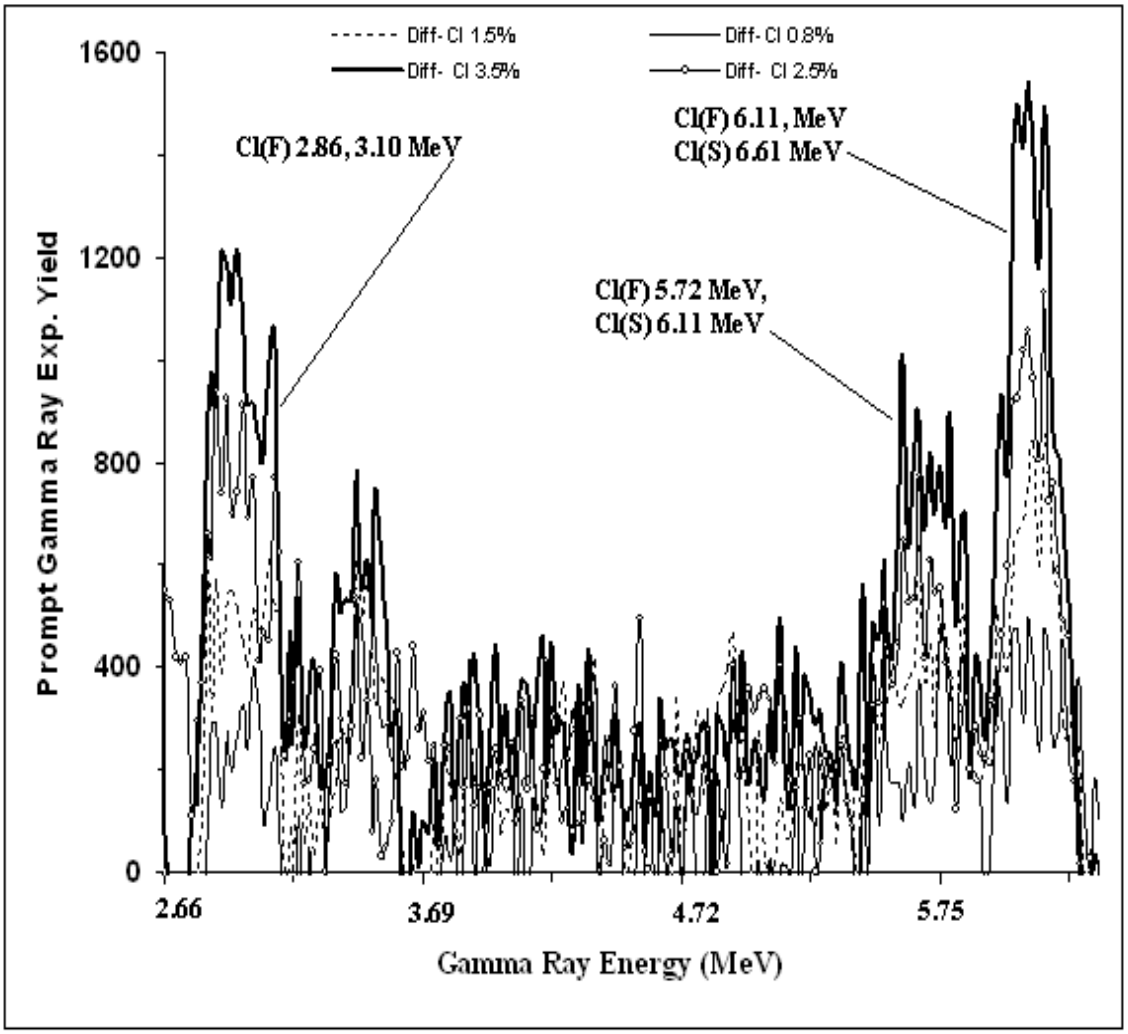

Figure 4.7: Enlarged prompt gamma-ray experimental pulse height spectra after background subtraction from the four SPZ cement concrete specimens, showing full energy and associated single escape prompt gamma-rays peaks for 2.86+3.1, 5.72 and 6.11 MeV.

4.3 Inter-Comparison of Experimental and Theoretical Results

Experimental results were compared with theoretical results of Monte Carlo simulations discussed in detail in Section 3.1. The counts under each peak were integrated from the spectra of FA, BFS and SPZ cement concrete containing different chloride concentrations. Figures 4.8 through 4.10 show the normalized experimental yield of 2.86+3.10, 5.72 and 6.11 MeV chlorine gamma-rays as a function of chloride concentration in the FA, BFS and SPZ cement concrete respectively. Within the experimental uncertainties, there is an excellent agreement with the normalized calculated yield of the prompt gamma-rays from chlorine in FA, BFS and SPZ cement concrete (shown with solid line) obtained through Monte Carlo simulations.

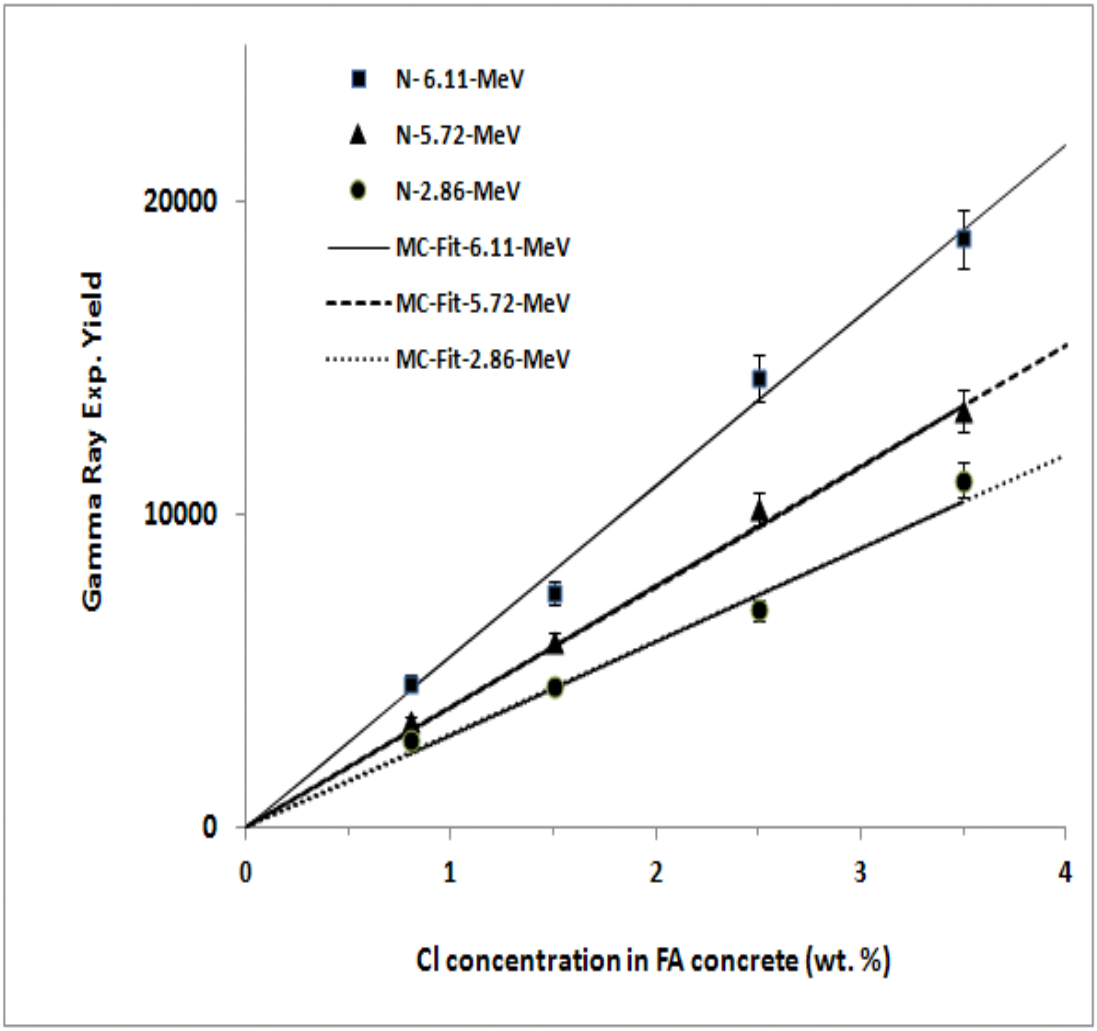

Figure 4.8: Integrated yield of 2.86+3.1, 5.72 and 6.11 MeV prompt gamma-ray as a function of chlorine concentration for the four FA cement concrete specimens. Solid line represents the calculated yield obtained through Monte Carlo simulations.

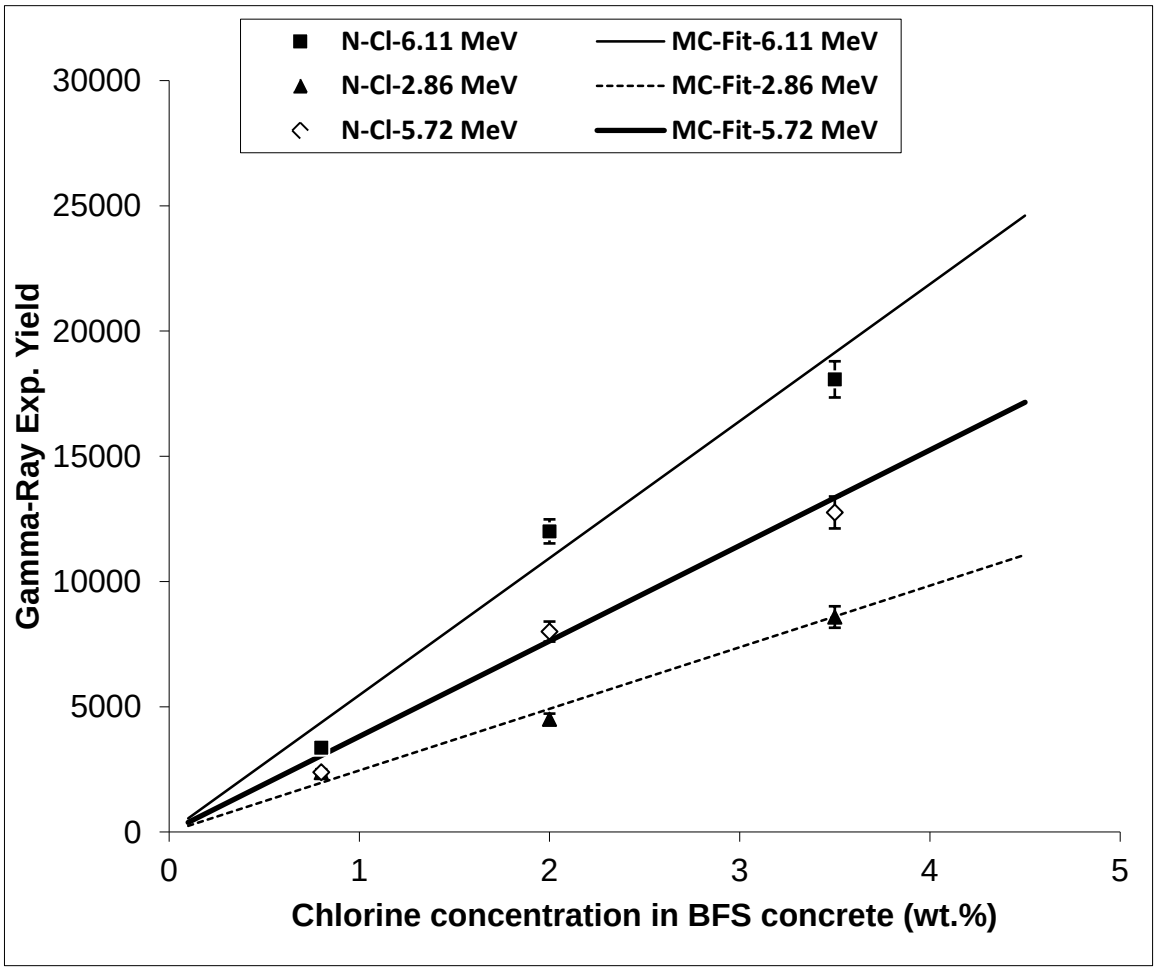

Figure 4.9: Integrated yield of 2.86+3.1, 5.72 and 6.11 MeV prompt gamma-ray as a function of chlorine concentration for the three BFS cement concrete specimens. Solid line represents the calculated yield obtained through Monte Carlo simulations.

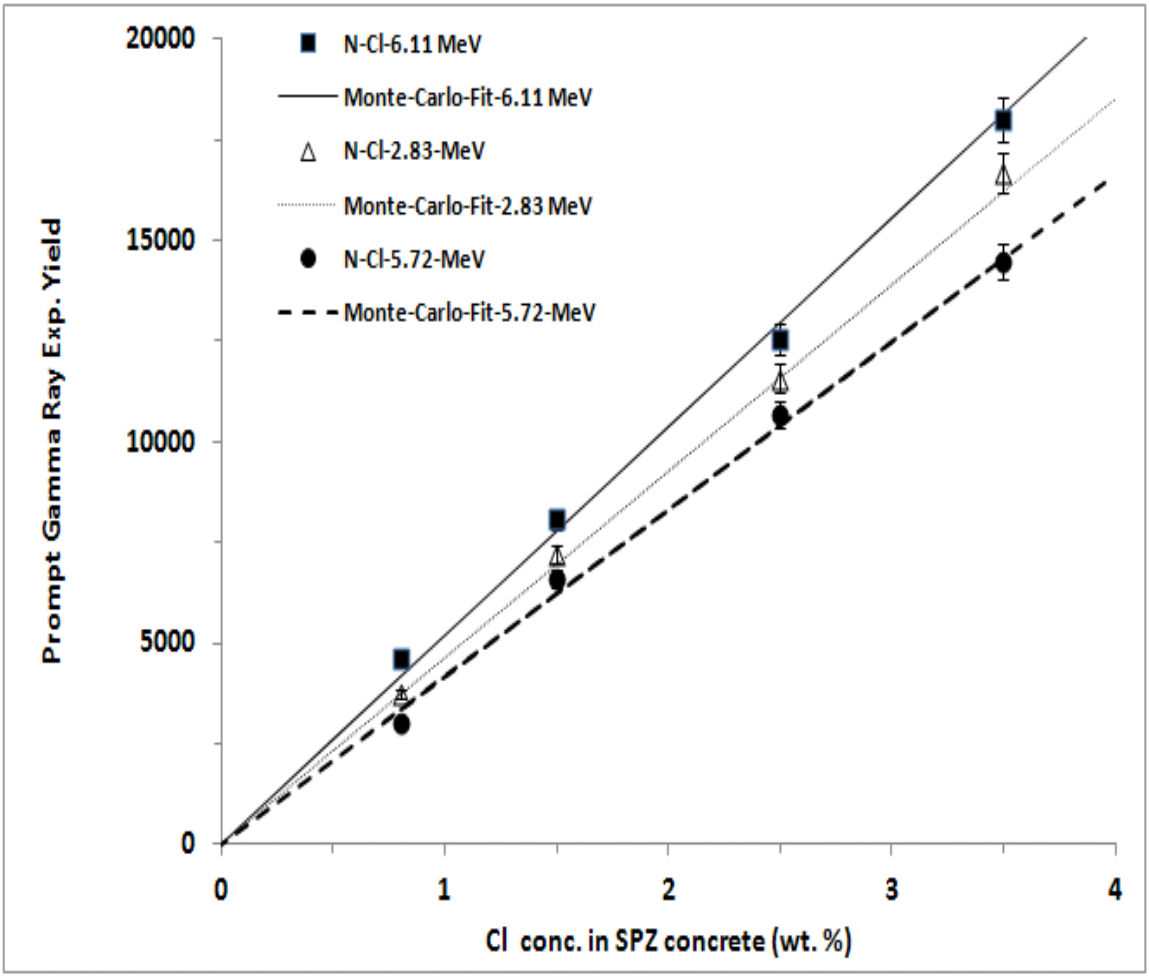

Figure 4.10: Integrated yield of 2.86+3.1, 5.72 and 6.11 MeV prompt gamma-ray as a function of chlorine concentration for the four SPZ cement concrete specimens. Solid line represents the calculated yield obtained through Monte Carlo simulations.

4.4 Generalized Calibration Curve

Chloride content in a structure can be measured using the developed PGNAA set-up in a reflectance mode. The gamma-ray yield obtained from FA, BFS and SPZ cement concrete specimens for different gamma-ray energies was plotted as a function of chloride concentration. The plots will serve as a ready reference for evaluating the chloride concentration in the concrete from the gamma-ray yield.

4.4.1 Calibration Curve for 2.86+3.10 MeV Gamma-Ray

The gamma-ray yield at 2.86+3.10 MeV from FA, BFS and SPZ cement concrete specimens is plotted against the chloride concentration in Figure 4.11.

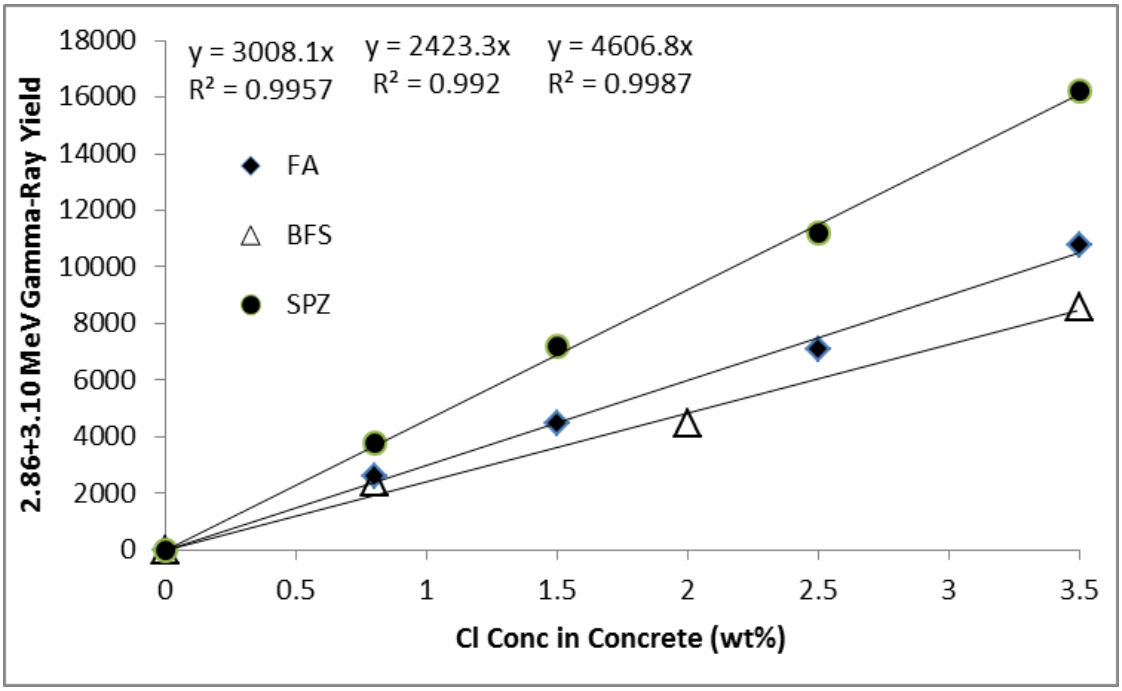

Figure 4.11: Prompt gamma-rays as a function of chloride concentration for FA, BFS and SPZ cement concrete specimens (2.86+3.10 MeV).

It is evident from Figure 4.11 that there is a good correlation between the gamma-ray yield and the chloride concentration. The R^2 was in the range of 0.992 to 0.998. However, the slope varied from 2400 to 4600 counts

In order to ascertain the possibility of developing a single correlation between the chloride concentration and the gamma-ray yield the data in Figure 4.11 were plotted as a single curve in Figure 4.12. Again an almost linear relationship was noted between the chloride concentration and the gamma-ray yield. However, the fit is not good, as R^2 is 0.83. Generally, an R^2 of more than 0.85 indicates a good fit. This suggests that a common correlation equation cannot be developed for 2.86+3.1 MeV gamma-rays. Subsequently, the chloride concentration in FA, BFS and SPZ concretes have to be determined using the respective curves in Figure 4.11. Alternatively, gamma-ray yield at higher energy, such as 5.72 or 6.11 MeV may be used.

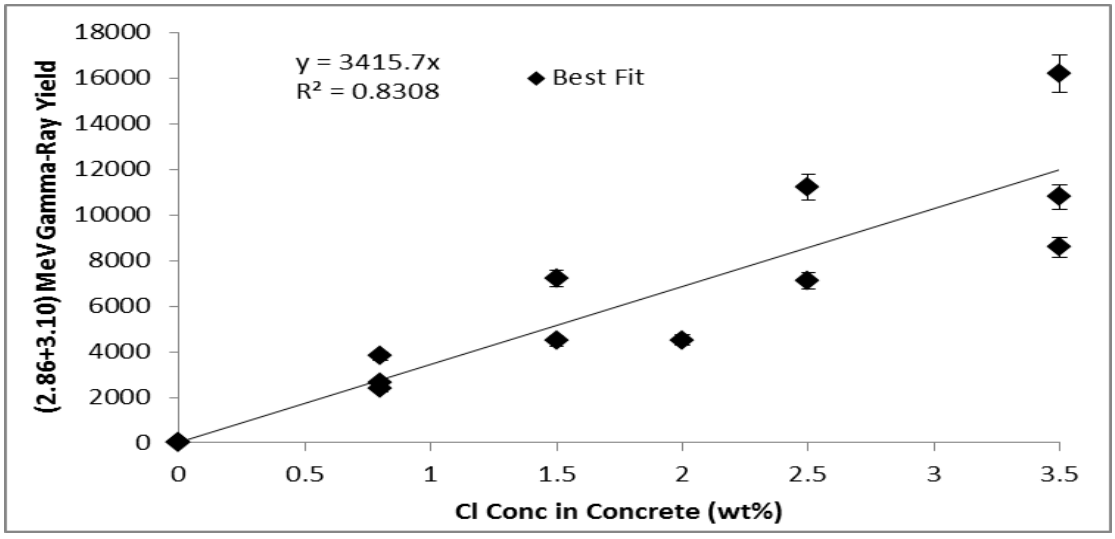

Figure 4.12: Prompt gamma-ray yield (2.86+3.10 MeV) as a function of chloride concentration in cement concrete specimens.

4.4.2 Gamma-Ray Calibration Curve for 5.72 MeV

Figure 4.13 shows gamma-ray yield at 5.72 MeV from FA, BFS and SPZ cement concrete specimens as a function of chloride concentration.

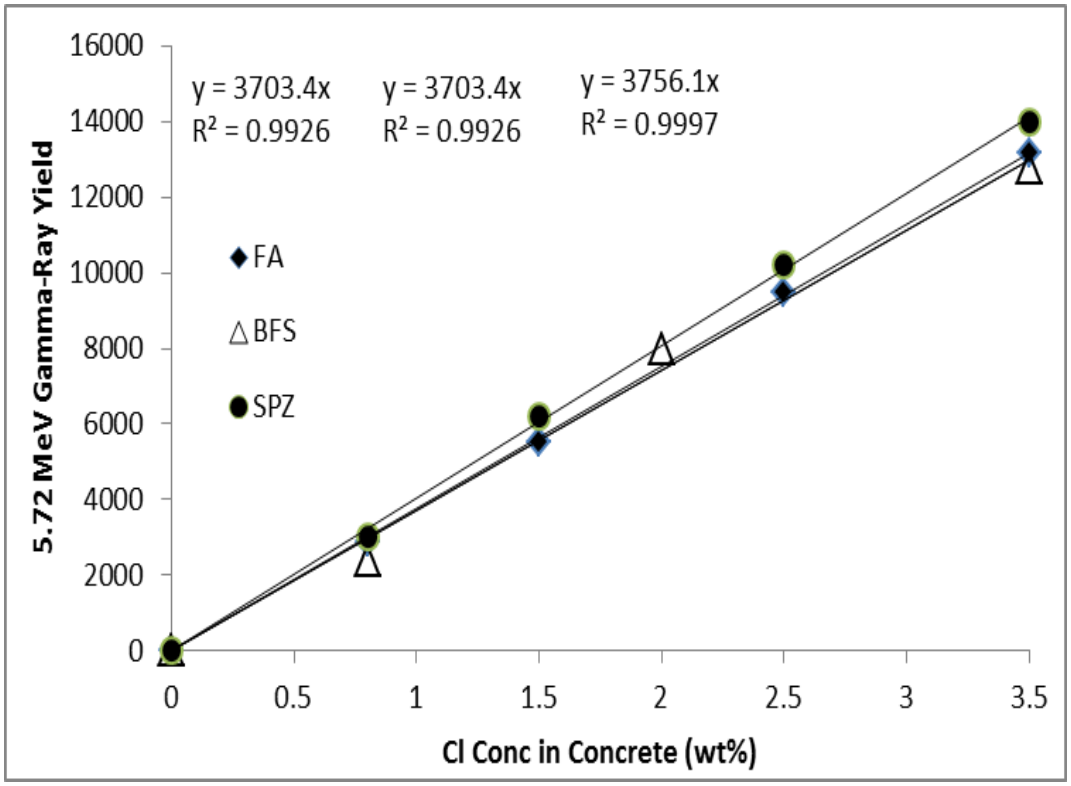

Figure 4.13: Yield of 5.72 MeV prompt gamma-rays as a function of chloride concentration for FA, BFS and SP cement concrete specimens.

A good correlation was noted between the gamma-ray yield and the chloride concentration. The R^2 was more than 0.99 in all the cases. Moreover, the slope was also in a close range, 3750 to 4000 counts. The gamma-ray yields of FA, BFS and SPZ cement concrete specimens are collectively plotted against chloride concentration in Figure 4.14.

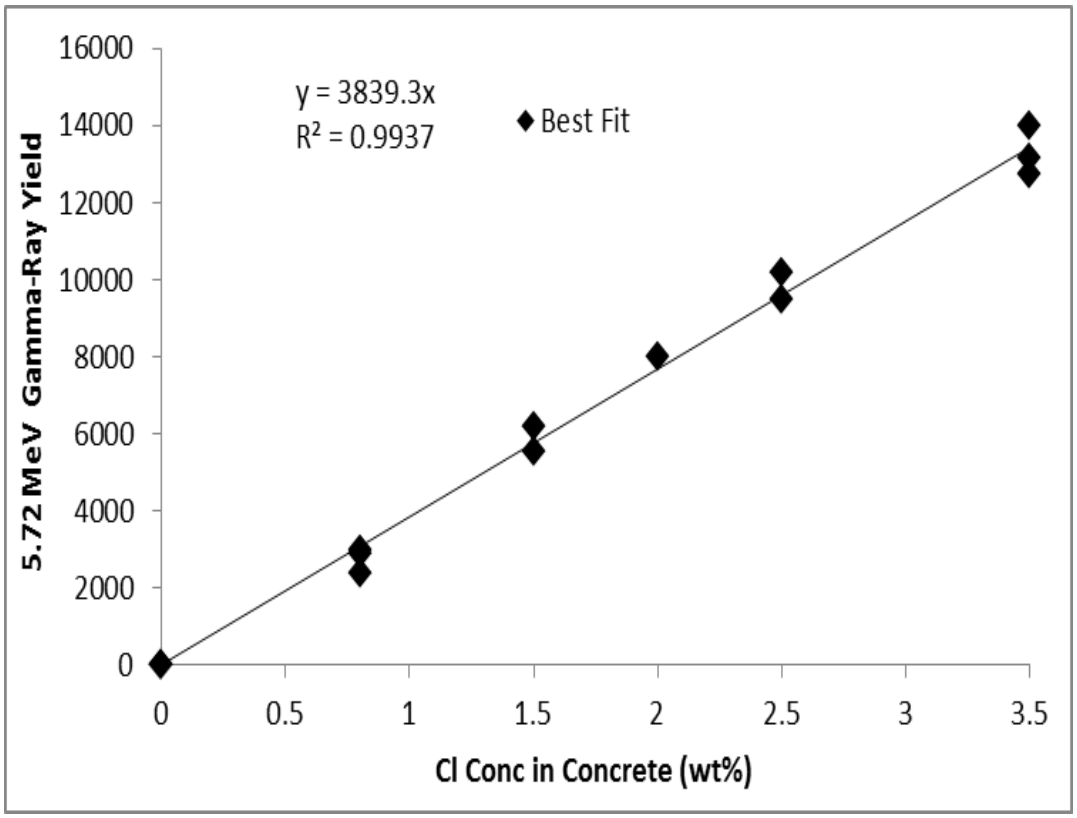

Figure 4.14: Yield of 5.72 MeV prompt gamma-rays as a function of chloride concentration in cement concrete specimens.

A linear correlation was noted between the gamma-ray yield and the chloride concentration and the relationship is as given below:

Chloride (wt.%) = (Gamma-Ray Yield)/3839

$R^2 = 0.993$.

Since the R^2 value is close to 1.0 the above equation could be utilized for determining the chloride concentration from the experimental yield.

4.4.3 Gamma-Ray Calibration Curve for 6.11 MeV

Figure 4.15 shows gamma-ray yield at 6.11 MeV from FA, BFS and SPZ cement concrete specimens as a function of chloride concentration.

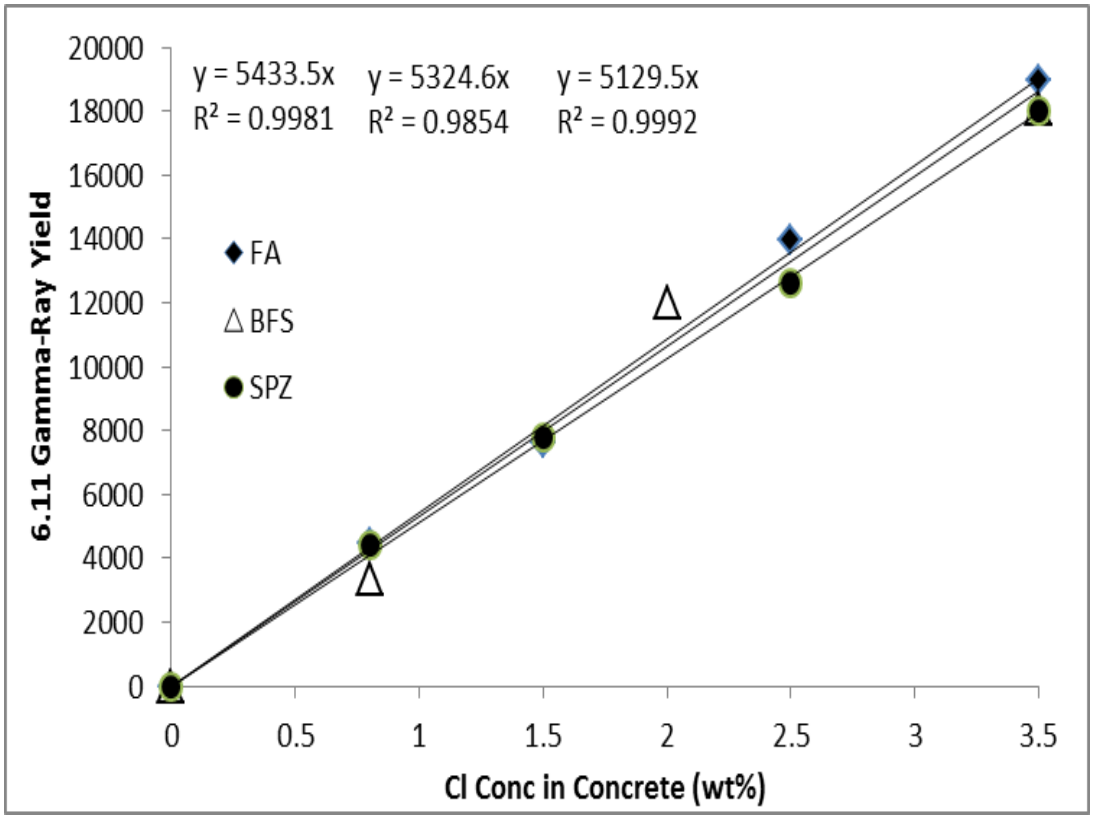

Figure 4.15: Prompt gamma-ray at 6.11 MeV as a function of chloride concentration for FA, BFS and SPZ cement concrete specimens.

An almost linear correlation was noted between the chloride concentration and gamma-ray yield. The R^2 was in the range of 0.985 to 0.999 and the slope was in the range of 5129 to 5433 counts. The experimental yield in FA, BFS and SPZ is collectively plotted against the chloride concentration in Figure 4.16.

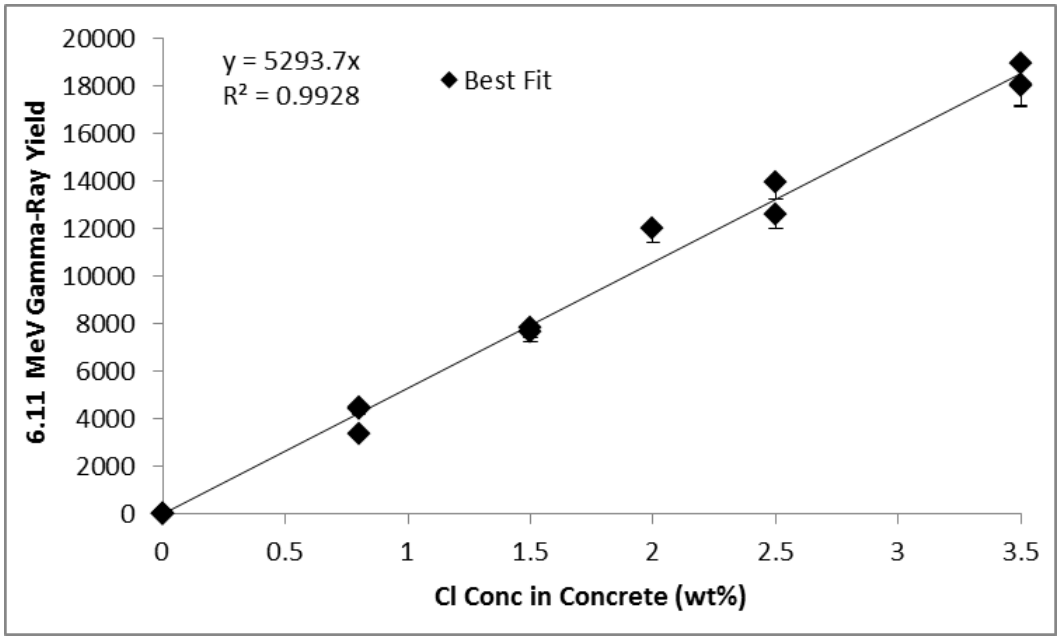

Figure 4.16: Prompt gamma-ray yield at 6.11 MeV as a function of chloride concentration in the cement concrete specimens.

From the Figure 4.16, the following relationship between the gamma-ray yield at 6.11 MeV and the chloride concentration is noted.

Chloride (wt.%) = (Gamma-Ray Yield)/5293

$R^2 = 0.992$.

This indicates that the gamma-ray yield at 6.11 MeV can also be utilized to determine the chloride concentration with high degree of accuracy. However, between the yield at 5.72 and 6.11 MeV, the latter is preferred as it has higher intensity of 6.59 units compared to 1.82 units at 5.72 MeV [43]. Further, the 6.11 MeV gamma-rays can detect low concentration as they have a higher intensity of 6.59.

4.5 Calculation of MDC of Chloride in Blended Cement Concretes

The MDC of chloride in cement concrete was calculated using the procedure described in Reference [41]. The MDC for an elemental concentration measured under a peak with net counts N_P and associated background counts N_B (under the peak) is defined by the following relation:

$MDC = 4.653*(C/N_P)*\sqrt{N_B}$

where C is the element's concentration in the peak.

The error in MDC $\sigma_{MDC} = (C/N_P)*[\sqrt{(2*N_B)}]$

Inspite of a reduction in the gamma-ray intensity due to the backward angle of the gamma-ray detector and relatively smaller neutron flux from a portable neutron generator, the values of MDC measured in the present study, are comparable with the MDC value for 6.11 MeV chlorine prompt gamma-rays measured in FA, SF and BFS cement concrete measured using transmission type PGNAA setup [47, 48].

4.5.1 FA Cement Concrete Data

Table 4.5 shows the MDC of chlorine in FA cement concrete specimens determined by the portable neutron generator-based PGNAA set-up for 2.86+3.10, 5.72 and 6.11 MeV chlorine prompt gamma-rays. Also included in Table 4.5 are MDC of chlorine prompt gamma-rays in plain, FA, SF [48] and BFS [47] cement concretes utilizing the previous transmission type PGNAA set-up. The MDC of chlorine prompt gamma-rays in the FA cement concrete specimens for the portable neutron generator based PGNAA set-up were

been measured as 0.033±0.010, 0.031±0.010, 0.032±0.010 wt % for 2.86+3.10, 5.72 and 6.11 MeV gamma-rays, respectively. The best value of MDC limit of chlorine in the FA cement concrete was found to be 0.031±0.010 for 5.72MeV prompt gamma-rays.

Table 4.5: Comparison of MDC of chlorine in FA cement concrete using Transmission and Reflection technique PGNAA

Gamma-Ray Energy (MeV)	MDC in Present Reflection Study	MDC in Previous Transmission Studies [47-48]			
	FA cement concrete	Plain cement concrete [48]	FA cement concrete[48]	SF cement concrete[48]	BFS cement concrete[47]
2.86+3.12	0.033±0.010	-	-	-	-
5.72	0.031±0.010	0.255±0.050	-	-	-
6.11	0.032±0.010	0.140±0.068	0.038±0.017	0.026±0.008	0.035±0.011

4.5.2 BFS Cement Concrete Data

Table 4.6 shows the MDC of chlorine in BFS cement concrete specimens determined by the portable neutron generator-based PGNAA set-up for 2.86+3.10, 5.72 and 6.11 MeV chlorine prompt gamma-rays. Also included in Table 4.6 are MDC of chlorine prompt gamma-rays in plain, FA, SF [48] and BFS [47] cement concretes utilizing the previous

transmission type PGNAA set-up. The MDC of chlorine prompt gamma-rays in the BFS cement concrete specimens for the portable neutron generator-based PGNAA set-up was 0.034±0.010, 0.032±0.010, 0.033±0.010 wt % for 2.86+3.10, 5.72 and 6.11 MeV gamma-rays, respectively. The best value of MDC limit of chlorine in the BFS cement concrete was found to be 0.032±0.010 for 5.72 MeV prompt gamma-rays.

Table 4.6: Comparison of MDC of chlorine in concrete in BFS cement concrete using Transmission and Reflection technique PGNAA

Gamma-Ray Energy (MeV)	MDC in Present Reflection Study	MDC in Previous Transmission Studies [47-48]			
	BFS cement concrete	Plain cement concrete [48]	FA cement concrete[48]	SF cement concrete[48]	BFS cement concrete[47]
2.86+3.12	0.034±0.010	-	-	-	-
5.72	0.032±0.010	0.255±0.050	-	-	-
6.11	0.033±0.010	0.140±0.068	0.038±0.017	0.026±0.008	0.035±0.011

4.5.3 SPZ Cement Concrete Data

Table 4.7 shows the MDC of chlorine in SPZ cement concrete specimens determined by the portable neutron generator-based PGNAA set-up for 2.86+3.10, 5.72 and 6.11 MeV chlorine prompt gamma-rays. Also included in Table 4.7 are MDC of chlorine prompt gamma-rays in plain, FA, SF [48] and BFS [47] cement concretes utilizing the previous transmission type PGNAA set-up. The MDC of chlorine prompt gamma rays in SPZ cement concrete specimens for the portable neutron generator based PGNAA set-up have been measured as 0.032±0.012, 0.037±0.012, 0.035±0.012 wt % for 2.86+3.10, 5.72 and 6.11 MeV gamma-rays, respectively. The best value of MDC limit of chlorine in the SPZ cement concrete was found to be 0.032±0.012 for 2.86+3.10 MeV prompt gamma-rays.

Table 4.7: Comparison of MDC of chlorine in SPZ cement concrete using Transmission and Reflection technique PGNAA

Gamma-Ray Energy (MeV)	MDC in Present Reflection Study	MDC in Previous Transmission Studies [47-48]			
	SPZ cement concrete	Plain cement concrete [48]	FA cement concrete[48]	SF cement concrete[48]	BFS cement concrete[47]
2.86+3.12	0.032±0.012	-	-	-	-
5.72	0.037±0.012	0.255±0.050	-	-	-
6.11	0.035±0.012	0.140±0.068	0.038±0.017	0.026±0.008	0.035±0.011

The value of MDC achieved in the present study (reflection mode) is comparable with previous results (transmission mode) for larger accelerator based PGNAA set-up. This shows the successful application of a portable neutron generator in the detection of chloride ions in concrete structures.

CHAPTER 5

DISCUSSION OF RESULTS

5.1 Conclusions

This research was conducted to assess the suitability of PGNAA technique in a reflectance mode in determining the chloride concentration in cement concrete specimens. The following conclusions can be drawn based on the data developed in this study:

1. A prompt gamma-ray neutron activation (PGNAA) setup has been designed utilizing a portable neutron generator for field measurements in reflectance mode. The setup has been tested through measurement of chlorine concentration in the concrete specimens in a reflectance mode utilizing a portable neutron generator.
2. The salient feature of the setup is the neutron source and shielded gamma-ray detector are placed on one side of the specimen for external scanning of the chloride concentration in concrete.
3. The chloride concentration was measured in chloride-contaminated FA, BFS and SPZ cement concrete specimens at 6.11, 5.72 and 2.86+3.10 MeV chlorine prompt-gamma rays. In spite of interference between gamma-rays from chlorine and calcium, an excellent agreement was observed between the experimental and theoretical yield of 6.11, 5.72 and 2.86+3.10 MeV chlorine prompt gamma-rays.

This shows the successful application of the portable neutron generator for evaluating the chloride contamination in the field.

4. The best values of MDC of chlorine in the FA, BFS and SPZ cement concrete specimens were measured to be 0.031±0.010, 0.032±0.010 and 0.032±0.012 respectively. These value are comparable to those measured with the transmission type measurements using a large 350 keV accelerator, showing excellent performance of the portable PGNAA neutron generator set-up.
5. Within the statistical uncertainty the lower bound of MDC of chlorine measured in the concrete using the portable neutron generator PGNAA set-up was 0.03 wt.% indicating that the developed set-up can be used for low chloride concentrations as well.
6. Based on the data obtained in this study, it can be concluded that the portable neutron generator based PGNAA setup can be used successfully to detect chloride concentration in the concrete specimens.
7. A good correlation was noted between the gamma-ray yield at 2.86+3.10 MeV for chloride in FA, BFS and SPZ cement concrete. However, the combined correlation between gamma-ray yield and chloride concentration was not reliable (R^2 = 0.83). As such, the correlation equation between gamma-ray yield at 2.86+3.10 MeV and chloride concentration cannot be used confidently.
8. A good correlation was noted between the gamma-ray yield at 5.72 and 6.11 MeV. Consequently, the chloride concentration can be determined from these relations:

Chloride (wt.%) = 5.72 MeV Gamma-Ray Counts / 3839

Chloride (wt.%) = 6.11 MeV Gamma-Ray Counts / 5293

However, the equation with 6.11 MeV is preferred as it has higher intensity and can detect low concentrations of chloride.

5.2 Recommendations

Based on the present study, the following recommendations are made:

1. Studies should be conducted to evaluate the suitability of the developed PGNAA set-up for field applications.
2. The detection efficiency of the PGNAA set-up should be improved by using portable neutron generator with higher neutron intensity.
3. The developed set-up should be evaluated to determine free and bound chlorides.

CHAPTER 6

REFERENCES

[1] Al-Amoudi, O.S.B., and Maslehuddin. M., "Concrete Protection in Aggressive Media", *Proceedings, Concrete in the Service of Mankind: Concrete Repair, Rehabilitation and Protection, R.K. Dhir and M.R. Jones (Editors),* E & FN Spon, London, 1996, pp. 141-154.

[2] ACI Committee 222, Proceedings, *"Corrosion of Metals in Concrete",* (ACI 222R-89), *American Concrete Institute, Detroit, USA, 1989. Also ACI Manuals of Concrete Practice, Part I.*

[3] Maslehuddin, M. and Al-Amoudi , O.S.B., "Corrosion of Reinforcing Steel in Concrete: Its Monitoring and Prevention", *Proceedings, Symposium on Corrosion and Its Control,* King Saud University, Riyadh, Saudi Arabia, May 1992, pp. 110-125.

[4] Al-Amoudi O.S.B., (Cordinator), *"A Short Course on Protection of Reinforced Concrete Structures in Hot and Aggressive Exposures",* KFUPM, Dhahran, May 21 to 25, 2011.

[5] Montemor, M. F., Simoes, A.M. P., Ferreira, M.G. S., "Chloride-induced Corrosion on Reinforcing Steel: From the Fundamentals to the Monitoring Techniques". *Cement & Concrete Composites,* Vol. 23, 2003, pp. 491–502.

[6] Tuutti, K., "Corrosion of Steel in Concrete", CBI Research Report no. 4.82, Swedish Cement and Concrete Research Institute, Stockholm, Sweden, 1982.

[7] Pourbaix, M., "Atlas of Electrochemical Equilibria in Aqueous Solutions". *Oxford: Pergamon Press;* 1966.

[8] Gjorv, O. E., and Vennesland, O., "Sea Salts and Alkalinity of Concrete", *Journal of American Concrete Institute,* Vol. 73, No. 9, 1976, pp. 512-516.

[9] Ogura, K., and Ohama, T., "Pit Formation in the Cathodic Polarization of Passive Iron: ii. Effects of Anions", *Corrosion*, Vol. 37, No. 10, 1981, pp. 572.

[10] Uhlig, H. H., *Corrosion and Corrosion Control*, 1983, John Wiley and Sons, New York.

[11] Ritter, J. J., and Rodriguez, M.J., "Corrosion Phenomena for Iron Covered with a Cellulose Nitrate Coating", *Corrosion*, Vol. 38, No. 4, 1982, pp. 223-226.

[12] Roberts, M. H., "Effects of Calcium Chloride on the Durability of Pre-tensioned Wire in Prestressed Concrete", *Magazine of Concrete Research*, Vol. 14, No. 42, 1962, pp. 143-152.

[13] Mehta, P.K., "Effect of Cement Composition on Corrosion of Reinforcing Steel in Concrete". *Chloride Corrosion of Steel in Concrete, ASTM STP-62,* Philadelphia, 1977, pp. 12.

[14] Page, C. L., Short, N. R., and Holden, W. R., "The Influence of Different Cements on Chloride-induced Corrosion of Reinforcing Steel", *Cement and Concrete Research*, Vol. 16, No. 1, 1986, pp. 79-86.

[15] American Concrete Institute (1996). *ACI 318-85 Building Code Requirements for Reinforced Concrete.* American Concrete Institute, Detroit.

[16] American Concrete Institute (1996). *ACI 224, Causes, Evaluation and Repair of Cracks in Concrete.* American Concrete Institute, Detroit.

[17] Rasheeduzzafar, Hussain S. E., an Al-Saadoun, S. S., "Effect of Tricalcium Aluminate Content of Cement on Chloride Binding and Corrosion of Reinforcing Steel in Concrete", *ACI Materials Journal*, Vol. 89, No. 1, 1992, pp. 3-12.

[18] Lambert, P., Page, C. L., and Vassie, P. R. W., "Investigations of Reinforcement Corrosion. 2. Electrochemical Monitoring of Steel in Chloride-contaminated Concrete", *Materials and Structures*, Vol. 24, 1991, pp. 351-358.

[19] Page, C. L., and Vennesland, O., "Pore Solution Composition and Chloride-binding Capacity of Silica-fume Cement Pastes", *Materials and Structures*, Vol. 16, No. 91, 1983, pp. 19-25.

[20] Rasheeduzzafar, Hussain, S. E., and Al-Saadoun, S. S., "Effect of Cement Composition on Chloride Binding and Corrosion of Reinforcing Steel in Concrete", *Cement and Concrete Research*, Vol. 21, No. 1, 1991, pp. 777-794.

[21] Tritthart, J., "Chloride Binding in Cement, II. The Influence of the Hydroxide Concentration in the Pore Solution of Hardened Cement Paste on Chloride Binding", *Cement and Concrete Research*, Vol. 21, No. 5, 1991, pp. 777-794.

[22] Hausmann, D. A., "Steel Corrosion in Concrete". *Materials Protection*, Vol. 6, No. 19, 1967.

[23] Gouda, V. K., "Corrosion and Corrosion Inhibition of Reinforcing Steel: I. Immersed in Alkaline Solution". *British Corrosion Journal*, Vol. 5, 1970, pp.198-203.

[24] Mangat, P. S., and Molloy, B. T., "Influence of PFA, Slag and Microsilica on Chloride Induced Corrosion of Reinforcement in Concrete". *Cement and Concrete Research*, Vol. 21, No. 5, 1991, pp. 819-834.

[25] Al-Amoudi, O. S. B., Rasheeduzzafar, Maslehuddin, M., and Abduljauwad, S. N., "Corrosion of Reinforcing Steel in Sabkha Environment", *Proceedings, Symposium on Corrosion and Its Control*, Riyadh, 16-18 May 1992, pp. 80-90.

[26] Jovancicevic, V., Bockris, J. O. M., Carbajal, J. L., Zelenay, P., Mizuno, T., "Adsorption and Absorption of Chloride Ions on Passive Iron Systems", *Journal of Electrochem Soc*, Vol. 133, No. 133, 1986, pp. 2219-2226.

[27] Leckie, H. P., Uhlig, H. H., "Environmental Factors Affecting Critical Potential for Pitting in 18-8 Stainless Steel", *Journal of Electrochem Soc*, Vol. 113, No. 12, 1966, pp. 1262-1267.

[28] Bohni, H., Uhlig, H. H., "Environmental Factors Affecting the Critical Pitting Potential of Aluminium", *Journal of Electrochem Soc*, Vol. 116, No. 7, 1969, pp. 906-910.

[29] Kolotorkyn, Ja. M., "Efffects of Anions on the Dissolution Kinetics of Metals", *Journal of Electrochem Soc*, Vol. 108, No. 3, 1961, pp. 209-216.

[30] Hoar, T.P., *Corrosion Science*, CRRSA, Vol. 7, 1967, pp. 341.

[31] Chao, C. Y., Lin, L. F., MacDonald, D. D., "A Point Defect Model for Anodic Passive Films", *Journal of Electrochem Soc*, Vol. 128, No. 6, 1981, pp. 1187-1194.

[32] Schiessl, P., Raupach, M., In: Page, C. L., Treadway, K. W., Bamforth, P. B., editors. *Proceedings, Third International Symposium On Corrosion of Reinforcement in Concrete. London: Elsevier Applied Science,* England, May 21-24, 1990, pp. 314-332.

[33] Glass, G. K., Buenfeld, N. R., In: Nilsson, L. O., Olivier, J. P., editors. "Chloride Penetration in Concrete", *Paris: Pub. RILEM;* 1997, pp. 429-441.

[34] Glass, G.K., Buenfeld, N. R., "The Presentation of the Chloride Threshold Level for Corrosion of Steel in Concrete", *Corrosion Science,* Vol. 39, No. 5, May 1997, pp. 1001-1013.

[35] Ali Akbar Sohanghpurwala., "Manual on Service Life of Corrosion-damaged Reinforced Concrete Bridge Superstructure Elements", *National Cooperative Highway Research Program, National Research Council (U.S.) Transportation Research Board*- 2006, pp. 59.

[36] Vogel, I. A., *"A Textbook of Quantitative Inorganic Analysis",* 5th Edition, Revised by Basset, J., Longman., London, 1985.

[37] Sowerby, B. D., and Watt, J. S., "Nuclear Techniques for On-line Analysis in the Minerals and Energy Industries," *Proceedings, 9th Pacific Basin Nuclear Conference*, Sydney, Australia, 1994, pp. 379-386.

[38] Laszlo szentmiklosi, "Application of Time-dependent Processes in the Prompt-gamma Activation Analysis", *PhD thesis, Institute of isotopes, Hungarian Academy of Sciences,* Budapest, 2006.

[39] Vedmedenko, E. Y., “Competing Interactions and Patterns in Nano-world”, Institute for Applied Physics, University of Hamburg, Hamburg, Germany.

[40] Audi, G., Wapstra, A. H., “The AME2003 Atomic Mass Evaluation”. *Nuclear Physics A*, Vol. 729, No. 1, 2003, pp. 337-676.

[41] Paul, R. L., Lindstrom, R. M., “Prompt Gamma-ray Activation Analysis: Fundamentals and Applications”, *Journal of Radioanaytical Nuclear Chemistry*, Vol. 243, No. 1, 1999, pp. 181-189.

[42] Molnar, G. L., Revay, Z., Belgya, T., “Accurate Absolute Intensities for the 35Cl (n,γ) Reaction Gamma-ray Standard”, *Nuclear Instruments and Methods B,* Vol. 213, 2004, pp. 32-35.

[43] Choi, H. D., Firestone, R. B., Lindstrom, R. M., Molnar, G. L., Mughabghab, S. F., Paviotti-Corcuera, R., Revay, Z. S., Trkov, A., and Zhou, C. M., “Database of Prompt Gamma Rays from Slow Neutron Capture for Elemental Analysis”. *International Atomic Energy Agency*, Vienna, 2006.

[44] Collico, D., Savio, L., Mariscotti, M. A. J., Ribeiro Guevara, S., “Elemental Analysis of a Concrete Sample by Capture Gamma-rays with a Radioisotope Neutron Source”, *Nuclear Instruments and Methods B,* Vol. 95, 1995, pp. 379-383.

[45] Rhodes, J. R., Stout, J. A., Sieberg, R. D., Schindler, J. S., “In Situ Determination of the Chloride Content of Portland Cement Concrete Bridge Decks FHW/RD-80/030”, National Technical Information Service, Springfield, VA, 1980, pp. 58.

[46] Zhang, W., Gardner, R. P., "The Analog Linear Interpolation Approach for Monte Carlo Simulation of PGNA: CEARPGA Code", *Nuclear Instruments and Methods B*, Vol. 213, 2004 pp. 116–123.

[47] Naqvi, A. A., Maslehuddin, M., Garwan, M. A., Nagadi, M. M., Al-Amoudi, O. S. B., Khateeb-ur-Rehman and Raashid, M., "Estimation of Minimum Detectable Concentration of Chlorine in the Blast Furnace Slag Cement Concrete", *Nuclear Instruments and Methods B,* Vol. 269, 2011, pp. 1–6.

[48] Naqvi, A. A., Maslehuddin, M., Garwan, M. A., Nagadi, M. M., Al-Amoudi, O. S. B., Raashid, M., and Khateeb-ur-Rehman., "Effect of Silica Fume Addition on the PGNAA Measurement of Chlorine in Concrete", *Applied Radiation and Isotopes,* Vol. 68, 2010, pp. 412-417.

[49] Livingston, R. A., Mohamad Al-Sheikhly., and Ali B. Mohamed. "Numerical Simulation of the PGNA Signal from Chlorine Diffusion Gradients in Concrete". *Applied Radiation and Isotopes,* Vol. 68, 2010, pp. 679–682.

[50] Idiri, Z., Mazrou, H., Amokrane, A., and Bedek, S., "Characterization of an Am-Be PGNAA Set-up Developed for In-situ Liquid Analysis: Application to Domestic Wastewater and Industrial Liquid Effluents Analysis". *Nuclear Instruments and Methods B: Beam Interactions with Materials and Atoms***,** Vol. 268, 2010, pp. 213-218.

[51] Khelifi, R., Amokrane, A., Bode, P., "Detection Limits of Pollutants in Water for PGNAA using Am-Be Source". *Nuclear Instruments and Methods B: Beam Interactions with Materials and Atoms,* Vol. 262, 2007, pp. 329-332.

[52] Lea, D. E., “Combination of Proton and Neutron”, *Nature*, Vol. 133, 1934, pp. 24-24.

[53] Amaldi, E., O. D., “Artificial Radioactivity Produced by Neutron Bombarment-II”. *Proceedings of the Royal Society of London,* Vol. 149, 1935, pp. 522-558.

[54] Groshev, L. V., A. M., “Atlas of Gamma-Ray Spectra from Radiative Capture of Thermal Neutrons”. *Los Angeles, California: Pergaman Press INC,* 1959.

[55] Bartholomew, G. A., A. D., “Compendium of Thermal Neutron Capture Gamma-Ray Measurments”, *Nuclear Data Section A,* 1967, pp. 367-650.

[56] Greenwood, R. C., J. H., “Prompt Gamma Rays from Radiative Capture of Thermal Neutrons”. *US Atomic Energy Commission & IIT Research Institute,* Vol. 1 & 2, 1965.

[57] Hamermesh Bernard, H. V., “Neutron Capture Gamma-Ray Spectra from the Elements z = 17-30 and z = 45-57”, *Physical Review*, Vol.88, 1952, pp. 916-919.

[58] Lussie, W. G., Brownlee, J. L. Jr., “The Measurement and Utilization of Neutron-Capture Gamma Radiation”, *Modern Trends in Activation Analysis,* College Station, Texas, U.S.A, Vol. 88, 1965, pp. 194-199.

[59] Lambar, S. M., & Isenhour, T. L., “Neutron Capture Gamma-Ray Activation Analysis Using Lithium Drift Germanium Semiconductor Detectors”, *Analytical Chemistry*, Vol. 40, No. 13, 1968, pp. 1990-1994.

[60] Molnar, G. L., “Hand Book of Prompt Gamma Activation Analysis”, *Boston/ London: Kluwer Academic Publishers,* London, 2004.

[61] Anderson, D. L., Faily, M. P., Zoller, W. H., Walters, W. B., Gordon, G. E., & Lindstrom, R. M., “Facility for Non-Destructive Analysis for Major and Trace

Elements using Neutron- Capture Gamma-Ray Spectrometry", *Journal of Radioanalytical Chemistry*, Vol. 63, No. 1, 1981, pp. 97-119.

[62] Revey, Z., Harrison, R. K., Alvarez, E., Biegalski, S. R., & Landsberger, S., "Construction and Characterization of the Redesigned PGNAA Facility at the University of Texas at Austin", *Nuclear Instruments and Methods A*, Vol. 577, No. 3, 2007, pp. 611-618.

[63] Belgya, T., Revay, Z., & Molnar, G. L., "Gamma-Ray Background at the Budapest PGAA Facility", *Journal of Radioanalytical and Nuclear Chemistry*, Vol. 265, No. 2, 2004, pp. 181-191.

[64] KFKI Atomic Energy Research Institute, (n.d.) *KFKI Reactor Department,* Retrieved December 11, 2008, from http://www.kfki.hu/brr/indexen.htm

[65] Saleh, H. H., Livingston, R. A., " Experimental Evaluation of a Portable Neutron-Based Gamma-Spectroscopy system for Chloride Measurements in Reinforced Concrete", *Journal of Radioanalytical and Nuclear Chemistry*, Vol. 244, No. 2, 2000, pp. 367-371.

[66] Khelifi, R., Idiri, Z., Omari, L., Seghir, M., "Prompt Gamma Neutron Activation Analysis of Bulk Concrete Samples with an Am-Be Neutron Source", *Applied Radiation and Isotopes*, Vol. 51, No. 1, 1999, pp. 9-13.

[67] Tickner, J. R., "Determination of the Spatial Response of Neutron Based Analysers using a Monte Carlo Based Method", *Applied Radiation and Isotopes*, Vol. 53, No. 4-5, 2000, pp. 507-513.

[68] Lim, C. S., Tickner, J. R., Sowerby, B. D., Abernethy, D. A., McEwan, A. J., Rainey, S., Stevans, R., Manias, C., Retallack, D., "An On-Belt Elemental Analyser for the Cement Industry", *Applied Radiation and Isotopes*, Vol. 54, No. 1, 2001, pp. 11-19.

[69] Oliveira, C., Salgado, J., Goncalves, i. F., Carvalho, F. G., Leitao, F., "Prompt Gamma-Ray Neutron Activation Analysis of Cement Raw Materials ", *Journal of Nuclear Geophysics*, Vol. 7, No. 3, 1993, pp. 431-444.

[70] Jiggins, A. H., Habbani, F. I., "Prompt Gamma-Ray Analysis using 3.29 MeV Neutron Inelalstic Scattering", *Applied Radiation and Isotopes*, Vol. 27, No. 12, 1976, pp. 689-693.

[71] Naqvi, A. A., Garwan, M. A., "Validity Test of Design Calculations of a PGNAA Setup", *Nuclear Instruments and Methods B*, Vol. 215, No. 1-2, 2003, pp. 283-291.

[72] Naqvi, A. A., Nagadi, M. M., Khateeb-ur-Rehman., Maslehuddin, M., Kidwai, S., "Monte Carlo Simulations for Design of the KFUPM PGNAA Facility", *Radiation Physics and Chemistry*, Vol. 66, No. 2, 2003, pp. 89-98.

[73] Naqvi A.A., Fazul-ur-Rehman., Al-Jarallah, M. I., Abujarad, F., Maslehuddin, M., "Performance Test of External Moderators of a PGNAA Setup", *Applied Radiation and Isotopes*, Vol. 58, No. 1, 2003, pp. 27-28.

[74] Collico Savio, D. L., Mariscotti, M. A. J., Guevara, S. R., "Elemental Analysis of Concrete Sample by Capture Gamma-rays with a Radioisotope Neutron Source", *Nuclear Instruments and Methods B*, Vol. 95, No. 3, 1995, pp. 379-388.

[75] Naqvi, A. A., Garwan, M. A., Nagadi, M. M., Maslehuddin, M., Al-Amoudi, O. S. B., and Khateeb-ur-Rehman., "Non-destructive Analysis of Chlorine in Fly Ash Cement Concrete" *Nuclear Instruments and Methods A,* Vol. 607, No. 2, 2009, pp. 446–450.

[76] Chichester, D. L., Simpson, J. D., Lemchak, M., "Advanced Compact Accelerator Neutron Generator Technology for Active Neutron Interrogation Field Work," *Journal of Radio analytical and Nuclear Chemistry,* Vol. 271, No. 3, pp. 629–637.

[77] Idiria, Z., Mazroua, H., Beddeka, S., Amokraneb, A., Azbouchea, A., "Monte Carlo Optimization of Sample Dimensions of an 241Am–Be Source-based PGNAA Setup for Water Rejects Analysis", *Nuclear Instruments and Methods A,* Vol. 578, 2007, pp. 279–288.

[78] Naqvi, A. A., Nagadi, M. M., Khateeb-ur-Rehman., Maslehuddin, M., and Kidwai, S., "Monte Carlo Simulations for Design of the KFUPM PGNAA Facility". *Radiation Physics and Chemistry,* Vol. 66, 2003, pp. 89 – 98.

[79] Robin, P., Gardner., and Charles Mayo, W., "NaI Detector Nonlinearity for PGNAA Applications", *Applied Radiation and Isotopes,* Vol. 51, 1999, pp. 189-195.

[80] Briesmeister, J. F., (Ed) "MCNP4B2 –A General Monte Carlo N-Particles TransportCode", *Los Alamos National Laboratory Report, LA-12625, Version 4A, Los Alamos National Laboratory Report,* LA-12625-M, 1997.

[81] Qadir, M., Ghafoor, A., Murtaza, G., "Cadmium Concentration in Vegetables Grown on Urban Soils Irrigated with Untreated Municipal Sewage Environment", *Development and Sustainability,* Vol. 2 (1), 2000, pp. 13–21.

[82] Garcia-Reyes, J. F., Ortega-Barrales, P., and Molina-Diaz, A., "Sensing of Trace Amounts of Cadmium in Drinking Water using a Single Fluorescence-based Optosensor", *Microchemical Journal,* Vol. 82, No. 1, 2006, pp. 94–99.

[83] Cengiz, K.A., Levent, T., Dikilitas, Murat, Ashraf, Muhammed, Koskeroglu, Sultan, Guneri, Murat, "Supplementary Phosphorus can Alleviate Boron Toxicity in Tomato". *Scientia Horticulturae,* Vol. 121, 2009, pp. 284–288.

[84] Vincke, H., Gschwendtner, E., Fabjan, C. W., and Otto, T.,."Response of a BGO Detector to Photon and Neutron Sources: Simulations and Measurements", *Nuclear Instruments and Methods A,* Vol. 484, 2002, pp. 102–110.

[85] Ciema, M., Balabanski, D., Csatlo, M., Daugas, J. M., Georgiev, G., Gulya, J., Kmiecik, M., Krasznahorkay, A., Lalkovski, S., Lefebvre-Schuhl, A., Lozeva, R., Maj, A., and Vitez, A., "Measurement of High-energy γ-rays with $LaBr_3$:Ce Detectors", *Nuclear Instruments and Methods A,* Vol. 608, 2009, pp. 76-79.

[86] Favallia, A., Mehner, H. C., Ciriello, V., Pedersen, B., "Investigation of the PGNAA using the $LaBr_3$ Scintillation Detector",*Applied Radiation and Isotopes*, Vol. 68, 2010, pp. 901–904.

[87] Mehnera, H. C., Simonellib, F., "Wide Energy Range Efficiency Calibration for a Lanthanum Bromide Scintillation Detector". *Radiation Measurements*, Vol. 43, 2008, pp. 506 – 509.

[88] Alexiev, D., Mo, L., Prokopovich, D. A., Smith, M. L., and Matuchova, M., "Comparison of $LaBr_3$:Ce and $LaCl_3$:Ce with NaI(TI) and Cadmium Zinc Telluride (CZT) Detectors", *IEEE Transactions on Nuclear Sciences*, Vol. 55, No. 3, JUNE 2008.

VITAE

Name : Zameer Kalakada.

Nationality : Indian.

Date of Birth : Feb 08, 1982.

Permanent Address : H.No: 5-807, Old Alwal,

Secunderabad – 500010, Andhra Pradesh, INDIA.

Present Address : Room#810/218, KFUPM, Dhahran, K.S.A.

Email : kalakadazameer@gmail.com

Phone : +91-9966426363

+966-551853208

Degrees:

Bachelor of Science in Civil Engineering from Osmania University (Sept. 2000 – April 2004).

Experience:

Research Assistant in Civil Engineering Department of King Fahd University of Petroleum & Minerals (KFUPM) (Oct. 2009 – March. 2012).